

Modelling and Analysis of Geocell Reinforced Foundations

- Faby Mole P.A-

A Dissertation Submitted to
Indian Institute of Technology Hyderabad
In Partial Fulfillment of the Requirements for
The Degree of Master of Technology/ Doctor of Philosophy



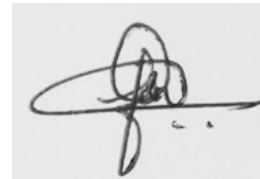
भारतीय प्रौद्योगिकी संस्थान हैदराबाद
Indian Institute of Technology Hyderabad

Department of Civil Engineering

July, 2013

Declaration

I declare that this written submission represents my ideas in my own words, and where others' ideas or words have been included, I have adequately cited and referenced the original sources. I also declare that I have to all principles of academic honesty and integrity and have not misrepresented or fabricated or falsified any idea/data/fact/source in my submission. I understand that any violation of the above will be a cause for disciplinary action by the Institute and can also evoke penal action from the sources that have thus not been properly cited, or from whom proper permission has not been taken when needed.

A handwritten signature in black ink, appearing to be 'Faby Mole P.A.', written on a light gray background.

Faby Mole P.A

CE11M02

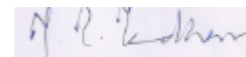
Approval Sheet

This thesis entitled “Modelling and Analysis of geocell reinforced foundations” by Faby Mole P.A. is approved for the degree of Master of Technology from IIT Hyderabad.

Dr. Umashankar Balunaini
Asst. Professor, Dept. of Civil Engg. , IIT Hyd
Examiner



Dr. Sireesh Saride
Asst. Professor, Dept. of Civil Engg. , IIT Hyd
Adviser



Prof. M.R Madhav
Visiting Professor, Dept. of Civil Engg. , IIT Hyd
Co-Adviser

Dr. Prasanth Kumar
Asst. Professor, Dept. of Mechanical Engg. , IIT Hyd
Chairman

Acknowledgements

This dissertation would not have been possible without the guidance and the help of several individuals who in one way or another contributed and extended their valuable assistance in the preparation and completion of this study.

First and foremost, my utmost gratitude to my thesis advisor, Dr. Sireesh Saride for the continuous support throughout my M-Tech research. Dr. Sireesh Saride has been my inspiration as I hurdle all the obstacles in the completion this research work. His interest and confidence in me has helped in the successful completion of my work.

I am also immensely indebted to Prof. Madhav Madhira for his valuable guidance and timely suggestions. I bow down before the immense knowledge and enthusiasm that he possess in exploring new frontiers in research. I am also extremely grateful to Dr. B. Umashankar for his kind concern, constant support and steadfast encouragement throughout my M-Tech study.

I am obliged to Praveen Throvagunta, Sasanka Mouli and Mrunalini Rao for unfailingly helping me to develop the solver. A special note of thanks to my classmates and friends Roji, Suraj, Rajasekhar, Saranya, Remya, Jancy, Sasanka Mouli, Hari Prasad, Bagat, Deepti, Vijay, Anita, Natasha and Akhila for the inexplicable love and affection that were showered on me. These people made my stay at IIT Hyd lovely and memorable. I am also grateful to my family for instilling confidence in me and giving me strength to plod on under difficult circumstances. Their stimulation, support and faith in me has helped in bringing out the best in me.

Faby Mole P.A

To my family who stood by me through thick and thin

Abstract

Geosynthetics, in the form of three dimensional geocell mattresses has emerged as a promising technique to improve the performance of foundations. This study pertains to the development of a mathematical formulation to predict the behaviour of footings (Strip and Circular footings) resting on geocell reinforced granular layer overlying soft soil. To obtain the approximate behaviour of the geocell reinforced system contact pressure distribution of the geocell reinforced bed was considered. The approach based on contact pressure distribution is demonstrative in understanding the pattern of bearing capacity improvement but for exact predictions of the same, numerical investigations using foundation models or experimental studies have to be conducted. Pasternak model was used to represent the geocell reinforced-footing system as it considers the material properties of geocell - subsoil system. Linear and nonlinear responses were considered to account for the behaviour at low and high settlements respectively. The predictions of the Pasternak model were found to hold good for lower range of settlements. The necessity of improvement of the model was understood since Pasternak model doesn't account for the confining stresses that act on the geocell system from which it derives its major strength. Hence, the stress dependent behaviour was also analyzed later in the research to fully understand the behaviour of geocell reinforced systems. To check the efficiency and applicability of the proposed models the results were validated in several ways (Theoretical, numerical, experimental validation) which indicated good agreement.

Nomenclature

Q^*	Normalized load (Non-dim)
R_g	Shear layer width ratio (Non-dim)
w	Settlement of shear layer from the edge of the footing (m)
W	Normalized settlement, (Non-dim)
W_0	Normalized footing settlement / prescribed settlement, (Non-dim)
x	Distance from center of the footing (m)
X	Normalized distance from center of the footing, (Non-dim)
α^2	$k_s \cdot B^2 / G_g H$,inverse of normalized shear stiffness of the geocell reinforced granular layer, (Non-dim)
μ	$k_s \cdot B / q_u$,inverse of normalized ultimate bearing capacity of unreinforced soft soil (Non-dim)
I_f	Improvement factor, (Non-dim)
C	Compaction Coefficient
R	Normalized radial distance (Circular footing)
n	Janbu's Parameter

Contents

Declaration.....	ii
Approval Sheet	iii
Acknowledgements.....	iv
Dedication.....	iv
Abstract.....	vi
Nomenclature	vii
1 Introduction.....	1
1.1 Preamble	1
1.2 Mechanism of Geocell Reinforcement	2
1.3 Objective and Scope of the Study.....	3
1.4 Organization of the Thesis.....	3
2 Literature Review	4
2.1 Introduction.....	4
2.2 Studies on Planar Reinforcement.....	4
2.3 Studies on Geocell reinforcement.....	7
2.4 Elastic Models of Soil Behaviour	10
2.4.1 Winkler Model	11
2.4.2 Filonenko- Borodich Model	11
2.4.3 Hetenyi Model.....	12
2.4.4 Pasternak Model.....	12
2.4.5 Vlazov Model.....	12
2.4.6 Reissner Model.....	13
2.5 Analytical or Numerical Modelling of Geocell Reinforcement.....	14
2.6 Summary.....	16
3 Prediction of Limit Bearing Capacity of Footings on Geocell Reinforced Foundations	18
3.1 Statement of the Problem.....	18
3.2 Analytical Approach	19
3.2.1 Strip footing.....	19
3.2.1.1 Short Geocell	19
3.2.1.2 Intermediate Width Geocell	20
3.2.1.3 Wide Geocell.....	20

3.2.2 Circular Footing.....	21
3.2.2.1 <i>Short Geocell</i>	21
3.2.2.2 <i>Intermediate width geocell</i>	21
3.2.2.3 <i>Wide Geocell</i>	22
3.3 Results and Discussions.....	22
3.4 Summary.....	27
4 Elasto-Plastic Behaviour of Rigid Strip Footing on Geocell Reinforced Soils	28
4.1 Statement of the problem.....	28
4.2 Theoretical formulation	30
4.2.1 Linear Formulation	30
4.2.2 Non-linear Formulation	35
4.2.3 Finite Difference Formulation	36
4.2.4 Boundary Conditions.....	37
4.3 Validation	37
4.3.1 Theoretical Validation	37
4.3.2 Experimental Validation.....	38
4.3.3 Numerical Validation	40
4.4 Results and discussion	41
4.4.1 Improvement Factors.....	47
4.4.2 Practical Significance	50
4.5 Summary.....	50
5 Elasto-Plastic Behaviour of Rigid Circular Footing on Geocell Reinforced Soils	53
5.1 Problem Statement.....	53
5.2 Theoretical Formulation	55
5.2.1 Linear Formulation	55
5.2.2 Non-linear Formulation	58
5.2.3 Finite Difference Formulation	59
5.2.4 Boundary Conditions.....	60
5.3 Validation	61
5.3.1 Theoretical Validation	61
5.3.2 Numerical Validation	61
5.4 Results and Discussion	62
5.5 Summary.....	72

6 Stress Dependent Behaviour of Rigid Strip Footing on Geocell Reinforced Soils	73
6.1 Problem Statement.....	73
6.2 Mathematical Formulation.....	75
6.2.1 Linear formulation.....	75
6.2.1.1 Validation	77
6.2.1.2 Results	78
6.2.2 Nonlinear formulation	79
6.2.3 Finite Difference Formulation	81
6.2.4 Boundary Conditions.....	82
6.3 Validation	82
6.3.1 Numerical Validation	82
6.3.2 Theoretical Validation	83
6.3.3 Experimental Validation.....	84
6.4 Results and Discussion	86
6.5 Summary.....	96
7 Stress Dependent Behaviour of Rigid Strip Footing on Geocell Reinforced Soils	98
7.1 Problem Statement.....	98
7.2 Mathematical Formulation.....	99
7.2.1 Linear Formulation.....	100
7.2.1.1 Validation	103
7.2.1.2 Results	104
7.2.2 Nonlinear formulation	106
7.2.3 Finite difference formulation.....	110
7.2.4 Boundary Conditions.....	112
7.3 Validation	112
7.3.1 Theoretical Validation	112
7.3.2 Numerical Validation	113
7.3.3 Experimental Validation.....	114
7.4 Results and Discussion	116
7.4.1. Improvement Factors.....	121
7.5 Summary.....	126
8 Conclusions	129
8.1 General.....	129

8.2 Conclusions	129
8.2.1 Limit Bearing Capacities through Contact Pressure Variations	130
8.2.2 Nonlinear Pasternak Model for Strip Footings.....	130
8.2.3 Modified Pasternak model – Circular Footing	132
8.2.4 Stress Dependent Model for Strip Footing	133
8.2.5 Stress Dependent Model for Circular Footing.....	134
8.3 Scope of Further work	135
References	137
Publications	141

Chapter 1

Introduction

1.1 Preamble

Land scarcity in the existing urban areas demands the use of sites that has soils of marginal quality. There are several ground improvement techniques that makes a site optimum for construction activities that have been employed over the decades. The concept of in situ reinforcement using timber fibers date back to 3000 B.C [Dewar, 1962; Koerner, 2005]. The first use of fabrics for reinforcing soft soils was experimented by the South Carolina Highway Development in 1926 [Koerner, 2005].

In the past decades, geosynthetics have emerged as exciting engineering material with a wide range of applications. According to ASTM D4439, a geosynthetic is defined as following:

Geosynthetic – a planar product manufactured from polymeric material used with soil, rock, earth or other geotechnical engineering related material as an integral part of a human made project, structure, or system

The geosynthetic material performs five major functions viz. separation, reinforcement, filtration, drainage and containment. The use of geosynthetic material is widely accepted due to its high performance and is a more economical solution for soft ground problems.

There are different types of geosynthetics viz. geotextiles, geogrids, geonet, geomembrane, geosynthetic clay liners, geopipe, geofoam and geocomposites. Widespread research on the use of geosynthetic as soil reinforcement has been carried out by various researchers [3,8]. A new introduction to the class of geosynthetics based on cellular confinement system was first developed and evaluated in France during late 1970s [21]. Netlon developed a similar concept with the introduction of Tensar geocell mattress [21]. Since then, the use of geocells

in the field of civil engineering construction has gained wide spread popularity due to its advantages over the two dimensional planar form of geosynthetics. Figure 1.1 shows a photograph of ready-made geocells.

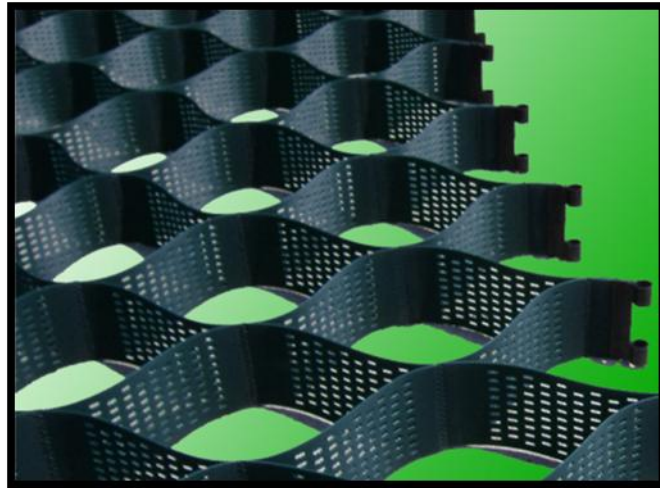


Figure 1.1: Typical readymade geocells (Pic courtesy: WCHPRCL)

1.2 Mechanism of Geocell Reinforcement

Geosynthetics rely on frictional resistance, arching and entanglement of fibers to improve the soil performance, whereas *geocell* derives its strength from the all-round confinement the three dimensional geocell mattress offers to the encapsulated soil as shown in the Figure 1.2.

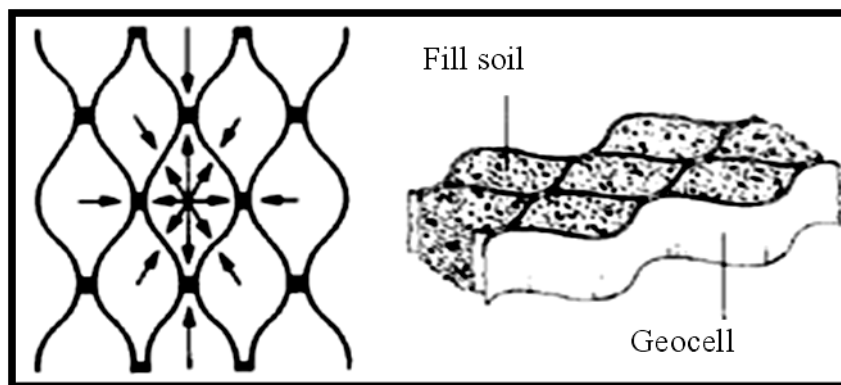


Figure 1.2: The concept of geocell reinforcement

There have been some exceptional research in the area of geocell reinforcement in the recent past (Bathrust and Jarrett, 1989; Bush et al, 1990; Mandal and Gupta, 1994; Krishnaswamy et al, 2000; Dash et al, 2001; Dash et al, 2003) and the use of geocells as a

reinforcement material has gained strength over the years. Since there are not many analytical or numerical models available to predict the behavior of geocell reinforced foundation beds, the current study focus on the development of a simple model to predict the geocell reinforced foundation behavior.

1.3 Objective and Scope of the Study

The major objective of the present study is to develop an understanding of the behavior of geocell reinforced foundations subjected to static loading on strip and circular footings using analytical and numerical modeling.

The scope of the present research is as follows:

- I. The primitive estimation of the bearing capacity of footings either strip or circular on geocell reinforced soils using contact pressure variation assumed based on the width and stiffness of the geocell reinforced soil.
- II. Develop a model in the lines of Pasternak Shear Layer model to evaluate the linear and non-linear behavior of strip and circular footings on geocell reinforced soils. Axisymmetric case will be considered for circular footings.
- III. Incorporation of effect *of confinement* to the infill material in the model to improve the model predictions. Development of design charts to design a strip or a circular footing resting on geocell reinforced soils.

1.4 Organization of the Thesis

In *Chapter 2* the literature available on reinforced soil has been discussed. Discussion has been carried on planar reinforcement, geocell reinforcement, foundation models and numerical and analytical modelling of geocell reinforcement. *Chapter 3* deals with the prediction of limit bearing capacity of geocell reinforced soil based on contact pressure variation. Contact pressures are assumed based on the width and stiffness of the geocell mattress. *Chapter 4* discusses the elasto plastic behaviour of rigid strip footing resting on Geocell reinforced soils with the aid of Pasternak model. Finite difference method was employed to obtain the solution of governing differential equations. The design charts were proposed for the design of geocell reinforced foundations. *Chapter 5* studies the elasto plastic behaviour of rigid circular footing resting on geocell reinforced soils. Axisymmetric

modelling was done since circular footing is involved. Linear and nonlinear analysis were conducted for low and high settlements respectively. *Chapter 6* covers the discussion on improvement of Pasternak model to include the effect of confining stresses on the geocell reinforced strip footing system. The proposed model predicts the behaviour of system accurately since it accounts for the stress dependent behaviour (Confining stresses) from which the geocell derives its major strength. The proposed design charts could be used for field applications. *Chapter 7* deals with the improved model for circular footing that accounts for confining stresses in the geocell reinforced system. The models were validated against experimental data and the results were found to be in good agreement. *Chapter 8* summarizes the results obtained from the study on different models and footings (strip and circular) and the major conclusions drawn from the study.

Chapter 2

Literature Review

2.1 Introduction

The reinforced soil technique has undergone considerable evolution over the years. The reinforcement of in-situ soils is an ancient process that date back to 3000 B.C. The concept of reinforced soil as a construction material was pioneered with the introduction of metal strips as reinforcement material. The use of geosynthetic as reinforcing material slowly gained momentum over the years and replaced the conventional materials. Geocells, which are relatively a new inclusion in the class of geosynthetics has been widely used in civil engineering applications due to its better performance, ease of construction and economy involved.

This chapter deals with the existing studies that were carried out on geosynthetics since its inception in 1960's. In this chapter, firstly discussion on current studies on planar geosynthetic reinforcement which was the initial entry to the class of geosynthetics was carried out. Later in the chapter, geocell reinforcement which was relatively new inclusion in the category of geosynthetics was studied extensively by various researchers and brief review of the same is discussed here. Further, a recap of analytical and numerical approaches to understand the behavior of geosynthetic reinforced foundations is reviewed in this chapter.

2.2 Studies on Planar Reinforcement

The invention of reinforced earth technique by the French engineer Henry Vidal in the 1960's combines horizontal metal strips with suitable granular backfill and prefabricated facing panels that are attached to the strips. The reinforced earth technique was originally employed in France in 1968 for the construction of highway retaining wall.

Binquet and Lee [1975 a] performed a series of model test on strip footing supported on homogeneous sand, sand overlying deep soft soil and sand above a deep finite pocket of soft material. Aluminium foils were used for reinforcement in their study. A non-dimensional term called bearing capacity ratio (BCR) which is the ratio of footing pressure of the reinforced bed at a particular settlement to the ultimate bearing pressure of the unreinforced bed. It was reported from the study that the ultimate bearing capacity increases with increase in the number of reinforcing layers and but shows negligible improvement after 8 layers of reinforcement.

Akinmusuru and Akinbolade [1981] carried out laboratory model tests on square footings supported on deep homogeneous sand beds reinforced with strips of fiber material. Various parameters viz. spacing of the strips, number of reinforcing layers and the depth of first reinforcement from the footing base were varied to determine their influence on the improvement in bearing capacity. It was observed from the study that spacing between the fibers should be lesser than 0.5 times the width of footing for better performance. Maximum improvement in BCR was achieved when the top layer of reinforcement was placed at a depth of 0.05 times the width of the footing with three or four reinforcement layers.

A series of laboratory model test were conducted on rectangular steel footing by Fragazsy and Lawton [1984] where aluminium strips were used as reinforcement. From the study, the optimum length of reinforcement strip was found to seven times the footing width. They also observed that the BCR is independent of soil density when calculated at a settlement equal to 10% of the footing width but at a settlement of 4% of the footing width the percentage increase in BCR was found to be less for loose sands than dense sands.

Geogrid and Geotextile slabs were tested by Guido et al. [1986] to determine the influence of vertical spacing of the layers, number of layers, placement depth of the first layer of reinforcement, width of a square sheet reinforcement and tensile strength of the reinforcement on the improvement. It was reported that for geogrids and geotextile after reaching the optimum width of reinforcement and number of layers the increase in bearing capacity was found to be marginal. The bearing capacity was found to be very high when the first layer of reinforcement was placed closed to the footing base and spacing between consecutive geogrid/geotextile layers smallest. In case of geotextile, the increase in bearing capacity is directly proportional to the increase in tensile strength of the geotextile, whereas

for a geogrid apart from tensile strength, aperture opening size also plays an important role in improvement.

Verma and Char [1986] conducted model tests on footings supported on vertically reinforced sand subgrade. The experiments performed on the subgrades concluded that for a given quantity of the reinforcement, bearing capacity was found to be a function of length and spacing of the reinforcement.

Plain strain model tests were headed by Huang and Tatsuoka [1990] to foretell the bearing capacity of a horizontal sandy ground reinforced with tensile reinforcement layers. The significant conclusions that were obtained from the study is that reinforcement layer of approximately the same width as that of footing provides high improvement in bearing capacity, however reinforcement layers lying outside the loaded area contributed in a secondary manner to the load carrying mechanism.

The impact of soil reinforcement on the bearing capacity of eccentrically loaded footings over granular soils was studied in detail by Raymond et al. [1992]. It was concluded from the study that placing the reinforcement near the foundation contact surface resulted in high bearing capacity irrespective of the eccentricity. The bearing capacity was found to increase with increase in reinforcement length up to 1.25 times the width of the footing and shows negligible improvement beyond that.

Omar et al. [1993a] compared model test results for the ultimate bearing capacity of strip and square footings on geogrid reinforced sand beds. The critical depth of reinforcement was found to be 2 times the width of footing and 1.4 times the width of footing for strip and square footings respectively. The maximum width of geogrid layers required for mobilization of bearing capacity is about 8 times the width of the footing for strip footing and 4.5 times the width of the footing for square footings. Omar et al. [1993b] further improved the studies by considering the influence of length to width ratios of model foundations supported by geogrid reinforced sand beds.

The bearing capacity of rectangular footings supported on geogrid reinforced sand beds was investigated by Yetmoglu et al. [1994] through laboratory model test. Similar trend of improvement as inferred from the previous studies were again confirmed from this study like the increase in bearing capacity is increased with increase in the number of

reinforcement layers and width of the reinforcement when it's placed at an effective zone below the footing. The optimum depth of reinforcement and effective spacing between the reinforcement were also reported from the study. It was also inferred from the study that increase in the axial stiffness of beyond 1000 kN/m would not bring in any improvement.

There had been an extensive and wide research on various modifications of planar reinforcement conducted by various researchers [Das et al, 1996; Michael et al, 1997; Gabr et al, 1998; Alawaji, 2001; Kumar and Saran, 2001; Shin et al, 2002; De Merchant et al, 2002; Yamamoto et al, 2002; Boushehrian and Hataf, 2003; Michalowski, 2004; Patra et al, 2005] especially on geogrid reinforced foundations studying the effect of various parameters [Khing et al, 1993; Omar et, 1993 etc.], on the improvement and arriving at the optimum dimensions of the reinforcement and their placement.

2.3 Studies on Geocell reinforcement

In the earlier days interconnected paper cells filled with sand was used as reinforced layer for construction of low cost highways. Ria and Mitchell [1978] pioneered the research on thick paper cells and the influence of ratio of radius of loaded area to cell width, ratio of cell width to cell height, sub grade stiffness and repeated loading were investigated.

A series of large scale static tests were undertaken by Bathrust and Jarret [1988] to investigate the load deformation behaviour of geocomposite mattresses (geocell or geoweb mattresses) constructed over a compressible peat subgrade and to compare this behaviour with that of comparable unreinforced gravel bases and gravel bases reinforced with a single layer of geotextile or geogrid at the gravel peat interface. The test showed that the geocomposite mattresses significantly improved the load –bearing capacity of the gravel base layer in comparison with equivalent depths of unreinforced gravel bases. It was also observed that a stiffer geoweb construction gave a greater load bearing capacity at a given rut depth than did a less stiff geocell construction. Comparisons between geoweb reinforced gravel bases and unreinforced bases showed that the geoweb composites were equivalent to about twice the thickness of unreinforced gravel bases in their effectiveness.

Laboratory plate load test on geoweb reinforced sand beds were performed by Guido et al. [1989]. Parametric study were conducted for the parameters texturisation roughness of the geoweb wall, number of layers of geoweb reinforcement, depth below the loaded plate to the top of the first layer of reinforcement, size of the geoweb reinforcement and relative

density of the fill material. It was reported from the study that for untextured geoweb, increasing the number of reinforcement beyond 4 doesn't bring in further improvement but for medium textured geoweb there was considerable improvement. The optimum geocell layer width ratio, R_g was reported as 2 and 3 for untextured and medium textured geocells respectively. It was also observed that for loose soils (effect of relative density) the improvement in load carrying capacity was found to be higher.

The use of geocell foundation mattresses were studied by Bush et al. [1990]. The incorporation of the geocell mattress induces a rough interface between the soft foundation and the contained granular fill of the mattress. The rigidity of the mattress distributes the load onto the foundation bringing forth a regular stress field within the soft foundation layer. To sum up, a restraining influence was exerted by the geocell mattress to prevent deformation in the soft foundation.

Model test were undertaken by Shimizu and Inui [1990] on geotextile cell wall used to strengthen soft soils. The influence of aspect ratio of the cell (height to width ratio) on bearing capacity improvement was found to be maximum for an aspect ratio of about 1.5. Explicitly, addition of the geocell increased the bearing capacity of the footing on soft soil and another observation from the study is that bearing capacity proportionately increases with increase in stiffness of the geocell.

The case study of performance of geocell supported embankment on soft clay were analyzed by Cowland and Wong [1993]. The embankment was fully instrumented during construction to monitor the performance of geocell mattress foundation and the recorded extensions of the geocell mattress were found to be less than 1% which indicates the geocell mattress behaved as a stiff raft to the embankment.

Laboratory model test were carried on geocell structure on a soft clay subgrade by Mhaikar and Mandal [1994] and also finite element analysis on the same were conducted. The experimental results were simulated in a finite element package ANSYS and close agreement between experimental and numerical results were obtained.

Mandal and Gupta [1994] conducted studies on the application of geocell reinforcement to stabilize the soft marine clay subgrade. A series of experiments were carried out on model strip footing resting on geocell reinforced sand overlying clay beds. The influence of geocell

opening size and height of the geocell on the entire behaviour of the foundation system has been studied.

Krishnaswamy et al. [2000] conducted laboratory model tests to quantify the improvement in the performance of embankments constructed on soft clays due to the provision of a geocell reinforcement layer at the base. The results of the test have shown that the provision of a layer of geocells at the base of the embankments improves the load capacity as well as vertical as well as lateral deformations of the embankment. The tensile stiffness of the geogrid used to manufacture the geocell and the aspect ratio of the geocell pockets have an important influence on the performance of geocell supported embankments.

Laboratory model tests on a strip footing supported by a sand bed reinforced with geocell mattress were undertaken by Dash et al. [2001]. The parameters that were varied in the testing program include pattern of geocell formation, pocket size, height and width of geocell mattress, the depth to top of geocell mattress, tensile stiffness of the geogrids used to fabricate geocell mattress and the relative density of sand. It was reported from the investigation that chevron pattern is more beneficial than diamond pattern.

Small scale laboratory model tests were conducted on a model circular footing by Dash et al. [2003] to determine the effectiveness of geocell reinforced granular fill overlying soft clay beds. Footing load, footing deformation and footing settlement on the fill surface were measured during the tests. It was reported from the study that a seven fold increase in the bearing capacity of the circular footing can be obtained by providing geocell reinforcement along with a basal geogrid layer in the sand bed underlying soft clay.

Sitaram and Sireesh [2005] reported the laboratory model test results on embedded circular footing supported on geogrid cell reinforced foundation beds. The cellular mattress used in the investigation was prepared from biaxial polymer called geogrid geocell. The parameters that were studied in the testing program include depth of placement of cellular mattress below the footing base, width and height of the geocell mattress. It was observed from the study that the effect of embedment depth of footing becomes marginal in case of sand beds compared when compared with clay beds at higher embedment depths. It was also reported that with the insertion of cellular mattress the footing pressure is distributed more uniformly over a wider area of footing embedment depth.

The performance of surface footing on geocell reinforced sand clay beds was studied by Sitharam et al [2007]. Geocells made of biaxial polymer geogrid were fabricated. It was reported from the study that the load carrying capacity of the clay bed increased by a factor of up to 4.5 times of the unreinforced bed. The maximum reduction in footing settlement observed with the provision of footing settlement of optimum size close to the footing is around 90%.

Sireesh et al. [2008] investigated the potential benefits of providing geocell reinforced sand mattress over clay subgrade through a series of laboratory scale model tests. The parameters varied in the test program were thickness of unreinforced sand layer above clay bed, width and height of geocell mattress, relative density of sand fill in the geocells, and influence of additional layer of planar geogrid placed at the base of the geocell mattress. The test results indicate substantial improvement. The test results indicate substantial improvement in performance can be obtained with the provision of geocell mattress, of adequate size, over the clay subgrade with void. The influence of the void over the performance of the footing reduces for height of geocell mattress greater than 1.8 times the diameter of the footing.

Moghaddas [2010] conducted laboratory investigations on strip footing supported on geocell reinforced sand bed under monotonic load. A series of different laboratory, pilot scale tests were performed to evaluate the bearing pressure and settlement of a strip footing supported by reinforced relatively dense sand with geocell with special emphasis on the reduction of footing settlement and on the improvement in bearing capacity of footings at the range of low to medium level settlement level, similar to those of interest in practice. The bearing capacity improvement, settlement reduction, typical height and width of geocell required etc. were reported from the study.

2.4 Elastic Models of Soil Behaviour

The inherent complexity in the behavior of real soils has led to development of many idealized models of soil behaviour especially for the analysis of soil-foundation interaction problems. A detailed account of the foundation models (Winkler, 1867; Filonenko-Borodich, 1940; Pasternak, 1954) has been presented by Selvadurai (1979) and Poulos and Davis (1974). In this section a brief exposition of some of the idealized models are presented.

2.4.1 Winkler Model

The idealized model proposed by Winkler (1867) assumes that the deflection, w of the soil medium at any point on the surface is directly proportional to the stress, q applied at that point and independent of stresses applied at other locations i.e.

$$q(x,y) = kw(x,y) \quad (2.1)$$

Where, k is the modulus of subgrade reaction with units of stress per unit length.

Some of the shortcomings that were encountered in the model are that the displacement occurs immediately under the loaded area and in the outside regions the displacements are zero and also the displacements under the loaded region would be same whether the soil is subjected to an infinitely rigid load or a uniform flexible load. The inherent deficiency of the Winkler model in depicting continuous behaviour has led to the development of physical models viz. Filonenko-Borodich (1940, 1945) Hetenyi (1946), Pasternak (1954) and Kerr (1964) where the interaction between the spring elements is provided by elastic membranes, elastic beams or elastic layers. Figure 2.1 shows the idealized Winkler model.

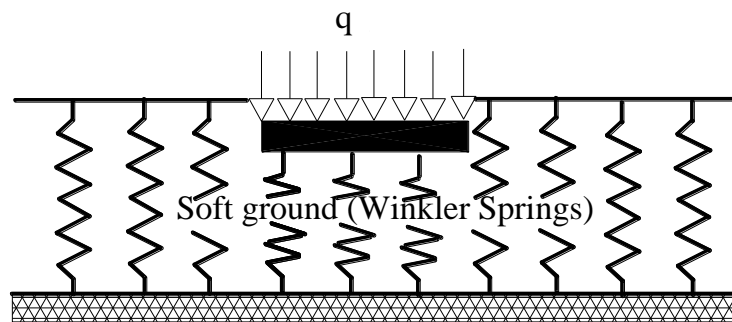


Figure 2.1: Winkler Model

2.4.2 Filonenko- Borodich Model

The model put forward by Filonenko-Borodich (1940, 1945) attains continuity between the spring elements by connecting them to a thin elastic membrane under constant tension, T .

The surface deflection of the soil medium due pressure q is given by

$$q(x,y) = kw(x,y) - T\nabla^2w(x,y) \quad (2.2)$$

$$\text{Where } \nabla^2 = \frac{\partial^2}{\partial x^2} + \frac{\partial^2}{\partial y^2}$$

Figure 2.2 represents the Filonenko-Borodich model.

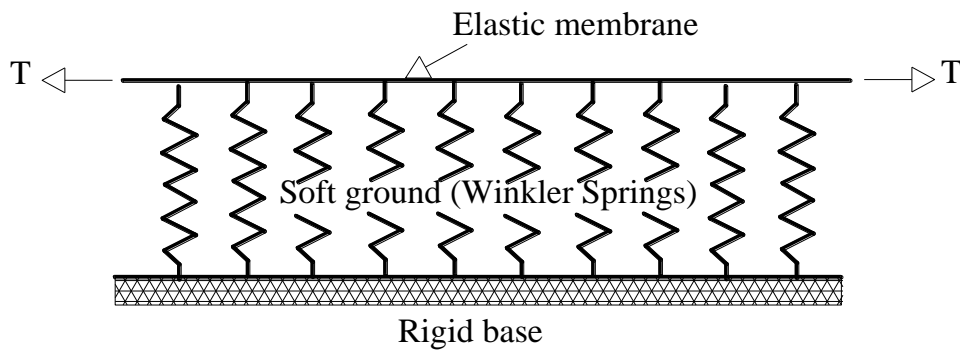


Figure 2.2: Filonenko – Borodich Model

2.4.3 Hetenyi Model

The model proposed by Hetenyi (1946), considers the interaction between the spring elements by incorporating an elastic plate in three dimensional problems or elastic beam in two dimensional problems. The response function of the model is given by

$$q(x, y) = kw(x, y) - D\nabla^4 w(x, y) \quad (2.3)$$

Where, $D = \frac{E_p h^3}{12(1-\mu_p^2)}$ is the flexural rigidity of the plate.

2.4.4 Pasternak Model

Pasternak proposed a model that assumes shear interaction between the spring elements. This can be accomplished by connecting the spring elements to a layer of incompressible vertical elements which deform in transverse shear only. This model is more appropriate to model soil as the shear behavior of soil is highly important during the failure of soil.

The surface deflection profile of this model due to pressure q is

$$q(x, y) = kw(x, y) - G_p \nabla^2 w(x, y) \quad (2.4)$$

Where G is the shear moduli of the shear layer.

Figure 2.3 shows the Pasternak foundation model which is used in the study.

2.4.5 Vlazov Model

The model proposed by Vlazov (1949 a,b) presents another approach of two-parameter elastic model which is derived by imposing displacement constraints that simplify the basic equation for a linear elastic isotropic continuum. Vlazov's method to the formulation is by application of variational method. The representation of Vlazov's model is shown in Figure 2.4.

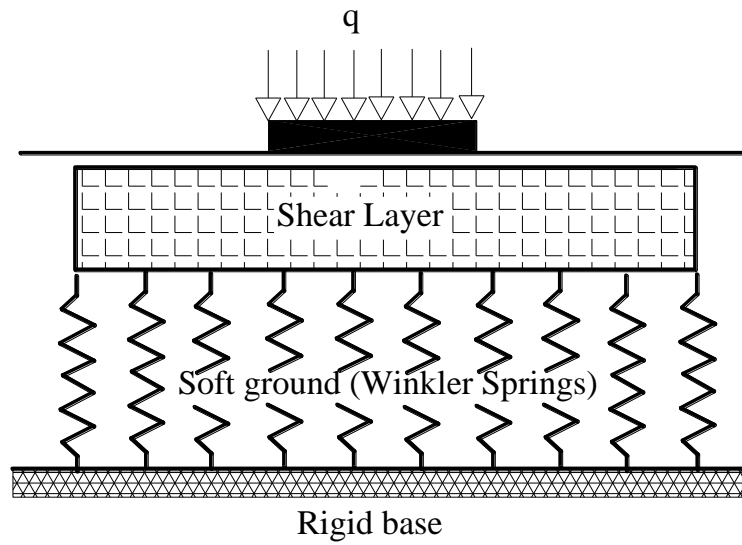


Figure 2.3: Pasternak Model

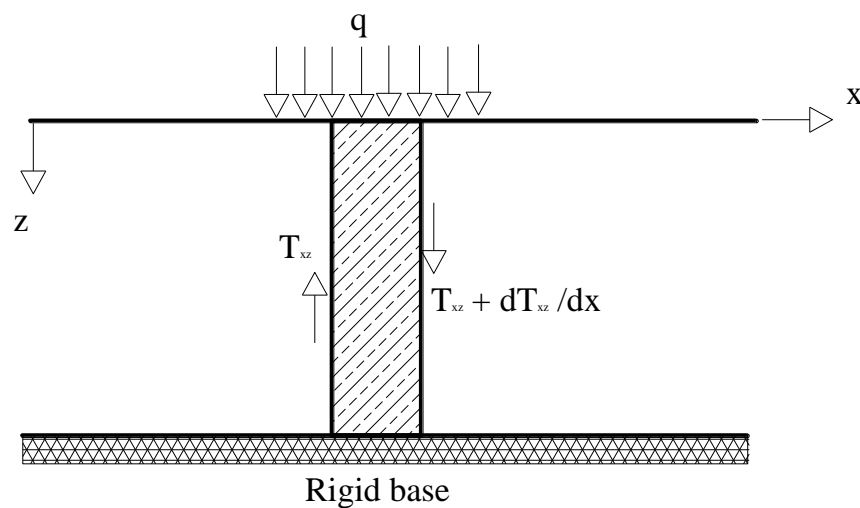


Figure 2.4: Vlazov's Model

2.4.6 Reissner Model

In a similar approach to Vlazov's model Reissner derived a model by introducing displacement and stress constraints that simplify the basic equations for a linear elastic isotropic continuum. By assuming that the in-plane stresses throughout the soil layer of thickness H are negligibly small and the displacement components u , v , w in the rectangular Cartesian coordinate directions x , y , z respectively satisfy the conditions

$$u = v = w = 0 \text{ on } z = H, u = v = 0 \text{ on } z = 0$$

The response function of the soil is given by

$$c_1 w - c_2 \nabla^2 w = q - \frac{c_2}{4c_1} \nabla^2 q \quad (2.5)$$

Where w is the vertical displacement and q is the external load. The constants c_1 and c_2 characterizing the soil response are related to E and μ . The Reissner model is given in Fig. 2.5.

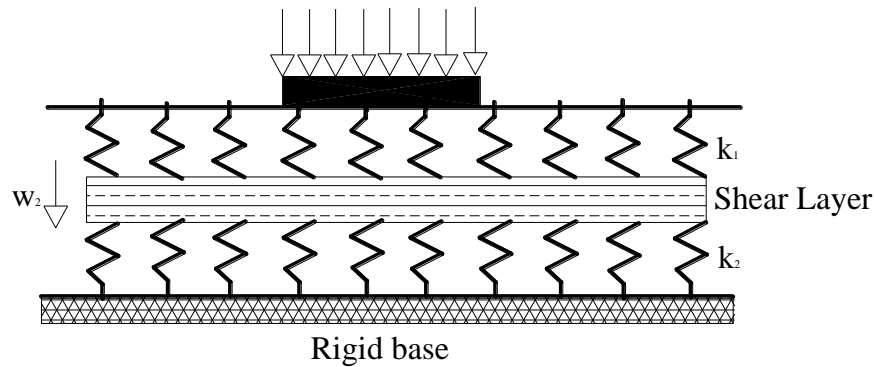


Figure 2.5: Reissner Model

Though there are other different numbers of models available in literature, the major soil response models are discussed here.

2.5 Analytical or Numerical Modelling of Geocell Reinforcement

Membrane effect of a reinforcement layer on the load settlement response of a reinforced granular fill soft soil foundation system was modelled with the help of a simple mathematical formulation by Ghosh and Madhav [1994]. A three parameter model that incorporates the load settlement and the shear stress -shear strain response respectively of the soft soil and the granular soil was proposed and the complete load settlement response of the strip footing obtained brings out the various parameters of the system. The improvement in the behavior of the composite system was studied.

Shukla and Chandra [1994] proposed a mechanical model for idealizing the settlement response of a geosynthetic reinforced compressible granular fill soft soil system by representing each subsystem by commonly used mechanical elements such as stretched, rough elastic membrane, Pasternak shear layer, Winkler springs and dashpot. The settlement profiles obtained from this work are in good agreement with the earlier reported works.

With the aid of foundation models viz. Pasternak various researchers have worked to develop an understanding of geosynthetic reinforced foundations. Madhav et al. (1989 a) embarked the work on geosynthetic reinforced foundations. He proposed a new model

which is an improvement of the Pasternak model by incorporating a rough membrane to simulate the behavior of geosynthetic. Further the same authors (1989 b) improved the earlier defined model to incorporate the confinement effect that take cares of the variation in modulus of deformation throughout the width of the geosynthetic.

Maheswari et al. [2004] studied the response of an infinite beam resting on reinforced granular bed overlying a soft soil strata subjected to a moving load with constant velocity is presented. The upper reinforced granular bed is modelled by a rough membrane embedded in Pasternak's shear layer overlying a series of compressible Winkler springs representing the underlying soft soil. the proposed model was successful in analyzing the response of moving loads on infinite beams resting on extensible geosynthetic reinforced granular fill soft soil system.

Deb et al. [2005] studied the development of a mechanical model to predict the behaviour of a multilayer geosynthetic reinforced granular fill soft soil system. The granular fill and the soft soil have been idealized as Pasternak shear layer and a layer of non-linear springs respectively. Stretched rough elastic membrane represent the geosynthetic reinforced layers. Parametric studies were conducted for a uniformly loaded strip footing and from the studies it was observed that significant reduction of settlement has been observed as a result of the use of multi-layer geosynthetic reinforcement system.

Deb et al. [2006] proposed a model for the analysis of granular foundation beds reinforced with several geosynthetic layers. The study is similar to the previous study except that the reinforcement is extensible which simulates the actual behaviour of geosynthetic reinforced beds. The reduction in settlement was found to less in comparison to the same for inextensible reinforcements.

Deb et al. [2007] developed a mechanical model to predict the behaviour of a geosynthetic-reinforced granular fill over soft soil improved with stone columns. The saturated soft soil was idealized by Kelvin-Voight model to represent its consolidation behaviour. The stone columns are idealized by stiffer springs. Pasternak shear layer and rough elastic membrane represents granular fill and geosynthetic reinforcement layer respectively. It was observed from the study that the inclusion of geosynthetic layer reduces the total as well as the differential settlement and the reduction is more for higher load intensity and higher modular ratio.

Madhavi Latha et al. [2009] reported the results of finite element simulations of the behaviour of strip footing resting on sand beds, with different densities of the soil reinforced with geocells of different dimensions. The strength and stiffness of sand confined with geocells is represented by an equivalent composite model developed from triaxial compression tests. The numerical model is able to predict the pressure settlement response of the model footings fairly well for various cases of cell dimensions, geocell width, placement of geocell mattress etc.

Sireesh et al [2009] numerically simulated geocell reinforced sand and soft clay beds using the finite difference package FLAC-3D. Simulations were carried out on both geocell reinforced sand beds and the conventional type planar geogrid reinforcement. The pressure settlement response of corresponding to geocell reinforced was found to be much stiffer in comparison in comparison with the unreinforced case indicating substantial reduction in settlement.

Avesani Neto et al [2013] proposed a method for the calculation of bearing capacity for soil reinforced with a geocell by taking into account the soil foundation bearing capacity and the geocell reinforcement mechanisms – the stress dispersion and the confinement effect. It was drawn from the analysis that the proposed method has a better approach than the other conventional methods for both sandy and clayey soil.

2.6 Summary

The review on existing literature brings to light the following:

There has been wide spread research on geosynthetics in various parts of the world since its commencement as a ground improvement technique. There has been boundless experimental investigations on geosynthetic reinforced beds viz. geogrids, geotextiles etc. Recently, geocell reinforcement is catching up as a promising solution and comprehensive experimental research has been conducted on the same.

The numerical or analytical researches conducted to study the behaviour of geosynthetic foundations are moderate and it is well understood from literature that studies on geocell reinforced foundations are very minimal. Another observations that was observed from the review is that very little attention has been paid on circular footing. Most of the research were carried out on strip footings.

From this detailed literature search, there is an understanding to conduct analytical and numerical studies on geocell reinforced soils. The responses of both strip and circular footing on geocell reinforced beds are necessary.. The approaches adopted to study the behaviour of foundations have been discussed in detail in the following chapters.

Chapter 3

Prediction of Limit Bearing Capacity of Footings on Geocell Reinforced Foundations

3.1 Statement of the Problem

The schematic of the geocell reinforced granular layer over a weak foundation soil underlying footing is shown in Figure 3.1. The ultimate bearing capacities of circular and strip footings were determined based on Terzaghi's general shear failure mechanism. On the basis of the dimensions of the geocell, different types of pressure distributions were considered (refer Fig. 3.2).

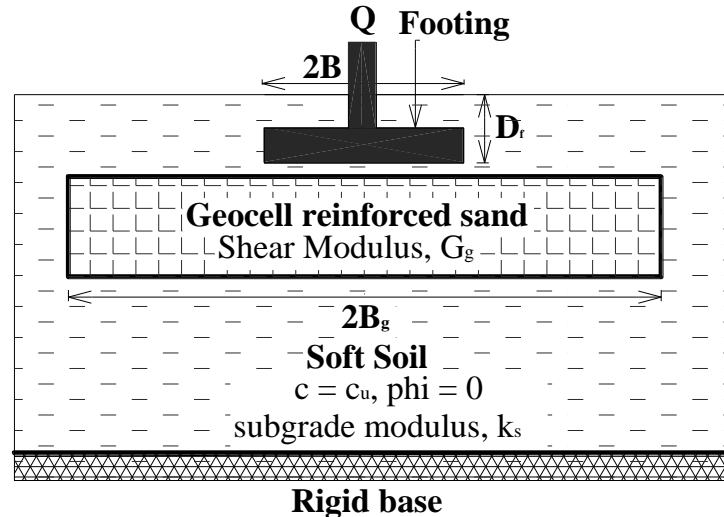


Figure 3.1: Definition sketch of footing on geocell reinforced soil.

In case of a short geocell, approximately the same width as that of the footing, it is assumed that the contact pressure distribution is uniform. For geocells of intermediate width, it is assumed that the contact stress decreases linearly from q_{uc} (ultimate bearing capacity) at the edge of the footing to zero at the edge of the geocell. For a very wide geocell, it is expected

that the contact stress decreases exponentially from q_{uc} at the edge of the footing and it tends to zero at the edge of the geocell. Using the concept of contact pressure variation, the improvement in bearing capacity of both strip and circular footing was studied. The present study is a primitive way of understanding the improvement rendered by the geocell reinforcement irrespective of the condition of the subsoil or the depth of embedment of the footing.

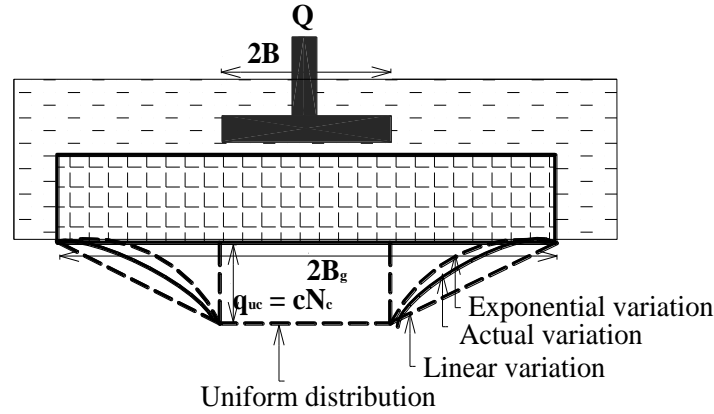


Figure 3.2: Assumed contact pressure distribution.

3.2 Analytical Approach

3.2.1 Strip footing

Let the width of the strip footing be $2B$ and width of the geocell layer, $2B_g$. The geocell layer width ratio, R_g is defined as the ratio of width of the geocell to the width of the footing i.e. $R_g = B_g/B$.

The ultimate bearing capacity of a strip footing as per Terzaghi's (1943) approach is

$$q_u = cN_c + qN_q + \frac{1}{2}\gamma BN_\gamma \quad (3.1)$$

3.2.1.1 Short Geocell

For a short geocell uniform distribution of contact pressure is assumed. The forces acting on the geocell layer are,

The ultimate bearing load of the unreinforced ground,

$$Q_{uc} = 2B_g q_{uc} \quad (3.2)$$

The bearing load of the geocell reinforced ground,

$$Q_{gc} = 2B q_{gc} \quad (3.3)$$

Now, the bearing capacity ratio (BCR) is defined as the ratio of bearing load of the geocell reinforced ground to the ultimate bearing load of the unreinforced ground.

$$BCR = \frac{Q_{gc}}{Q_{uc}} = \frac{B_g}{B} = R_g \quad (3.4)$$

Equation 3.4 represents that the BCR is equal to R_g for a strip footing.

3.2.1.2 Intermediate Width Geocell

The contact stress remains the same beneath the footing but decreases linearly from the edge of the footing to the edge of the geocell. The governing equation of the pressure distribution curve is as follows:

$$q(x) = q_u \left(1 - \frac{x-B}{B_g - B} \right) \quad (3.5)$$

where $q(x)$ is the contact pressure at a distance x from the center of the footing.

Applying the boundary condition in Eq.3.5

$$@x=B; q(x) = q_u$$

$$@x=B_g; q(x) = 0$$

The bearing load of the geocell reinforced ground is,

$$Q_{gc} = 2Bq_u \left(1 + \frac{1}{2}(R_g - 1) \right) \quad (3.6)$$

$$BCR = \frac{Q_{gc}}{Q_{uc}} = 1 + \frac{1}{2}(R_g - 1) \quad (3.7)$$

Equation 3.7 represents that the BCR is a function of R_g a strip footing.

3.2.1.3 Wide Geocell

For a wider geocell case, the contact stress assumed to decrease from q_{uc} at the edge of the footing and tends to zero at the edge of the geocell. The governing equation of the pressure distribution curve is as follows:

$$q(x) = q_u e^{-\beta \left(\frac{x-B}{B_g - B} \right)} \quad (3.8)$$

Where β is the decay parameter that defines the rate of decay of contact pressure from the edge of the geocell to the edge of the footing.

Applying the boundary conditions in Eq. 3.8,

$$@x=B; q(x) = q_u$$

$$@x=B_g; q(x) = q_u e^{-\beta}$$

The bearing load of the geocell reinforced ground is,

$$Q_{gc} = 2Bq_{uc} + 2q_{uc} \int_B^{B_g} e^{-\beta \frac{x-B}{B_g-B}} dx \quad (3.9)$$

Changing the variables of integration to non-dimensional form we obtain,

$$Q_{gc} = 2Bq_{uc} \left(1 + \frac{1}{\beta'} \left[1 - e^{-\beta'(R_g-1)} \right] \right) \text{ where, } X = \frac{x}{B}, \beta' = \frac{\beta}{B_g - B}, dX = \frac{dx}{B} \quad (3.10)$$

$$BCR = \frac{Q_{gc}}{Q_{uc}} = 1 + \frac{1}{\beta'} \left[1 - e^{-\beta'(R_g-1)} \right] \quad (3.11)$$

Equation 3.11 represents that the BCR is a function of R_g and the decay parameter, β for a strip footing.

3.2.2 Circular Footing

Let the diameter of the circular footing be $2B$ and the diameter of the geocell layer be $2B_g$. The ultimate bearing capacity of a circular footing as per Terzaghi's (1943) theory is,

$$q_{uc} = 1.3cN_c + qN_q + 0.3\gamma BN_\gamma \quad (3.12)$$

3.2.2.1 Short Geocell

The ultimate bearing load of the unreinforced ground,

$$Q_{uc} = \pi B^2 q_{uc} \quad (3.13)$$

The bearing load of the geocell reinforced ground,

$$Q_{gc} = \pi B_g^2 q_{uc} \quad (3.14)$$

The bearing capacity ratio, BCR

$$BCR = \frac{Q_{gc}}{Q_{uc}} = \frac{B_g^2}{B^2} = R_g^2 \quad (3.15)$$

Equation 3.14 represents that the BCR is equal to R_g^2 for a circular footing.

3.2.2.2 Intermediate width geocell

The contact stress decreases linearly from q_{uc} at the edge of the footing to 0 at the edge of the geocell. The governing equation of the pressure distribution curve is

$$q(r) = q_{uc} \left(1 - \frac{r-B}{B_g-B} \right) \quad (3.16)$$

Where, $q(r)$ is the contact pressure at a radial distance r from the center of the footing.

The bearing load of the geocell reinforced ground is,

$$Q_{gc} = \pi B^2 q_{uc} + \int_0^{2\pi} \int_B^{B_g} q(r) r dr d\theta \quad (3.17)$$

On simplification we obtain,

$$Q_{gc} = \pi B^2 q_{uc} + 2\pi B^2 q_{uc} \frac{R_g^2 + R_g - 2}{6} \quad (3.18)$$

$$BCR = \frac{Q_{gc}}{Q_{uc}} = 1 + \frac{1}{3}(R_g^2 + R_g - 2) \quad (3.19)$$

3.2.2.3 Wide Geocell

The contact stress decreases exponentially from q_{uc} at the edge of the footing to a very small value at the edge of the geocell.

The governing equation of the load distribution curve is

$$q(r) = q_{uc} e^{-\beta \left(\frac{x-B}{R_g-B} \right)} \quad (3.20)$$

The bearing load of the geocell reinforced ground is

$$Q_{gc} = \pi B^2 q_{uc} + \int_0^{2\pi} \int_B^{R_g} q(r) r dr d\theta \quad (3.21)$$

On simplification we obtain,

$$Q_{gc} = \pi B^2 q_{uc} + 2\pi B^2 q_{uc} \left[e^{\beta'} \left(\frac{R_g e^{-\beta' R_g}}{-\beta'} + \frac{e^{-\beta'}}{\beta'} \right) + \frac{e^{\beta'}}{\beta'} \left(\frac{e^{-\beta' R_g}}{-\beta'} + \frac{e^{-\beta'}}{\beta'} \right) \right] \quad (3.22)$$

Where
$$\beta' = \frac{\beta}{B_g - B}$$

$$BCR = \frac{Q_{gc}}{Q_{uc}} = 1 - \frac{2e^{\beta'} e^{-\beta' R_g}}{\beta'} \left(R_g + \frac{1}{\beta'} \right) + 2 \left(\frac{1}{\beta'} + \frac{1}{\beta'^2} \right) \quad (3.23)$$

Equation 3.22 represents that the BCR is a function of R_g and β for a circular footing.

3.3 Results and Discussions

The analytical approach of determining the contact pressure variation based on assumed simple variation has been studied. The presented results show comparison of circular and strip footing on geocell reinforced soils. Figure 3.3 illustrates the variation of the contact pressure assumed (linear and exponential variation) for intermediate width and wide geocells from the edge of the footing to the edge of the geocell. Similar pattern of pressure distribution is expected on both sides of the strip footing and throughout the perimeter in case of circular footing. In exponential variation of contact pressure, with the variation of decay parameter, β the pressure distribution pattern changes remarkably and hence the area covered under the

curve varies which leads to variation in BCR. The contact pressure becomes asymptotic to the X-axis at the edge of the geocell but doesn't become exactly zero for exponential variation of contact pressure. Appropriate pressure distribution diagram has to be assumed depending on the width of the geocell. A befitting value of decay parameter, β has to be chosen for wide geocells to predict its approximate behavior. For short geocells, the pressure distribution remains constant i.e. the pressure distributed beneath the footing and geocell layer remains the same. Hence, when uniform or linear distribution of pressure is assumed for wide geocells it predicts higher than the actual variation and exponential variation used for short and intermediate width geocells predicts lesser than the exact value.

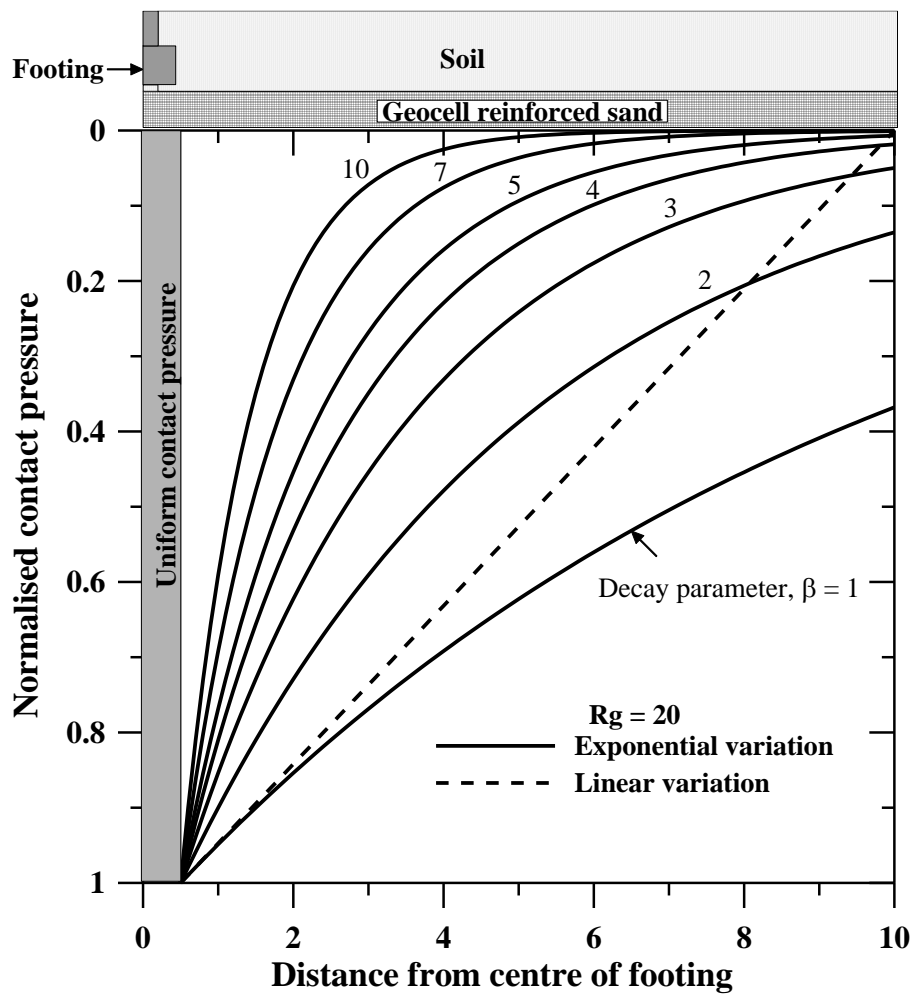


Figure 3.3: Variation of normalised contact pressure with distance from the centre of the footing (Strip and Circular)

The bearing capacity ratio, BCR were plotted against geocell layer width ratio, R_g for different widths of the geocell as shown in Figures 3.4 and 3.5. The variation in improvement of strip and circular footing could be clearly identified, there is a ten fold increase in the bearing capacity improvement factor for circular footing compared to that of strip footing for the same geocell layer width ratio. Short geocell represents the upper bound criterion and wide geocells represents the lower bound criterion in estimating BCR. While intergrating the pressure distribution of the footing, the area covered by short geocell is the highest, intermediate value for intermediate width geocell and lowest value for wide geocells. Hence, for low values of R_g uniform pressure distribution is assumed, for intermediate width geocells linear variation and wide geocells exponential variation is assumed.

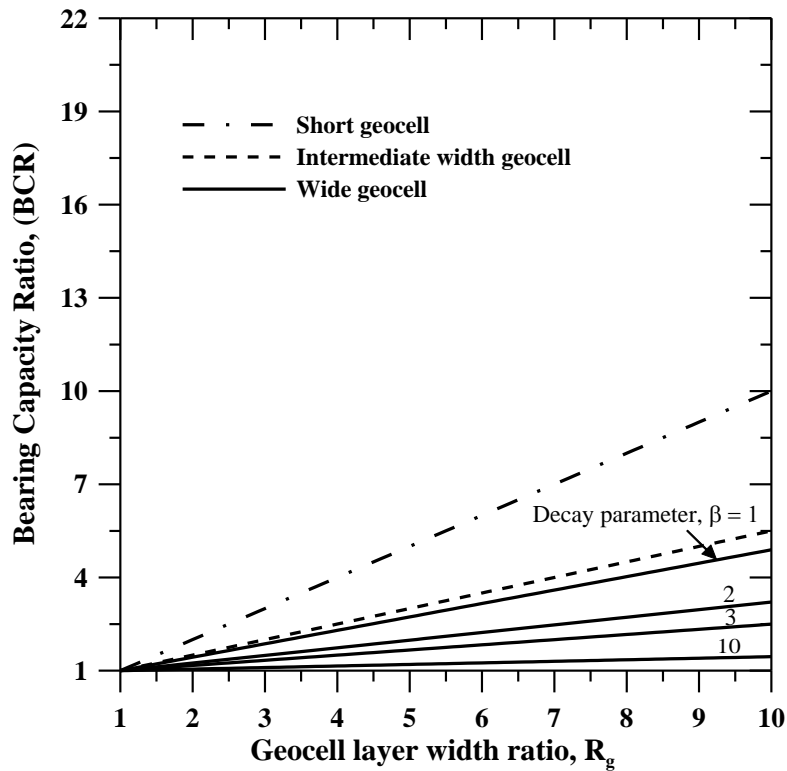


Figure 3.4: Variation of BCR with R_g for a strip footing

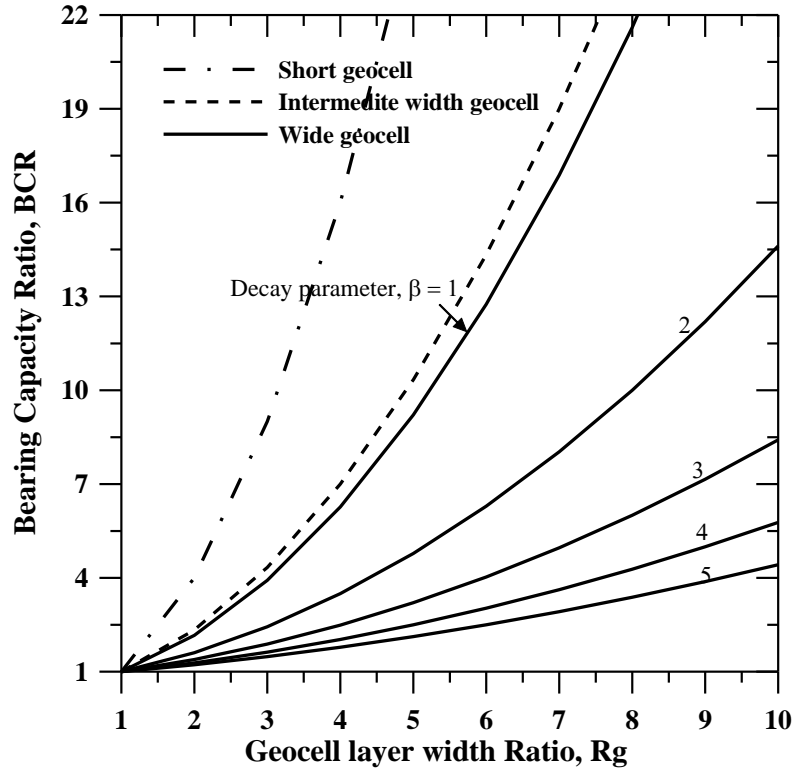


Figure 3.5: Variation of BCR with R_g for a circular footing

The results of the present analytical model were compared with two independent experiments conducted by Dash et al (2001 & 2003) as depicted in Figures 3.6 and 3.7. The results were found to be in range as per the formulation for short, intermediate width and wide geocells. Reasonable agreement between analytical and experimental result were found in case of lower settlements of strip footing and the results were found to be in range for high settlements of the order of 30% of circular footing settlement. The improvement in ground is not significant for geocell layer width ratio, R_g greater than 5. Increasing the geocell layer width doesn't bring in further improvement of the ground but helps in reducing differential settlement and is widely used in pavements. The ability to choose appropriate pressure distribution and decay parameter are the key parameters for determining the bearing capacity improvement character of the geocell reinforced ground.

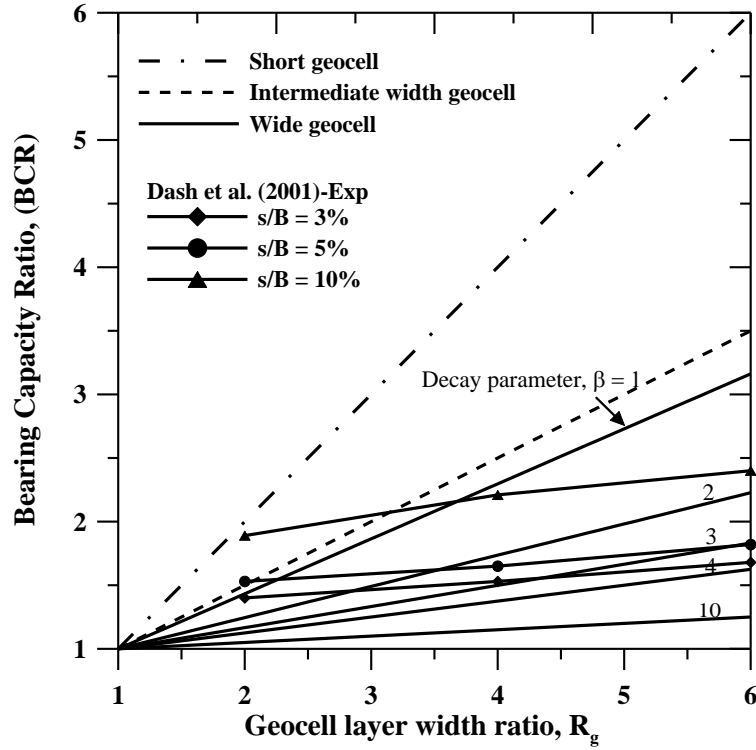
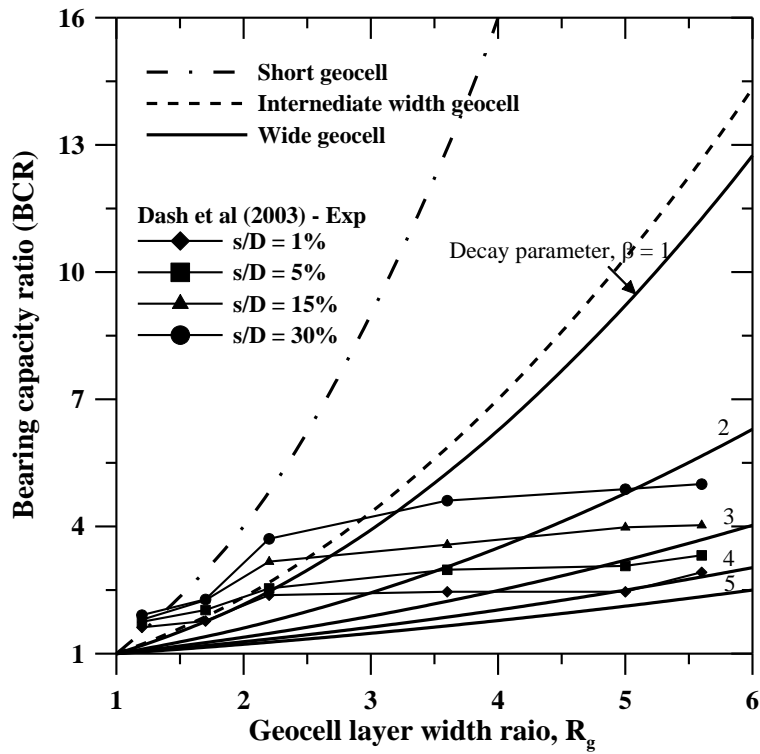


Figure 3.6: Variation bearing capacity ratio, BCR with geocell layer width ratio, R_g for a strip footing – Comparison of analytical and experimental results



3.7: Variation bearing capacity ratio, BCR with geocell layer width ratio, R_g for a circular footing – Comparison of analytical and experimental results

3.4 Summary

The methods discussed have proved successful in indicating the potential improvement in bearing capacity the geocell reinforced sand layer brings to the circular and strip footings. The present approach is demonstrative in understanding the pattern of bearing capacity improvement but for exact predictions of the same, numerical investigations using foundation models or experimental studies have to be conducted. The following conclusions were inferred from the study

- The improvement in bearing capacity of circular footing was found to be much higher than the strip footing improvement. In short circular footings performed better than the strip footing.
- The variations in contact pressure that were assumed were found to hold good i.e. uniform pressure distribution (short geocell), linear distribution (intermediate width geocell) and exponential variation (wide geocell). Decay parameter, β has to be chosen appropriately for wide width geocell.
- Increasing geocell layer width ratio, R_g beyond 5 only provides marginal increase in the improvement of the soft ground. Providing very large geocell layer width has wide applications in pavements and improvement of soft grounds where differential settlements are anticipated.
- Appropriate contact pressure has to be chosen for accurate prediction of BCR.

In summary, the present approach provides a simplistic way of predicting the improvement in bearing capacity the geocell reinforced sand layer brings in to circular and strip footings. However, for accurate prediction of bearing capacities, present model needs to be improved by incorporating the confining effect provided by the geocell to the infill material as well as the accurate contact pressure distribution and deflection profiles of the geocell mattress upon loading. Following chapters discuss the improvements to the model.

Chapter 4

Elasto-Plastic Behaviour of Rigid Strip Footing on Geocell Reinforced Soils

4.1 Statement of the problem

The schematic of the geocell reinforced granular layer over soft soil under rigid strip footing is shown in Figure 4.1. The system is idealized by considering two parameter elastic Pasternak model as shown in Figure 4.2a.

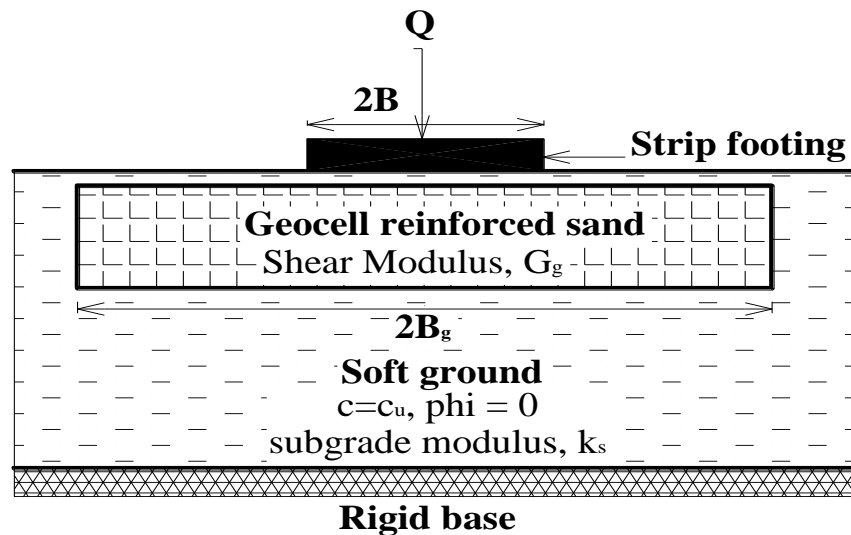


Figure 4.1: Definition sketch of strip footing on geocell reinforced foundation bed

The geocell reinforced granular fill and the soft foundation soil are idealized using Pasternak shear layer and a series of Winkler springs respectively. The settlement profile of the geocell reinforced foundation on soft soil is assumed as shown in Figure 4.2b. It is assumed that for a given unit displacement (w_0) on the rigid strip footing, the shear layer deflects to the same

displacement over the width of the footing (B). The deflection profile under the loading area (strip footing) is considered as uniform and the deflection from the edge of the footing to the edge of the shear layer of width (B_g) has been represented by second order differential equation that tends to a constant value at the end of the shear layer. The relative stiffness of the geocell reinforced shear layer and foundation soil are the key parameters to understand the behavior of geocell reinforced granular beds over soft soils. These parameters have been considered in the analysis to obtain design charts. The following sections briefly describe the theoretical linear and nonlinear formulation of the geocell reinforced granular layer supported rigid strip footing on soft soil.

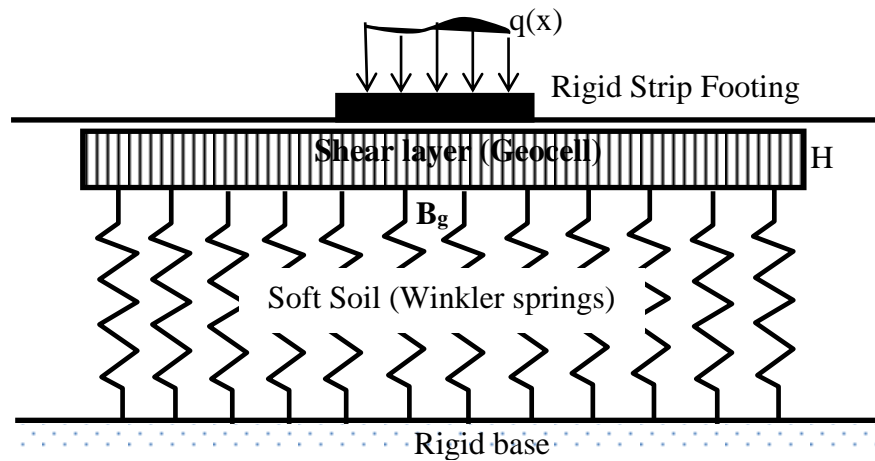


Fig. 4.2a Idealized Pasternak shear layer over Winkler springs

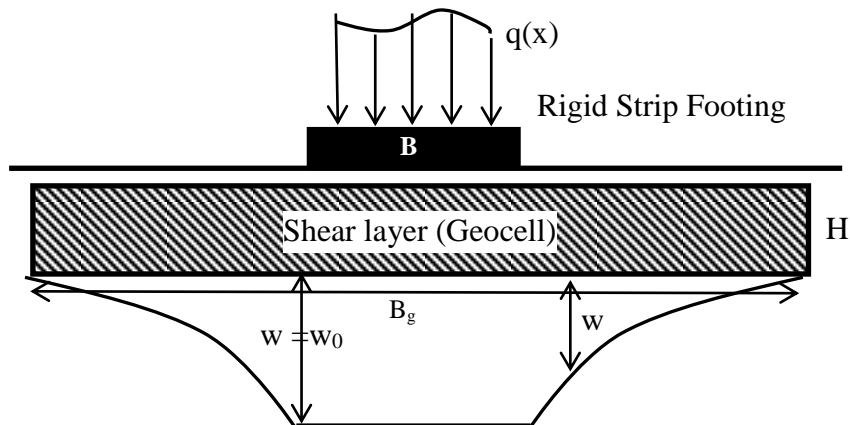


Fig. 4.2b Deflection profile of Pasternak shear layer over Winkler springs

Figure 4.2: Problem definition and deflected profile of the foundation system

4.2 Theoretical formulation

The load settlement behavior of a rigid footing resting on an elastic half space can easily be modeled using the concept of Winkler springs, which simulates the stiffness of the foundation soil. Pasternak [1954] improved the Winkler model by introducing a shear layer in between the rigid footing and the foundation soil. The shear layer is introduced to take the shear resistance of the soil into account in supporting the footing load, similar to a geocell mattress in the case of reinforced soil beds. This model is an advancement of Filonenko-Boridich model where the Winkler springs were considered to be connected through an elastic thin membrane under a constant tension.

In the present model, a linear load settlement relationship is considered for lesser footing settlements ($w_0 < 1$ percent of the footing width, B). For higher footing settlements, as expected, nonlinear relation between load-settlement must be assumed.

4.2.1 Linear Formulation

The governing equation for the load-deflection pattern of the problem considering the shear layer representing the geocell mattress, as described in Pasternak model, is presented below:

$$q(x) = k_s \cdot w_o \quad \text{For} \quad 0 \leq |x| \leq \frac{B}{2} \quad (4.1)$$

$$k_s \cdot w - G_s \cdot H \cdot \frac{d^2 w}{dx^2} = 0 \quad \text{For} \quad \frac{B}{2} \leq |x| \leq \frac{B_s}{2} \quad (4.2)$$

To represent the terms in non-dimensional form, let $X = \frac{x}{B}$, $W = \frac{w}{B}$

Simplifying Equation 4.2 the governing equation reduces to

$$\frac{d^2 W}{dX^2} - \alpha^2 W = 0 \quad \text{Where} \quad \alpha^2 = \left(\frac{k_s \cdot B^2}{G_s \cdot H} \right) \quad (4.3)$$

The solution of this second order differential equation is

$$W = C_1 e^{\alpha X} + C_2 e^{-\alpha X} \quad (4.4)$$

Applying the known boundary condition

$$\text{@ } X = 0.5 \rightarrow W = W_0$$

$$\text{@ } X = \frac{R_s}{2} \rightarrow \frac{dW}{dX} = 0$$

The solution yields the constants

$$C_1 = \left[\frac{W_0 e^{-R_g \alpha}}{e^{(0.5-R_g)\alpha} + e^{-0.5\alpha}} \right]$$

$$C_2 = \left[\frac{W_0}{e^{(0.5-R_g)\alpha} + e^{-0.5\alpha}} \right]$$

Now the load deflection equation of this formulation is

$$q(x).B = Q = k_s B w_0 + 2 \int_{B/2}^{B_g/2} k_s w dx \quad (4.5)$$

Dividing Equation 4.5 with $(k_s B^2)$ yields

$$Q^* = W_0 + 2 \int_{0.5}^{R_g/2} W dX \quad (4.6)$$

$$Q^* = W_0 + \frac{2}{\alpha} \left[C_1 \left(e^{(0.5R_g\alpha)} - e^{0.5\alpha} \right) - C_2 \left(e^{(-0.5R_g\alpha)} - e^{-0.5\alpha} \right) \right] \quad (4.7)$$

Equation (4.7) is the final form of the normalized load (Q^*) on the footing as a function of normalized footing settlement (W_0), inverse of normalized shear stiffness (α) and shear layer width ratio (R_g). Table 4.1 shows the typical range of values of these model parameters used in the current analysis and the results are presented in Figures 4.3-4.6.

Figure 4.3 shows the variation of Q^* with R_g for W_0 of 1% and 2%. The inverse of the normalized shear stiffness, (α) was varied within the practical range to understand the influence of improved geocell reinforced ground on the load bearing capacity of the soil. As expected, it could be found from the analysis that for lower values of α (when shear stiffness of the geocell reinforced ground is high) the load is high for similar subsoil conditions. For higher values of α , Q^* attains a constant value after R_g is about 3 i.e. for a bed with low shear stiffness, increasing the width of shear layer doesn't further improve the characteristics of the reinforced bed.

Figure 4.4 shows the settlement profile for varying α and shear layer width ratio, R_g . It could be observed that for lower values of α there is a significant difference in the settlement pattern with increase in R_g . This could be due to the high pressure on the footing in the case of smaller size of shear layer which has shown large settlements than the wider shear layer.

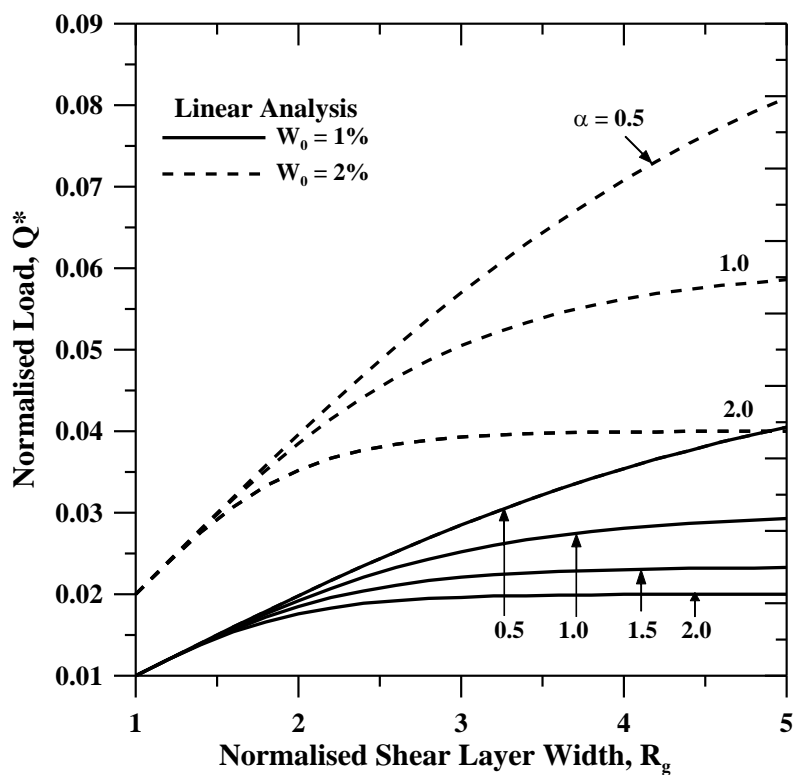


Figure 4.3: Variation of normalized load (Q^*) with shear layer width ratio (R_g) for different values of α

Table 4.1 Typical values of model parameters used in this study

Parameter	Unit	Range
W_0	%	1 to 5
R_g	dimensionless	1 to 5 and 10
μ	dimensionless	0 to 100
α	dimensionless	0.5 to 2
k_s (Bowels, 1997)	kN/m ³	5,000 to 80,000
G_g (Sireesh, 2006)	MPa	10 to 18

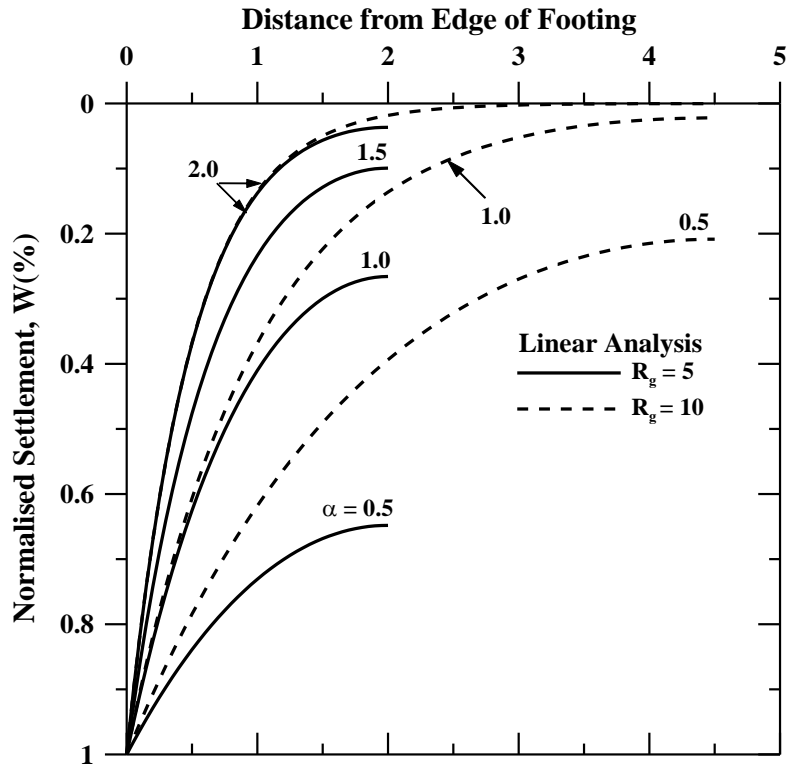


Figure 4.4: Settlement profile from the edge of the footing for different values of α

Figure 4.5 shows the linear load-settlement profile of the reinforced bed up to a W_0 of 1%. It can be noticed that for a reinforced bed with lower shear stiffness ($\alpha > 1$), the improvement in load bearing capacity of soil is insignificant with increase in R_g . However, a significant improvement is observed for reinforced bed with higher shear stiffness. The variation of α with Q^* has been plotted in semi-log scale as shown in Figure 4.6. In this case, the value of α was varied from 0.1 to 5.0 to verify its influence on the untreated ground. For higher values of R_g , Q^* is high for low values of α and attains a constant value with increase in α (for $\alpha > 1$). For a shear layer width ratio (R_g) of 1, it could be observed that load bearing capacity of the soil is independent of α , which is considered as unreinforced bed condition. This graph may be used as a design chart to obtain the value of α for a given R_g and Q^* .

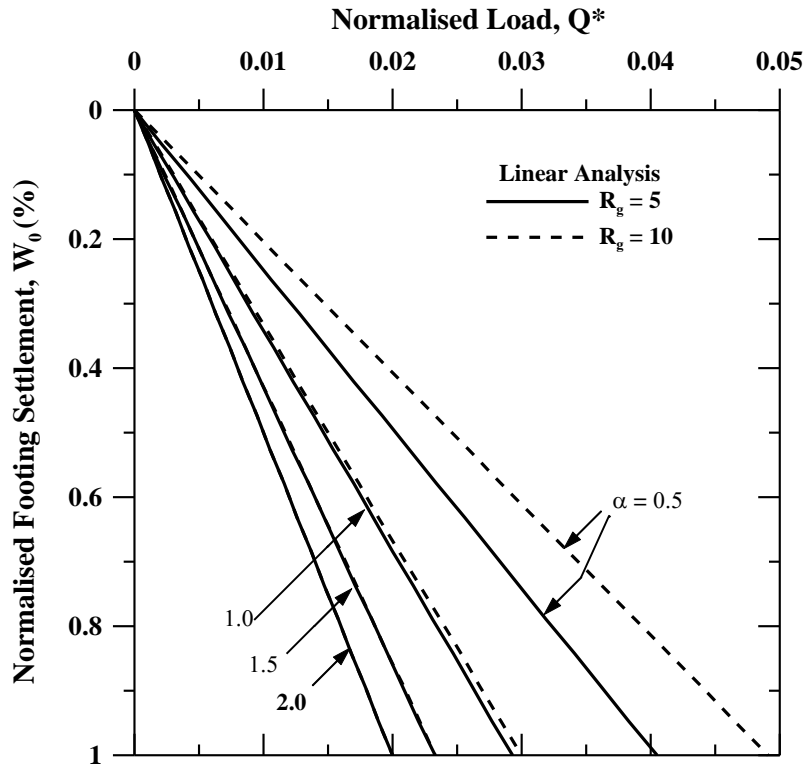


Figure 4.5: Variation of normalized load (Q^*) with normalized footing settlement (W_0) for different values of α

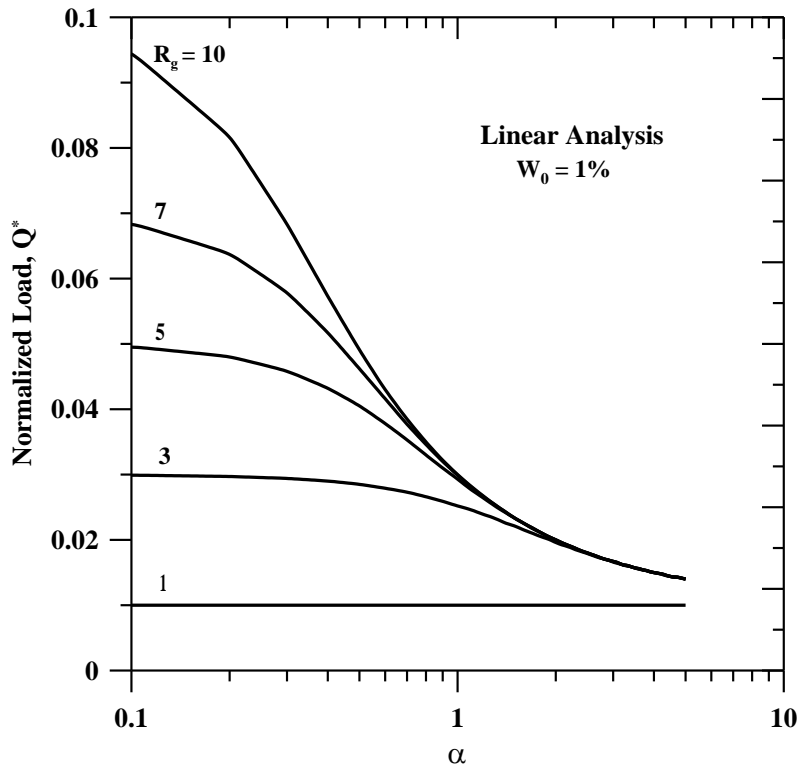


Figure 4.6: Variation of normalized load (Q^*) with α for different shear layer width ratios (R_g)

4.2.2 Non-linear Formulation

The nonlinear stress-displacement response of the soil can be represented by hyperbolic relation presented by Kondner [1963] as follows:

$$q(x) = \frac{k_s \cdot w_0}{1 + \frac{k_s}{q_u} \cdot w_0} \quad \text{For} \quad 0 \leq x \leq \frac{B}{2} \quad (4.8)$$

$$\frac{k_s \cdot w}{1 + \frac{k_s}{q_u} \cdot w} - G_g H \frac{d^2 w}{dx^2} = 0 \quad \text{For} \quad \frac{B}{2} \leq x \leq \frac{B_g}{2} \quad (4.9)$$

To represent the terms in non-dimensional form, let $X = \frac{x}{B}$, $W = \frac{w}{B}$

Simplifying Equation 4.9 the governing equation reduces to

$$\frac{d^2 W}{dX^2} - \alpha^2 \frac{W}{1 + \mu W} = 0 \quad \text{Where} \quad \alpha^2 = \left(\frac{k_s \cdot B^2}{G_g H} \right) \quad \text{and} \quad \mu = \frac{k_s \cdot B}{q_u} \quad (4.10)$$

Rearranging Equation 4.10 we obtain

$$\frac{W}{1 + \mu W} = \frac{1}{\alpha^2} \left(\frac{d^2 W}{dX^2} \right) \quad (4.11)$$

Now the load deflection equation of the formulation is

$$q_f(x) \cdot B = Q_f = \frac{k_s B w_0}{1 + \frac{k_s w_0}{q_u}} + 2 \int_{B/2}^{B_g/2} \frac{k_s w}{1 + \frac{k_s w}{q_u}} dx \quad (4.12)$$

$$Q_f = \frac{k_s B^2 W_0}{1 + \mu W_0} + 2 \int_{B/2}^{B_g/2} \frac{k_s B W}{1 + \mu W} dx \quad (4.13)$$

$$Q_f = \frac{k_s B^2 W_0}{1 + \mu W_0} + 2 \int_{0.5}^{R_g/2} \frac{k_s B^2 W}{1 + \mu W} dX \quad (4.14)$$

$$\frac{Q_f}{k_s B^2} = Q^* = \frac{W_0}{1 + \mu W_0} + 2 \int_{0.5}^{R_g/2} \frac{W}{1 + \mu W} dX \quad (4.15)$$

Using Equation 4.11, Equation 4.15 has been modified

$$Q^* = \frac{W_0}{1 + \mu W_0} + \frac{2}{\alpha^2} \int_{0.5}^{R_g/2} \left(\frac{d^2 W}{dX^2} \right) dX \quad (4.16)$$

Since the slope of the curve at $R_g/2$ is zero, Equation 4.16 can be rewritten as

$$Q^* = \frac{W_0}{1 + \mu W_0} - \frac{2}{\alpha^2} \left[\frac{dW}{dX} \right]_{0.5} \quad (4.17)$$

The nonlinear ordinary differential equation (Equation 4.16) is solved using finite difference scheme.

4.2.3 Finite Difference Formulation

The finite difference method has been employed to solve the nonlinear ordinary differential equation. In these equations, the derivatives have been discretized using central difference scheme [Crank-Nicolson method, 1947]. The length L/B has been divided into '(n-1)' number of elements with 'n' number of node points; thus the mesh size (dX) can be written as $dX=L/B/(n-1)$ (refer Figure 4.7). Writing equations in finite difference form for any interior node (i), leads to the following equation:

$$\frac{w(i+1) - 2w(i) + w(i-1))}{dx^2} - \alpha^2 \frac{w(i)}{1 + \mu w(i)} = 0 \quad (4.18)$$

Since the discretized ordinary differential equation is in non-linear form direct approaches for solving linear algebraic equations viz. tri-diagonal matrix method, Gauss elimination, Gauss-Siedel method etc. cannot be directly used to solve this finite difference formulation. The above nonlinear equation was linearized to the following form:

$$\frac{w(i+1) - 2w(i) + w(i-1))}{dx^2} - g(i)w(i) = 0 \quad (4.19)$$

Where, $g(i) = \frac{\alpha^2}{1 + \mu w(i)}$

An initial guess for $g(i)$ was adopted and using the iterative Gauss-Siedel procedure the equations were solved.

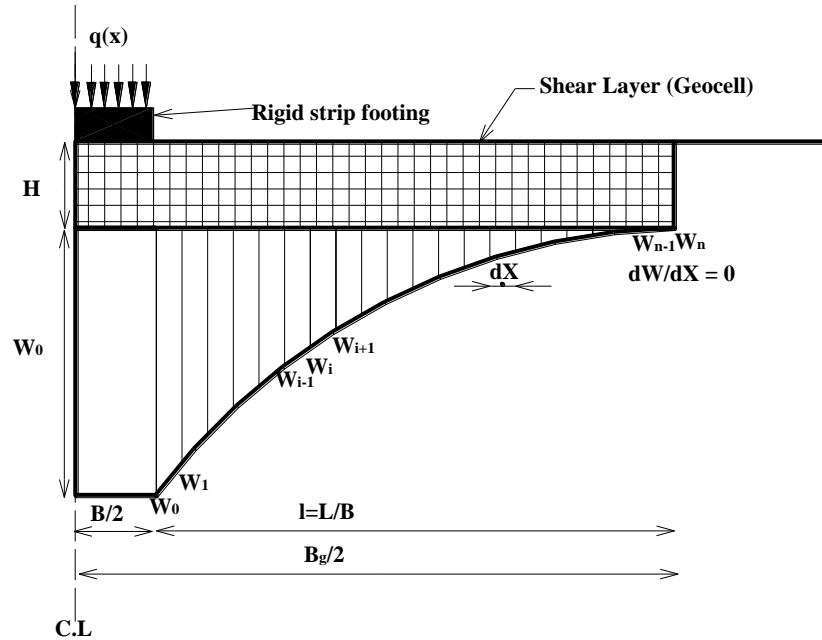


Figure 4.7: Definition sketch of finite difference discretization of the foundation model

4.2.4 Boundary Conditions

The settlement of the rigid strip footing is considered as uniform under the loading area. Hence at the edge of the footing ($X=0.5$), W is equal to W_0 . The slope (dW/dX) of the settlement profile (as shown in Figure 4.2b) will also be zero at the edge of the shear layer ($X=R_g/2$). By introducing these two boundary conditions in to the boundary value problem, the final equation (Equation 4.17) for Q^* can be solved using the iterative Gauss-Siedel technique (after linearization) as discussed earlier.

4.3 Validation

4.3.1 Theoretical Validation

Equation 4.17 depicts the complete solution for the load-settlement pattern for rigid strip footing resting on geocell reinforced sand overlying soft clay foundation. For $\mu = 0$, Equation 4.17 should give the solution for linear analysis. Figure 4.8 shows the validation of the numerical solution with respect to theoretical and experimental results. Theoretical validation of the numerical solution is shown in Figure 4.8 in terms of the variation of Q^* with W_0 for $R_g=10$ and $\mu=0$. The deviation between the theoretical and numerical solutions is negligible.

The recorded deviations between the two analyses can be attributed to the truncation errors accumulated over elimination of higher order terms in the finite difference scheme.

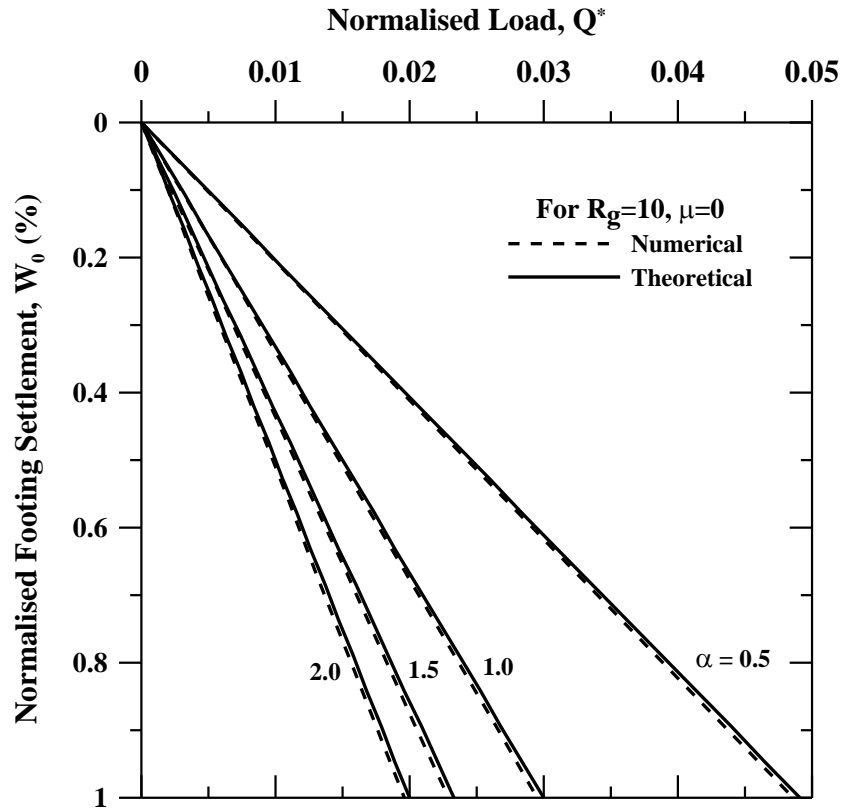


Figure 4.8: Variation of normalized load (Q^*) with normalized footing settlement (W_0)- Comparison of numerical and theoretical results

4.3.2 Experimental Validation

The present model is validated with independent experimental data obtained by Mandal and Gupta [1994] and Dash et al [2001]. Mandal and Gupta [1994] have conducted series of experiments on geocells, made out of polypropylene geotextile, reinforced clay subgrades to verify the bearing capacity improvement of a strip footing. In this study, the geometry of the geocells was varied to obtain a modified bearing capacity factors. From the experimental data, subgrade modulus, k_s was calculated as 3500 kN/m^3 and ultimate bearing capacity, q_u of the marine clay was found to be 25.7 kPa . Similarly, Dash et al [2001] have conducted several experiments on strip footing supported on geocell reinforced sand beds. In this case, geocells were prepared out of planar geogrids. The values of k_s and q_u of the sand beds were

found to be 22,222 kN/m³ and 200kPa respectively. The conditions that were used to perform the experiments viz. soil and geocell properties were accounted in the numerical program by the non-dimensional model parameters, α and μ . These model parameters were defined earlier. The following procedure was adopted for calculating the model parameters, α and μ :

1. The modulus of subgrade reaction (k_s), the width of the footing (B), ultimate bearing capacity of unreinforced ground (q_u) and width of shear layers (B_g) were obtained from the experimental data.
2. The normalized load, Q^* was calculated for lower W_0 (1-3%) using the formula: $Q^* = q/k_s.B$. From the design chart (Figure 6), the model parameter, α was determined for a given R_g (step 1) and Q^* (step 2).
3. The inverse of the normalized ultimate bearing capacity, μ could be directly calculated using the formula, $\mu = k_s.B/q_u$.

Based on the above described procedure, the model parameters, μ and α are back calculated from the experimental data and found to be 9.94 and 1.4 respectively for geocell reinforced sand overlying marine clay beds (Mandal and Gupta, 1994) and 11.11 and 1.6 respectively for geocell reinforced homogeneous sand beds (Dash et al, 2001). Then the numerical analysis was carried with these available input parameters (μ , α and R_g) to obtain the Q^* at different W_0 . Figure 4.9 shows the validation of numerical solution with the independent experimental data. Comparisons are made with respect to the variation of W_0 with the Q^* for different values of α and μ . Over the range of W_0 (0-5%), a very good agreement between the experimental data and numerical data can be seen.

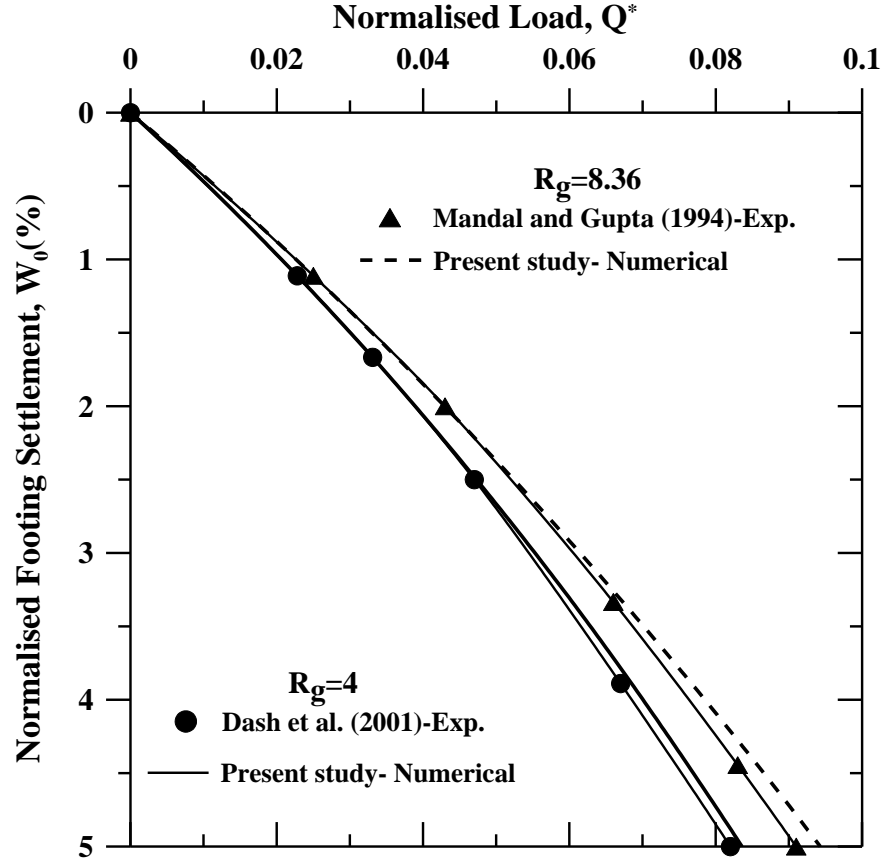


Figure 4.9: Variation of normalized load (Q^*) with normalized footing settlement (W_0)- Comparison of numerical and experimental results

4.3.3 Numerical Validation

An attempt has been made to validate the current model numerically. It can be seen numerically that for a very high settlement, the load-settlement curve converges to a constant Q^* .

At very high settlements, Equation 4.15 gets modified to

$$Q^* = \frac{1}{\mu} + 2 \int_{0.5}^{\frac{R_g}{2}} \frac{1}{\mu} dx = \frac{1}{\mu} + \frac{2}{\mu} \left(\frac{R_g}{2} - 0.5 \right) \quad (4.20)$$

In a trial, substituting the value of $R_g = 11$ and $\mu = 100$ in Equation 4.20, the value of Q^* becomes 0.11. The value obtained from numerical (MATLAB) analysis for 75% settlement for $\alpha = 0.5$ and $\mu = 100$ is 0.1070. The percentage error is 2.73% and is considered to be very minimal and acceptable (refer Figure 4.10). This error is due to truncation and round off errors in finite difference method. Hence the present model has been validated both qualitatively and quantitatively.

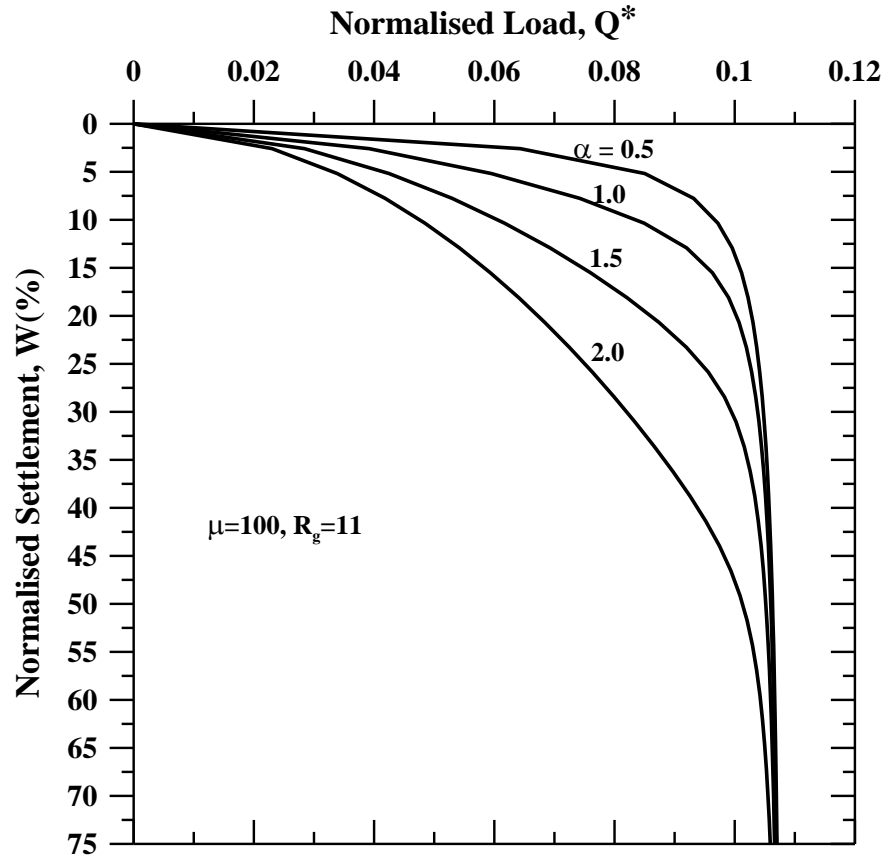


Figure 4.10: Variation of normalized load (Q^*) with normalized footing settlement (W_0) at high settlements.

4.4 Results and discussion

The deflection profiles of the normalized settlement (W) from the edge of the footing to the edge of the shear layer are presented in Figures 4.11 and 4.12. The Equation 4.17 presents the non-linear relationship between the normalized load (Q^*) and the W in terms of the model parameters α and μ , and the normalized footing settlement (W_0). The corresponding load-settlement curves are presented in Figures 4.14 and 4.15. A series of numerical analyses were performed using the finite difference code developed in MATLAB to ascertain the beneficial effects of using geocell reinforcement in a granular layer over soft soil subgrades. The model parameters viz. α and μ are varied along with the other variables such as R_g and W_0 for a range of values presented in Table 4.1 in different series of trials to develop design charts. These design charts are presented in terms of improvement factors (I_f), defined as the ratio of load bearing capacity of the reinforced ground to the unreinforced ground, with respect to each model parameter would give an insight of the behavior of geocell reinforcement.

The variations of settlement with distance from the edge of the footing for different values of the inverse of the normalized shear stiffness (α) and a constant normalized value of the inverse of ultimate bearing capacity of soft soil ($\mu = 50$) are shown in Figure 4.11. It is clear that for a stiffer and shorter granular-geocell layer ($\alpha=0.5$, $R_g=5$) the deflection profile is uniform beyond the edge of the footing and spreads the load uniformly over the soft foundation soil for W_0 of 5%. For increasing value of α , a non-uniform deflection profile of the shear layer beyond the edge of the footing is noticed depicting an unequal distribution of load over soft foundation soil owing to its lower flexural rigidity of the geocell (for $\alpha=0.5$, $R_g=10$). However, the load carrying capacity of the shorter shear layer is lower than the wider shear layer.

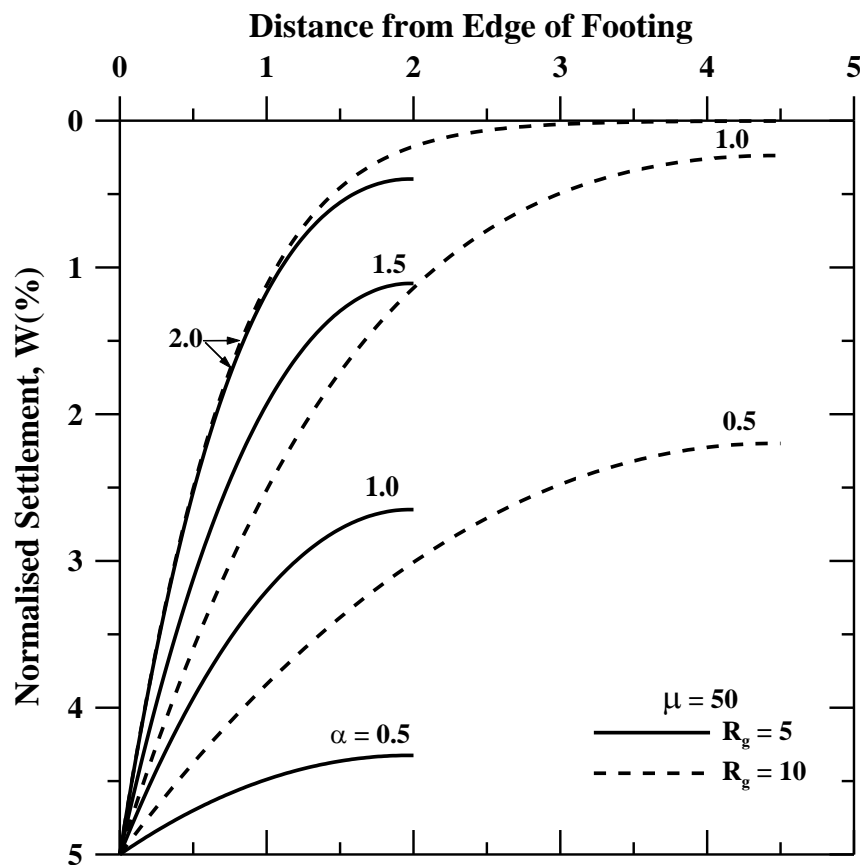


Figure 4.11: The settlement profile from the edge of the footing- Effect of α for $\mu=50$

Besides, the settlement profiles for different values of μ and a constant value of α ($\alpha = 1$) are shown in Figure 4.12. Figures 4.12a. and 4.12b. show this variation for shear layer width ratio, $R_g = 5$ and 10 respectively. It can be inferred from the comparison of Figures 4.12a. and

4.12b. that for a given value of α ($\alpha=1$), the settlement profile is relatively uniform for shorter shear layer ($R_g = 5$) than the wider ($R_g = 10$) depicting that the load distribution is almost uniform in the case of shorter shear layer. However, the load carrying capacity of the wider shear layer is higher. This is due to higher flexural rigidity expected for the shorter shear layer, which undergoes uniform larger settlements than the wider shear layer with lower shear stiffness for a given load. Comparing Figures 4.12a. and 4.12b., it could also be observed that even for soft subsoil conditions ($\mu > 50$) there is a considerable reduction in settlement by increasing the shear layer width ratio (R_g). The settlement profile pattern is similar for both cases of R_g but softer subsoil ($\mu > 50$) experiences higher settlement in spite of being subjected to lesser loads.

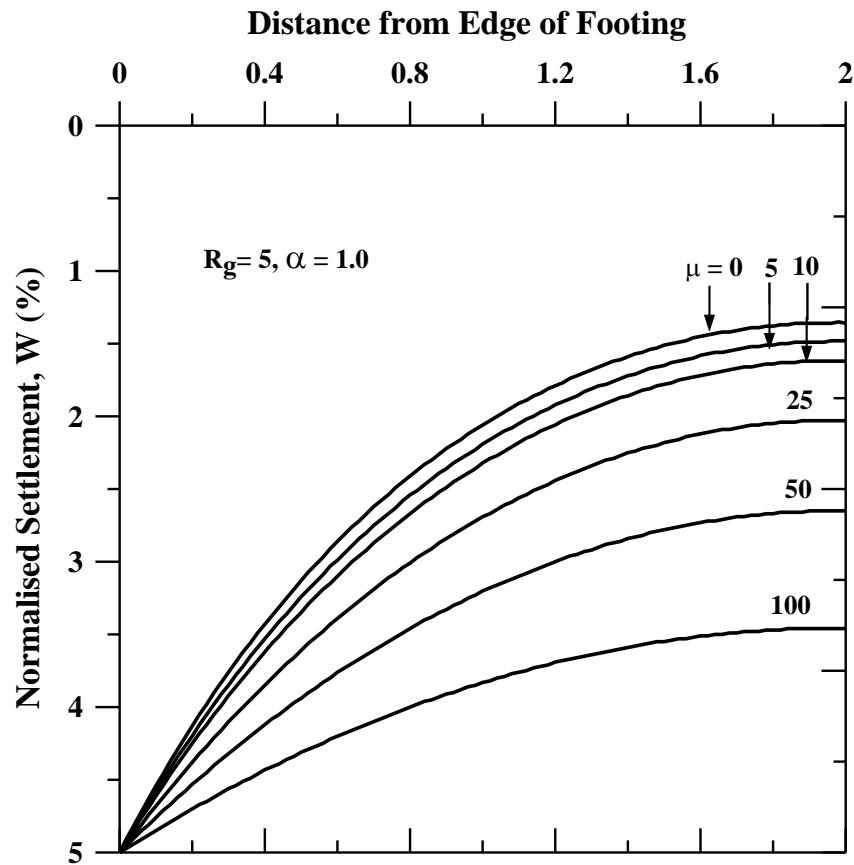
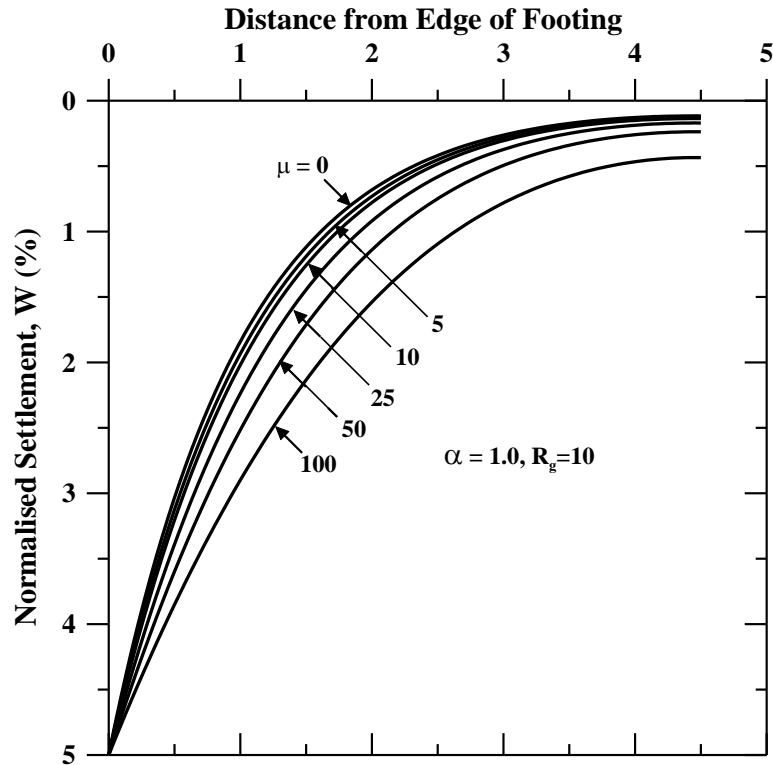


Fig. 12a Effect of μ for $R_g=5$ & $\alpha=1.0$

Fig. 12b Effect of μ for $R_g=10$ & $\alpha=1.0$ **Figure 4.12: Settlement profiles from the edge of the footing**

Figures 4.13-4.15 present the normalized load-settlement profiles for both unreinforced and reinforced beds. Figure 4.13 shows the normalized load settlement curve for unreinforced ground. The load that can be bore by the unreinforced ground is comparatively small even for soils with high bearing capacity (i.e. for low μ values). The influence of the model parameters α and μ can be seen on the normalized load-settlement responses of uniformly loaded strip footing resting on geocell reinforced soft soils in Figures 4.14 and 4.15 respectively. It could be observed from Figure 4.14 that with decrease in the value of α , as expected, the load carrying capacity of the composite ground increases. Similar trends are observed even for the case of wider shear layers on the soft foundation soil. However, the influence of α beyond 1.0 seems insignificant on the load-settlement response, even though there is an increase in the shear layer width ratio.

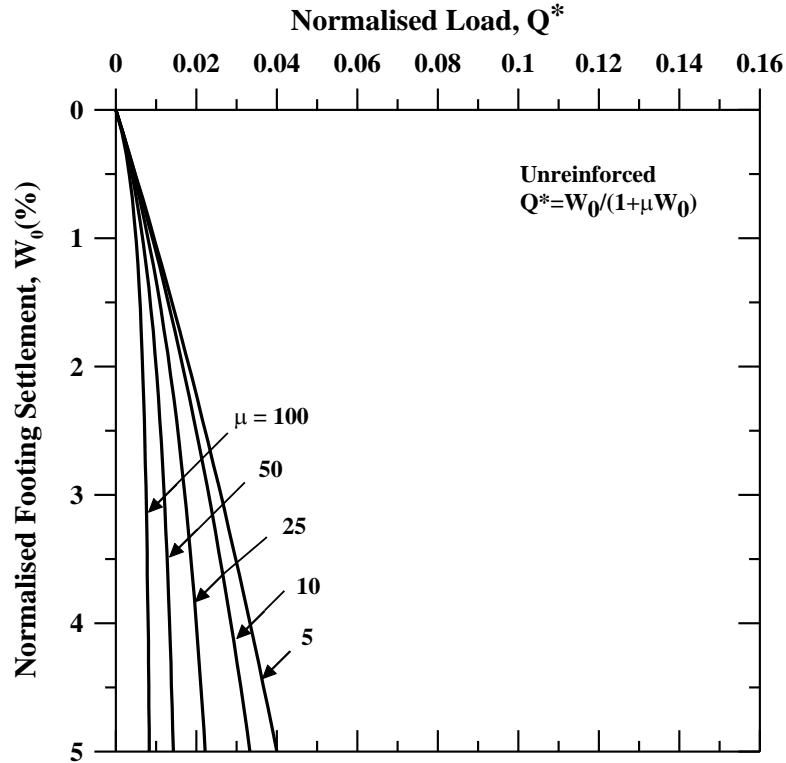


Figure 4.13: Variation of normalized load (Q^*) with normalized footing settlement (W_0) for unreinforced soil- Effect of μ

The inverse of the normalized ultimate bearing capacity (μ) has a significant effect on the load settlement response of a uniformly loaded strip footing resting on geocell reinforced soft soil (Figure 4.13). The load carrying capacity of the composite ground decreases with increase in the value of μ . This influence of $\mu \leq 10$ is found to be negligible on the load-settlement response as the foundation soils are expected to be very stiff at these values. It can be seen that for $\mu=0$ (i.e. theoretically the ultimate bearing capacity of soft soil reaches infinity), the load-settlement response is linear depicting that the foundation soil is much stiffer than the reinforced granular layer. In this case, the influence of R_g on the load settlement response is also negligible.

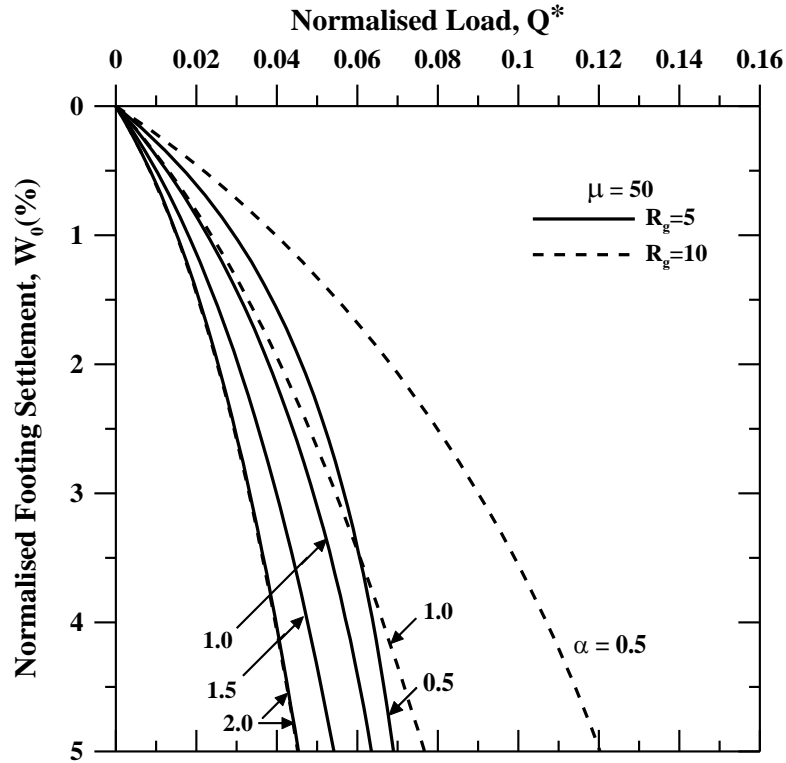


Figure 4.14: Variation of normalized load (Q^*) with normalized footing settlement (W_0) - Effect of α for $\mu=50$

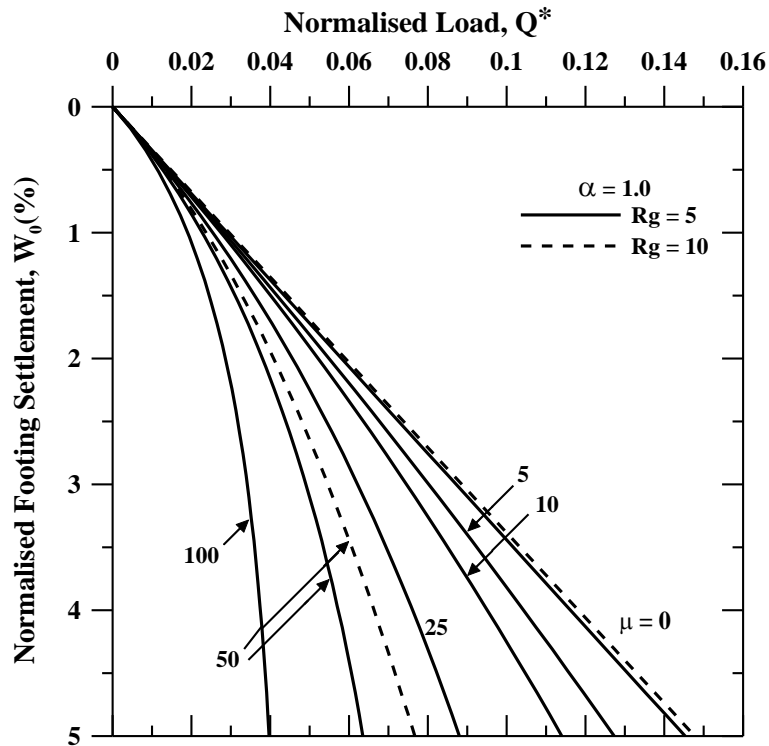


Figure 4.15: Variation of normalized Load (Q^*) normalized footing settlement (W_0) with -Effect of μ for $\alpha=1.0$

4.4.1 Improvement Factors

The beneficial effects of the geocell reinforced granular layer on the soft soil are expressed in terms of non-dimensional factor called improvement factor, I_f . Higher value of this factor indicates higher load carrying capacity of the composite ground. Figures 4.16 and 4.17 present the variation of improvement factors (I_f) with respect to the parameters α and R_g respectively. Figure 4.16 expresses the variation of I_f for different W_0 . As expected, higher I_f is noticed for higher W_0 ($W_0=5\%$).

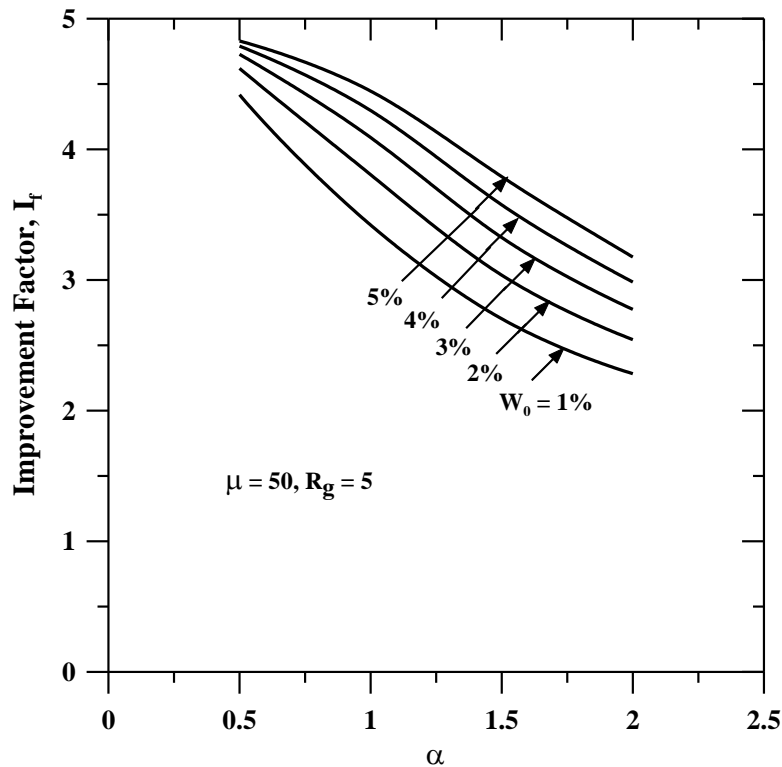


Figure 4.16: Variation of improvement factor, I_f with the inverse of the normalized shear stiffness, α - Effect of W_0 for $\mu=50$ and $R_g=5$

Figure 4.17 shows the variation of I_f with α . An interesting observation can be drawn from this Figure is that for a very stiff subsoil i.e. $\mu=0$, the I_f obtained is low in spite of stiffer subsoil having higher load bearing capacity. This is due to the higher stiffness of the subsoil which cannot be further improved with the addition of geocell reinforcement or in other words, the advantage of introducing geocell reinforcement on stiffer subsoil is negligible.

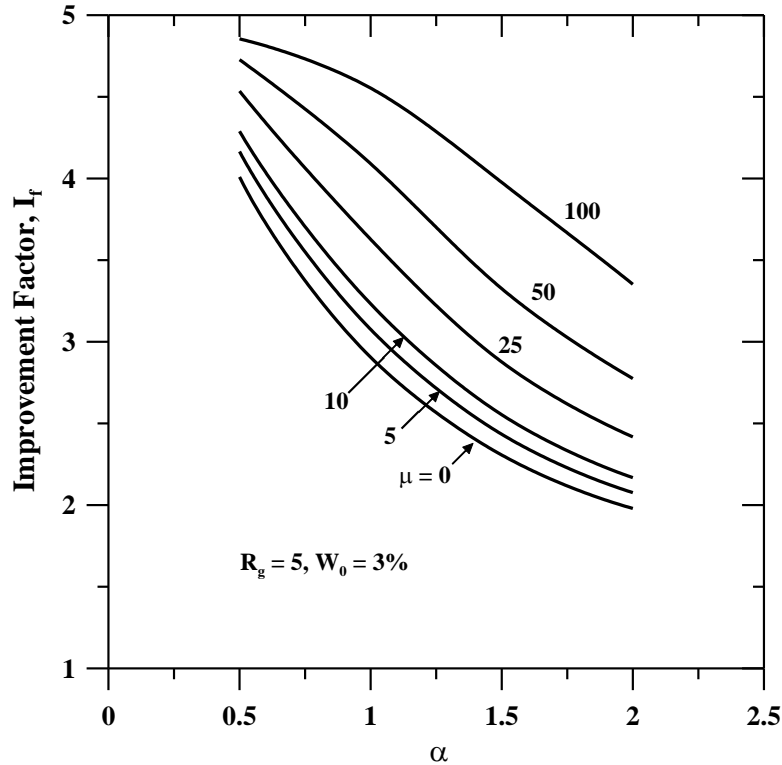


Figure 4.17: Variation of improvement factor, I_f with the inverse of the normalized shear stiffness, α - Effect of μ for $W = 3$ and $R_g=5$

Figure 4.18 shows the variation of I_f with R_g . It could be observed from Figure 4.18a that for lower values of μ (0-25) there is no improvement after increasing R_g beyond 5. But significant improvement is brought by soils with low ultimate bearing capacity ($\mu > 25$). Figure 18b demonstrates that the inclusion of geocell with higher shear stiffness ($\alpha=0.5$) brings in 8 fold increase in the improvement of ground. Besides, geocell with low shear stiffness ($\alpha=2$) doesn't show any improvement with the increase in shear layer width ratio beyond 5. Figure 18c shows the variation in improvement factor with shear layer width ratio for varying footing settlements. The percentage increase in improvement factor for various settlements remains same. In addition, there is no much improvement observed beyond $R_g = 5$.

In summary, the improvement factors with different model parameters show a clear trend of improvement in bearing capacity of reinforced ground. Each model parameter has certain influence on the performance of the reinforced ground.

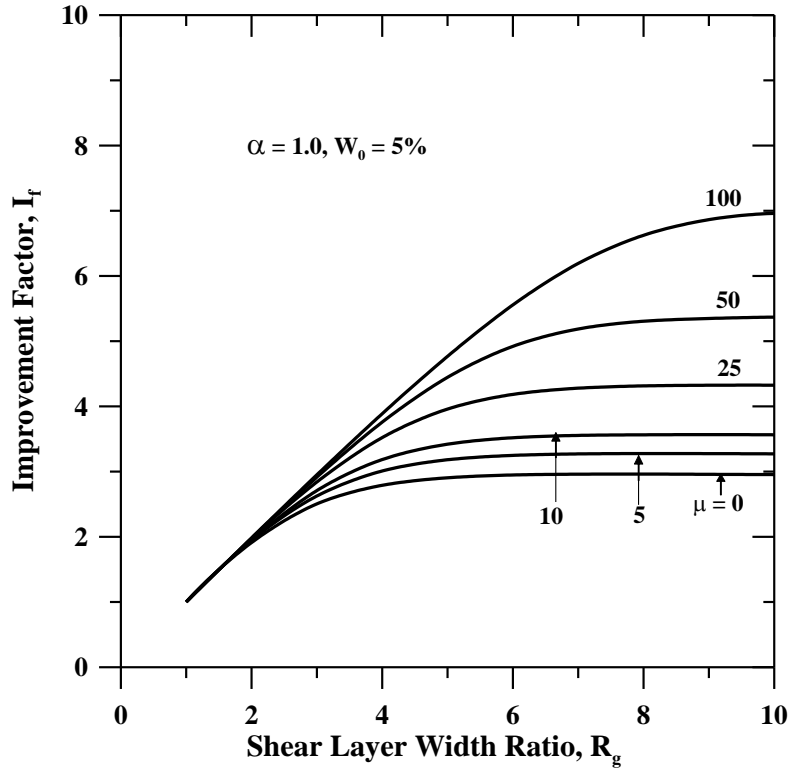


Figure 4.18 a: Effect of μ for $\alpha=1$ and $W=5\%$

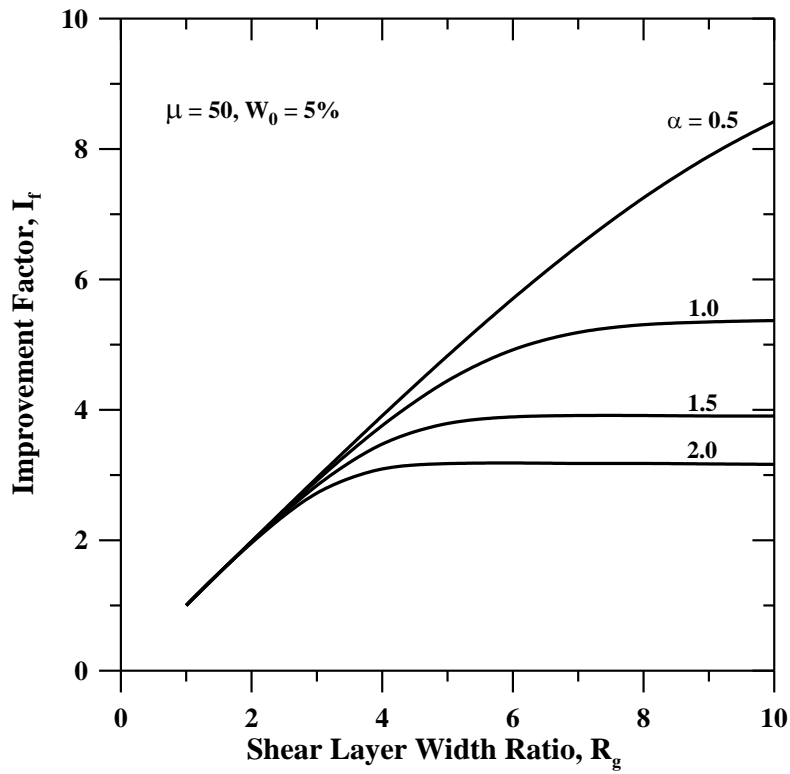
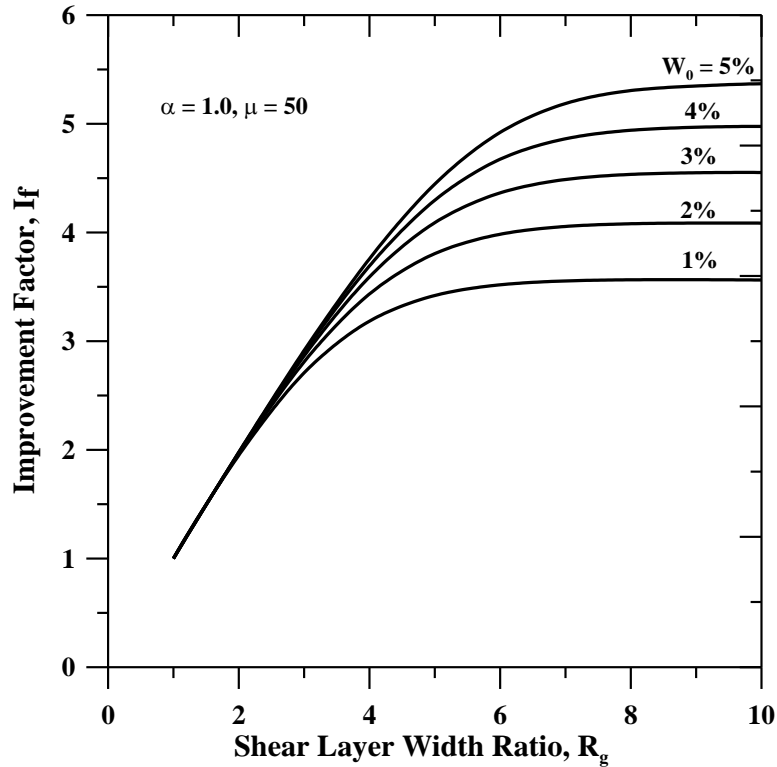


Figure 4.18 b: of α for $\mu=50$ and $W=5\%$

Figure 4.18c: Effect of W for $\mu=50$ and $\alpha=1.0$ Figure 4.18: Variation of improvement factor, I_f with shear layer width ratio, R_g

4.4.2 Practical Significance

Designing with geosynthetics especially with geocells has been drawing interest of design engineers for geotechnical structures. However, to the author's knowledge, there are no preferred design criteria or design charts available in the literature to adopt this new construction technic though, several experimental data are available. In this study an attempt has been made to develop design charts in terms of composite soil-geocell properties. These design charts are useful in selecting the model parameters required (α and R_g) to improve the soft ground of known conditions (q_u and μ). The degree of improvement expected governs the model parameters as well. Using these design charts, one can easily design foundations of structures on a soft ground reinforced with geocells.

4.5 Summary

An attempt has been made to numerically simulate the elasto-plastic behavior of rigid strip footing on geocell reinforced sand beds overlying soft clay beds. Linear and non-linear load settlement behavior of reinforced beds was obtained by considering the reinforced granular

layer as a Pasternak shear layer. The deflection profile of the Pasternak shear layer was analyzed to obtain the load-settlement profiles. Following important conclusions are drawn from this study:

- A non-linear relationship between the normalized load (Q^*) and normalized footing settlement (W_0) in terms of the non-dimensional model parameters α and μ is obtained based on the deflection profile of the Pasternak shear layer. The second order non-linear differential equations were solved using finite difference scheme.
- Numerical results are compared with two independent experimental data and observed that there is a good match between the load-deflection profiles from experiments and numerical study.
- It has been observed that the normalized load-deflection profiles have significant influence on the model parameters viz. the shear layer width ratio, R_g ; inverse of normalized shear stiffness of the reinforced granular layer, α ; inverse of the normalized ultimate bearing capacity of the soft clay bed, μ .
- Lower value of μ represents higher stiffness of the soft foundation clay layer. Besides, lower the value of α represents higher flexural rigidity and stiffness of the Pasternak shear layer with geocell reinforcement.
- It is seen that a stiffer granular-geocell layer ($\alpha=0.5$) sustains a higher load for W_0 of 5% and spreads the load uniformly over the soft foundation soil. Further increase in value of α , the load supported by the geocell-granular layer decreases owing to its lower flexural stiffness.
- For a given value of inverse of normalized shear stiffness of reinforced granular layer ($\alpha=1.0$), the settlement profile is uniform for shorter shear layer ($R_g = 5$) than for wider shear layer ($R_g = 10$). This observation concurs with the fact that highly rigid foundations undergo uniform settlements. Besides, there is a reduction in settlement with increase in shear layer width, R_g for a given value of α , even for weaker subsoil conditions (i.e. with increase in μ).
- With decrease in the value of inverse of normalized shear stiffness (α), the load carrying capacity of the composite ground increases. However, the influence of α beyond 1.0 seems insignificant on the load-settlement response, even though there is an increase in the shear layer width ratio.

- The load carrying capacity of the composite ground decreases with increase in the value of μ . This influence of $\mu \leq 10$ is found to be negligible on the load-settlement response as the foundation soils are expected to be very stiff at these values.
- Design charts in terms of improvement factors are presented with respect to various model parameters. For lower values of μ (0-25), it is seen that there is no improvement after increasing the shear layer width ratio (R_g) beyond 5. But significant improvement is brought by soils with low ultimate bearing capacity ($\mu > 25$).
- The inclusion of geocell with higher shear stiffness ($\alpha = 0.5$) brings in 8 fold increase in the improvement of ground.

In summary, the improvement factors with different model parameters show a clear trend of improvement in bearing capacity of reinforced ground

Chapter 5

Elasto-Plastic Behaviour of Rigid Circular Footing on Geocell Reinforced Soils

5.1 Problem Statement

The definition sketch of the geocell reinforced granular layer over soft soil under rigid circular footing is shown in Figure 5.1. The rigid circular footing resting on soft soil (undrained cohesive strength, $c = c_u$; friction angle, $\phi = 0$; Modulus of subgrade, k_s), which is reinforced with geocell (Shear modulus, G_g). The system is idealised with the aid of two parameter elastic Pasternak model as shown in Figure 5.2. The geocell reinforced granular fill and soft foundation soil are idealised using Pasternak shear layer and Winkler springs respectively. The cross sectional view of settlement profile of the circular footing supported on geocell reinforced granular fill is shown in Figure 5.3. Since analysis is done on circular footing axisymmetric model is considered. A uniform unit displacement was assumed beneath the footing and a hyperbolic second order differential equation was assumed to represent the deflection profile from the edge of the footing to the edge of the geocell layer. The shear stiffness (a product of shear modulus and height) of the geocell reinforced granular fill and the ultimate bearing capacity of the soft soil, q_u are the crucial parameters that helps in understanding the behaviour of the geocell reinforced soils. Linear and nonlinear analysis was carried out to determine the performance of the circular footing under various range of settlements.

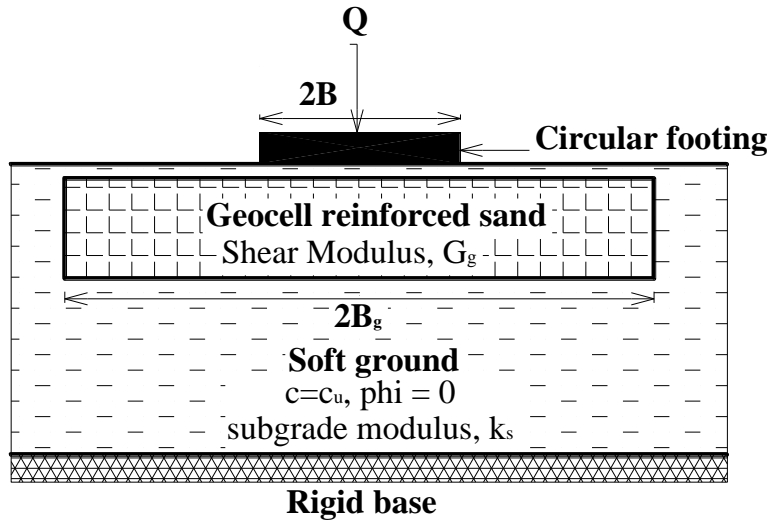


Figure 5.1: Definition sketch of circular footing on geocell reinforced soils

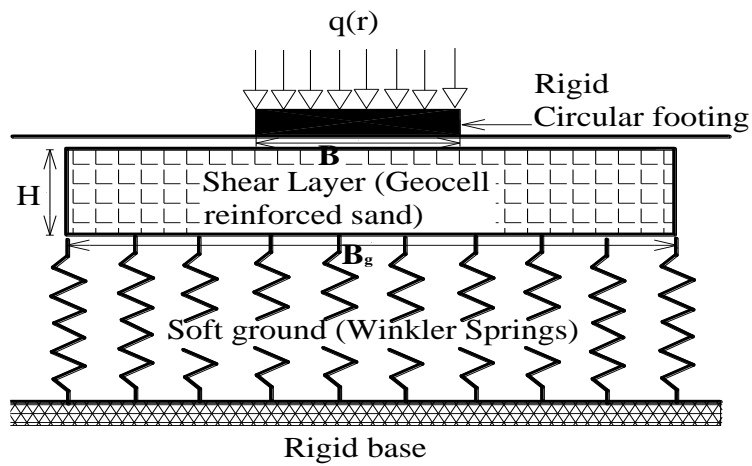


Figure 5.2: Idealisation of Geocell reinforced soils – Pasternak model

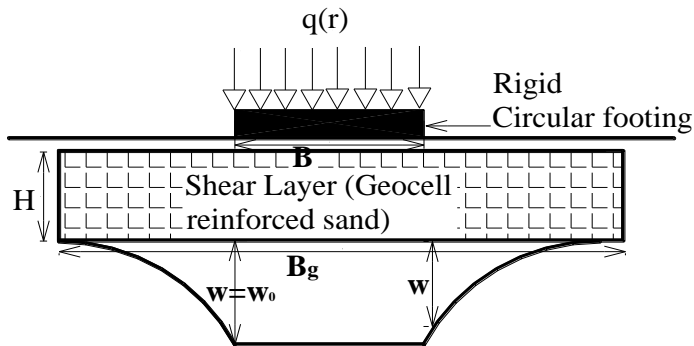


Figure 5.3: Cross-sectional view of the deflection profile of rigid circular footing.

5.2 Theoretical Formulation

The inherent complexity in understanding the behaviour of soils gave rise to many idealised models of soil behaviour. The response of circular footing resting on geocell reinforced soils was modelled with the aid of modified Pasternak foundation model. Axisymmetric model was considered for circular footing for symmetric distribution of loads around the central axis. In the current model, linear analysis is performed for lesser footing settlements ($w_0 < 1\%$ of the footing width, B) and non-linear analysis is carried out for higher settlements to simulate the actual behaviour of the circular footing.

5.2.1 Linear Formulation

The governing equation for the load-deflection pattern of the problem considering the shear layer representing the geocell mattress, as described in Pasternak model, is as follows (see Fig. 5.3):

$$q(r) = k_s \cdot w_o \text{ for } |r| \leq \frac{B}{2} \quad (5.1)$$

$$k_s w - G_g H \left(\frac{d^2 w}{dr^2} + \frac{1}{r} \frac{dw}{dr} \right) \text{ for } |r| \geq \frac{B}{2} \quad (5.2)$$

Let r be the radial distance from the central axis, w be the settlement.

Expressing the terms in non-dimensional form,

Let $R=r/B$ and $W=w/B$ where B is the diameter of the footing.

Simplifying Equation (5.2) the governing differential equation reduces to

$$\frac{d^2 W}{dR^2} + \frac{1}{R} \frac{dW}{dR} - \alpha^2 W = 0 \text{ Where } \alpha = \frac{k_s B^2}{G_g H} \quad (5.3)$$

Now the load deflection equation of the formulation is

$$Q = \int_0^{2\pi} \int_0^{B/2} k_s w_o r dr d\theta + \int_0^{2\pi} \int_{B/2}^{B_g/2} k_s w r dr d\theta \quad (5.4)$$

$$Q = \int_0^{2\pi} \int_0^{1/2} k_s B^3 W_o R dR d\theta + \int_0^{2\pi} \int_{1/2}^{R_g/2} k_s B^3 W R dR d\theta \quad (5.5)$$

$$Q^* = \int_0^{2\pi} \int_0^{1/2} W_o R dR d\theta + \int_0^{2\pi} \int_{1/2}^{R_g/2} W R dR d\theta \quad \text{where } Q^* = \frac{Q}{k_s B^3} \quad (5.6)$$

$$Q^* = \frac{\pi}{4} W_0 + 2\pi \int_{0.5}^{R_g/2} WRdR \quad (5.7)$$

Equation (5.7) represents the normalized load (Q^*) as a function of normalized settlement. From Equation (5.3), it could be understood that the settlement profile is a function of geocell layer stiffness. Trapezoidal rule was employed for numerical integration by discretizing the region into very fine elements. Table 5.1 shows the range of non-dimensional parameters used in the present analysis.

Table 5.1: Typical values of model parameters used in this study

Parameter	Unit	Range
W_0	%	1 to 5
R_g	Dimensionless	1 to 5 and 10
μ	Dimensionless	0 to 100
α	Dimensionless	0.5 to 2
k_s (Bowels, 1997)	kN/m ³	5,000 to 80,000
G_g (Sireesh, 2006)	MPa	10 to 18

The results obtained from linear analysis for low values of settlements are presented below. The settlement profile from the edge of the footing to the edge of the geocell for small settlements ($W \approx 1\%$) is shown in Figure 5.4a. Figure 5.4b shows the magnified view of the same. It could be inferred from the figure that when the geocell layer stiffness is very high ($\alpha = 0.5$), the reinforced bed is able to bear higher load and spreads the load more uniformly. In this analysis, constant settlement is enforced at the edge of the footing and therefore the geocell layer with higher stiffness settles more due to the higher load that can be borne by the system to attain the same settlement as that of the low stiffness geocell reinforced ground.

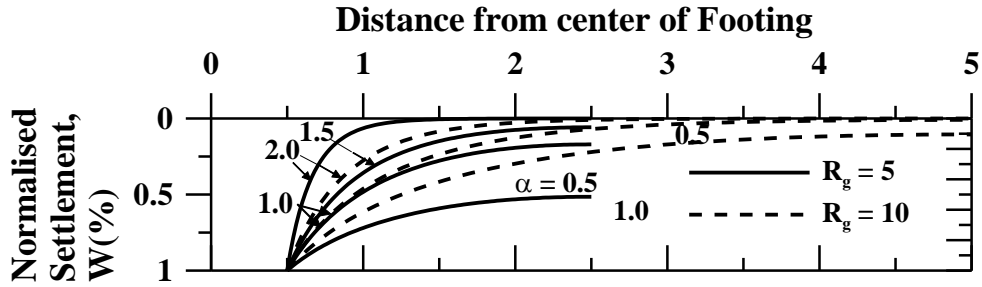


Figure 5.4a: Settlement Profile (Linear analysis)

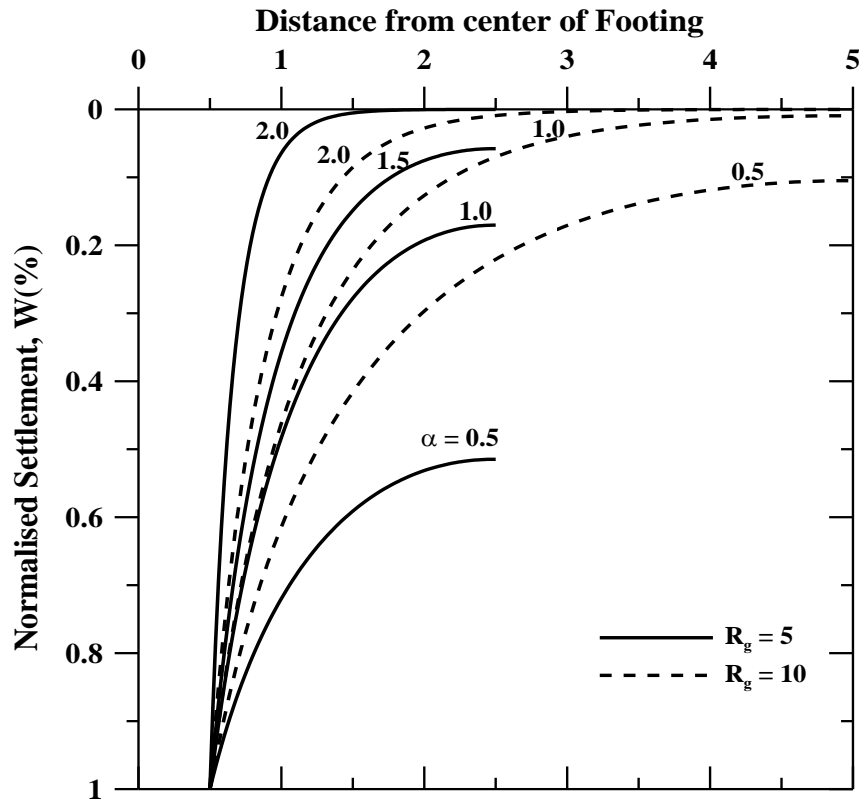


Figure 5.4b: Settlement Profile (Magnified view)

Figure 5.4: Settlement Profile from the edge of footing to the edge of the geocell layer

Figure 5.5 shows the linear load settlement response of the reinforced bed for a settlement up to 1% which helps in better understanding of the settlement profile of the geocell reinforced ground. The load experience by stiffer geocell layer ($\alpha=0.5$) is very high compared to that of softer geocell layer ($\alpha=2$). For geocell reinforced beds of high stiffness, the load bearing capacity of the reinforced bed increases with increase in geocell layer width however the increase in geocell layer width has negligible influence for low shear stiffness geocell beds.

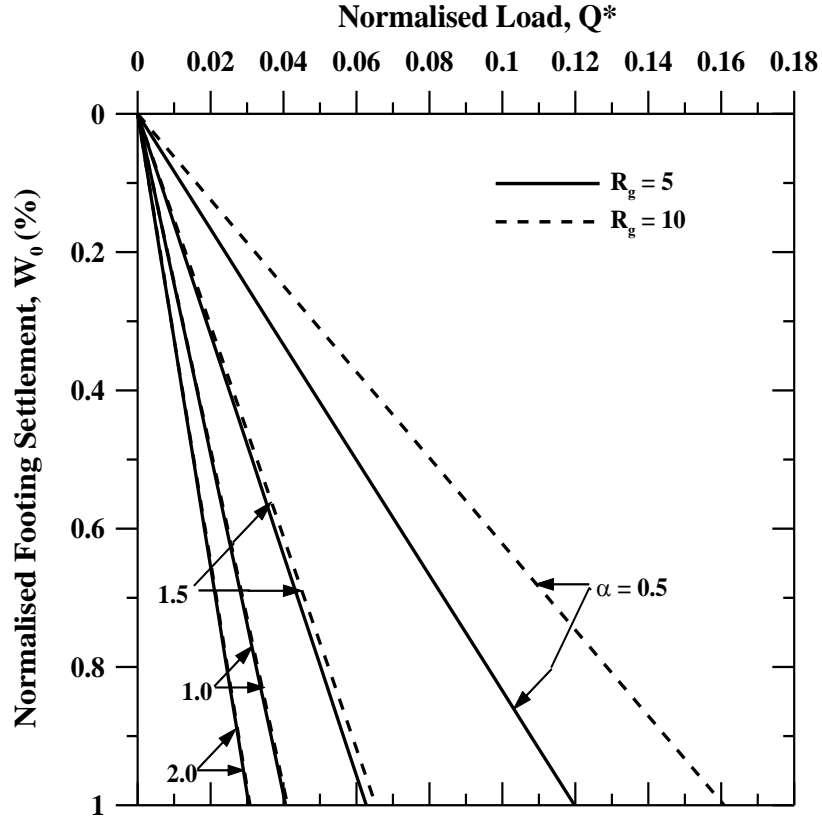


Figure 5.5: Variation of normalised load (Q^*) with normalised footing settlement (W_0) with variation in α

5.2.2 Non-linear Formulation

The nonlinear stress displacement response of the soil can be represented by the hyperbolic relation given by Kondner [1963] as follows:

$$q(r) = \frac{k_s w_0}{1 + \frac{k_s w_0}{q_u}} \quad \text{for } |r| \leq \frac{B}{2} \quad (5.8)$$

$$\frac{k_s w_0}{1 + \frac{k_s w_0}{q_u}} - G_g H \left(\frac{d^2 w}{dr^2} + \frac{1}{r} \frac{dw}{dr} \right) = 0 \quad \text{for } |r| \geq \frac{B}{2} \quad (5.9)$$

Expressing the terms in non-dimensional form,

Let $R=r/D$ and $W=w/D$

$$\frac{d^2 W}{dR^2} + \frac{1}{R} \frac{dW}{dR} - \frac{\alpha^2 W}{1 + \mu W} = 0 \quad (5.10)$$

$$\alpha = \frac{k_s B^2}{G_g H} \quad \mu = \frac{k_s B}{q_u}$$

Where,

Now the load deflection equation of the formulation is

$$Q = \int_0^{2\pi} \int_0^{B/2} \frac{k_s W_o}{1 + \frac{k_s W_o}{q_u}} r dr d\theta + \int_0^{2\pi} \int_{B/2}^{B_g/2} \frac{k_s W}{1 + \frac{k_s W}{q_u}} r dr d\theta \quad (5.11)$$

Changing the limits of integration and expressing in non-dimensional form

$$Q = \int_0^{2\pi} \int_0^{B/2} k_s B^3 \frac{W_o}{1 + \mu W_o} R dR d\theta + \int_0^{2\pi} \int_{1/2}^{R_g/2} k_s B^3 \frac{W}{1 + \mu W} R dR d\theta \quad (5.12)$$

$$Q^* = \int_0^{2\pi} \int_0^{1/2} \frac{W_o}{1 + \mu W_o} R dR d\theta + \int_0^{2\pi} \int_{1/2}^{R_g/2} \frac{W}{1 + \mu W} R dR d\theta \quad \text{where, } Q^* = \frac{Q}{k_s B^3} \quad (5.13)$$

$$Q^* = \frac{\pi}{4} \left(\frac{W_o}{1 + \mu W_o} \right) + 2\pi \int_{0.5}^{R_g/2} \frac{W}{1 + \mu W} R dR \quad (5.14)$$

5.2.3 Finite Difference Formulation

Both the linear and nonlinear ordinary differential equations were difficult to solve analytically. Finite difference method, numerical method for approximating the solution of differential equations was employed. Central difference scheme (Crank – Nicolson method, 1947) was employed to discretise second order terms and forward difference scheme (Explicit method) was used to discretise first order terms. The normalised length, L has been divided into '(n-1)' number of elements with 'n' number of node points. The mesh size (dX) can be written as dX=L/n (refer Figure 5.6). Writing the equation for any interior node 'i', for the linear ordinary differential equation leads to the following:

$$\frac{W_{i-1} - 2W_i + W_{i+1}}{(\Delta R)^2} + \frac{1}{R_i} \frac{W_{i+1} - W_i}{\Delta R} - \alpha^2 W_i = 0 \quad (5.15)$$

Tridiagonal matrix method, a simplified form of Gaussian elimination was used to solve the linear algebraic equations.

The nonlinear ordinary differential equation can be discretised to the following form

$$\frac{W_{i-1} - 2W_i + W_{i+1}}{(\Delta R)^2} + \frac{1}{R_i} \frac{W_{i+1} - W_i}{\Delta R} - \frac{\alpha^2 W_i}{1 + \mu W_i} = 0 \quad (5.16)$$

Since the discretised equation is in nonlinear form direct approaches viz. Gauss elimination, Gauss- Seidel, Tridiagonal matrix method etc. cannot be employed. The nonlinear algebraic equation (5.16) has to be linearized.

$$\frac{W_{i-1} - 2W_i + W_{i+1}}{(\Delta R)^2} + \frac{1}{R_i} \frac{W_{i+1} - W_i}{\Delta R} - g_i W_i = 0 \quad (5.17)$$

Where $g_i = \frac{\alpha^2}{1 + \mu W_i}$

An initial guess for g_i was adopted and the iterative Gauss-Siedel procedure for obtaining solution of linear algebraic equations was used to obtain the solution.

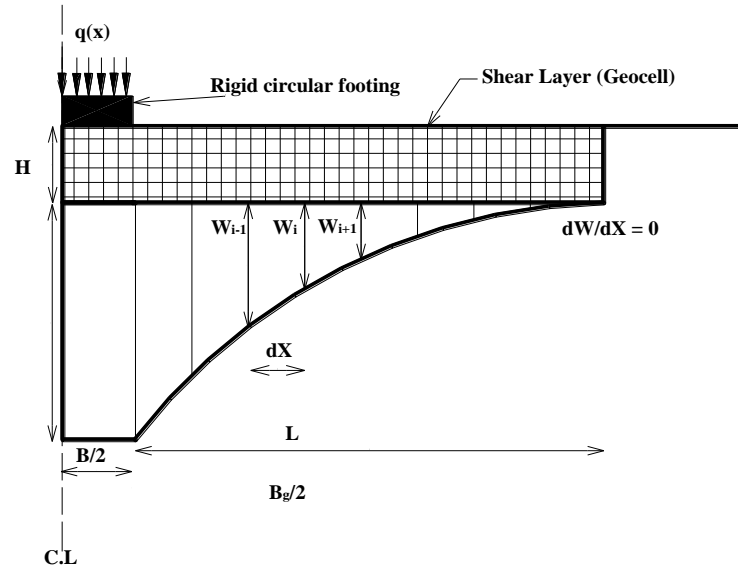


Figure 5.6: Finite difference discretization (Cross-sectional view)

5.2.4 Boundary Conditions

The settlement of the rigid circular footing is considered as uniform under the loaded circular footing area. Hence the normalised settlement (W) at the edge of the footing is equal to the normalised footing settlement (W_0). The slope of the settlement profile (gradient of the settlement profile, dW/dR) is zero at the edge of the geocell layer, ie $R=R_g/2$. These two boundary conditions has been instrumental in solving both linear and non-linear ordinary differential equations.

In mathematical form it can be written as:

$$@R = 0.5, W = W_0$$

$$@R = R_g/2, dW/dX = 0$$

5.3 Validation

5.3.1 Theoretical Validation

The complete solution for the load settlement behaviour for a rigid circular footing supported on geocell reinforced soil is expressed in Equation (5.14). When $\mu = 0$, the results obtained from Equation (5.14) should match with the results of linear load settlement pattern. Figure 5.7 shows the validation of the nonlinear numerical model with that of the linear model. It could be seen that both the curves are found to overlap each other since the same finite difference method was employed to solve both the linear and nonlinear equations.

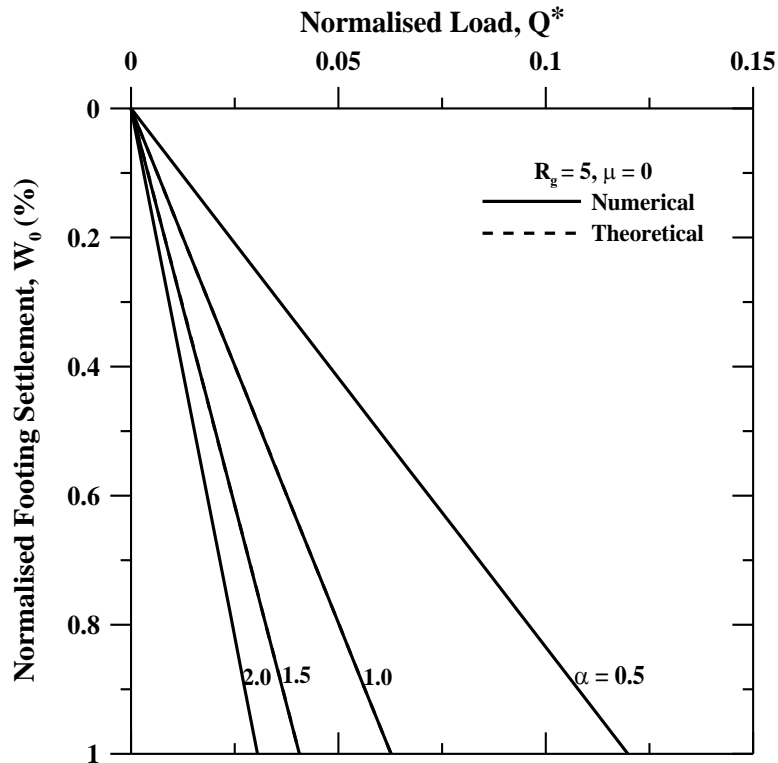


Figure 5.7: Validation of the nonlinear model with linear analysis

5.3.2 Numerical Validation

At very high settlements, Equation (5.14) converges to a constant normalized load (Limiting value), Q^* as follows:

$$Q^* = \frac{\pi}{4\mu} R_g^2 \quad (5.18)$$

Substituting $R_g = 5$, $\mu = 100$ in equation (5.18), Q^* becomes 0.196. For high settlements, numerical (MATLAB) analysis were carried out for 75% and for a particular μ ($\mu = 100$) and

R_g ($R_g = 5$) the Q^* was found to converge to 0.1937. The percentage error is -1.17% which is due to truncation and round off errors.

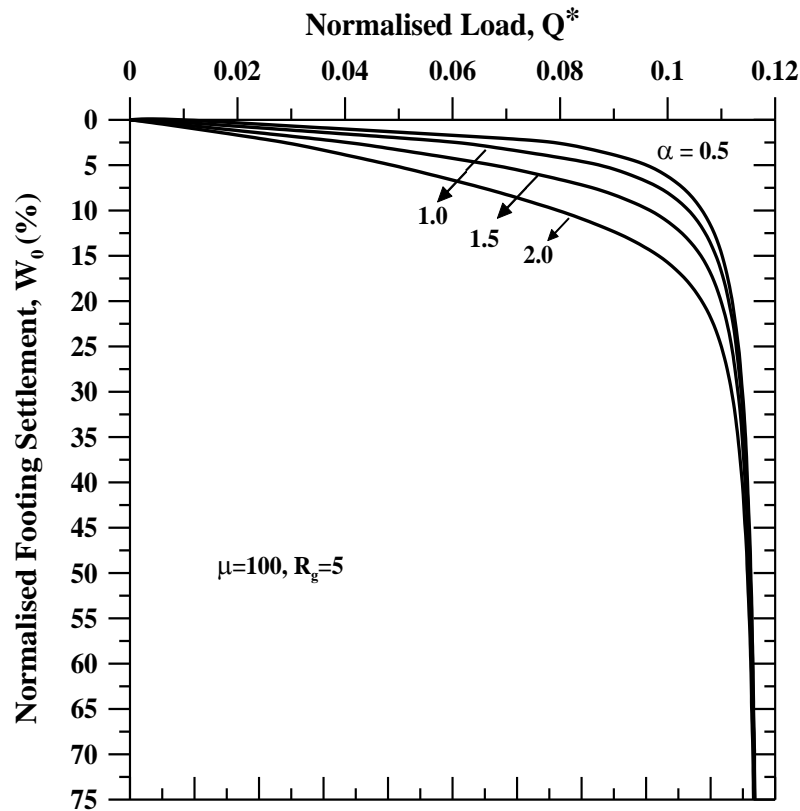


Figure 5.8: Normalised load settlement curve at high settlements – Numerical Validation

5.4 Results and Discussion

The settlement profile from the edge of the footing to the edge of the geocell layer is shown in Figures 5.9 and 5.10. The corresponding load settlement curves are plotted in Figures 5.12 and 5.13. The nonlinear response is close to actual soil behaviour. Improvement factors, I_f were also reported later in the study to give an insight into the beneficial effects of using geocell reinforcement in soft subgrades under circular footing.

The settlement profile for varying shear stiffness of the geocell reinforced ground and constant ultimate bearing capacity of the subsoil is plotted in Figure 5.9. Similar trend, as seen in linear analysis, is followed here. In linear analysis the subsoil is considered to be infinitely stiff whereas in nonlinear analysis the subsoil conditions are also accounted.

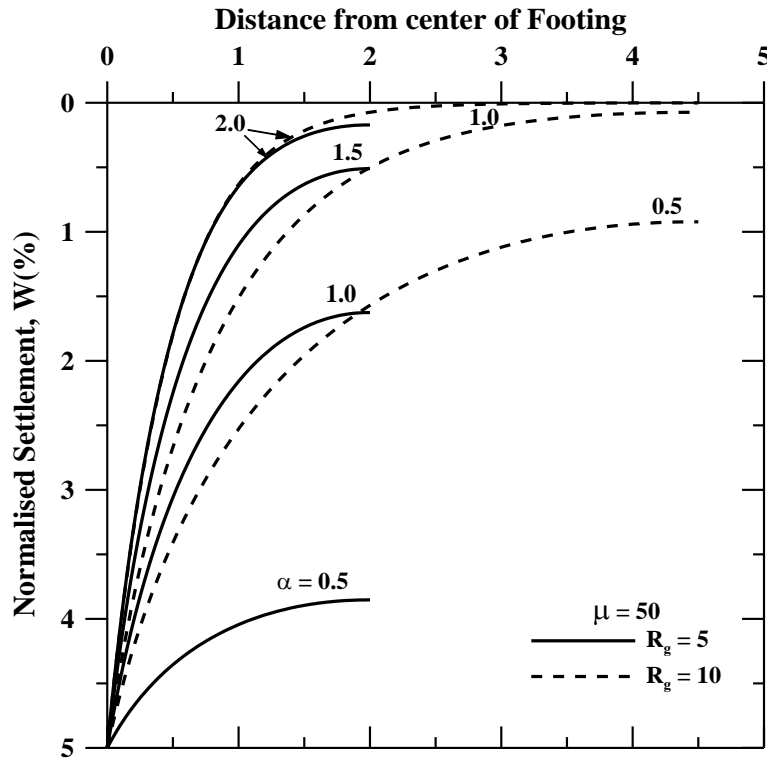


Figure 5.9: Settlement profile from the edge of the footing to the edge of the geocell layer (different α and constant μ)

Analysis was also carried out for varying subsoil conditions and a constant value of geocell layer stiffness for obtaining the settlement profile as shown in Figure 5.10. It could be observed that when shear layer width ratio, R_g is 5, the settlement pattern varies remarkably for different subsoil conditions (Figure 5.10a) whereas for higher geocell layer width there is negligible difference in settlement pattern for varying subsoil conditions (Figure 5.10b). It could also be inferred that subsoil with high ultimate bearing capacity, in spite of bearing higher load, undergoes lesser settlement. Load distribution is more uniform for soils with low ultimate bearing capacity.

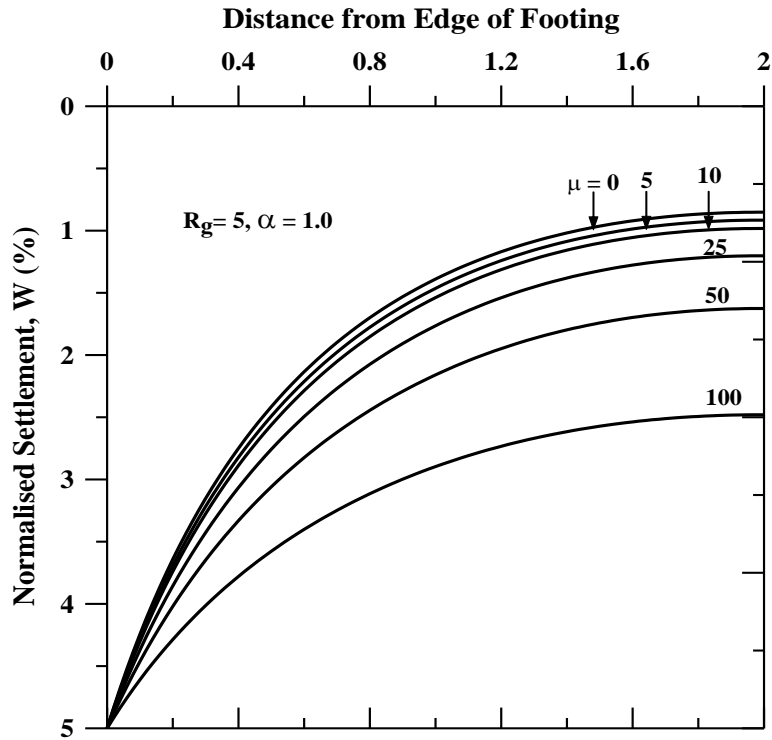


Figure 5.10a: Settlement profile for shear layer width ratio, $R_g = 5$.

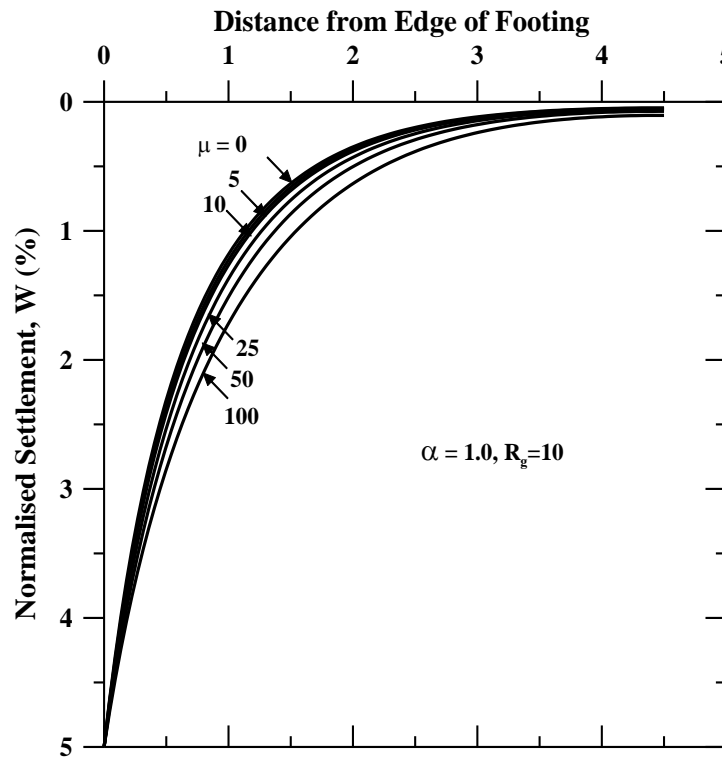


Figure 5.10b: Settlement profile for shear layer width ratio, $R_g = 10$

Figure 5.10: Settlement profile from the edge of the footing to the edge of the geocell (constant α and different μ)

The normalised load settlement curves for both reinforced and unreinforced beds are shown in Figures 5.11-5.13. The load settlement curve of the unreinforced bed is shown in Figure 5.11. It could be clearly understood from the figure that the load bore by the unreinforced ground is very small even under good subsoil conditions. Figure 5.11b shows the magnified view of the same. There is a clear trend of increase in load with increase in the subsoil stiffness.

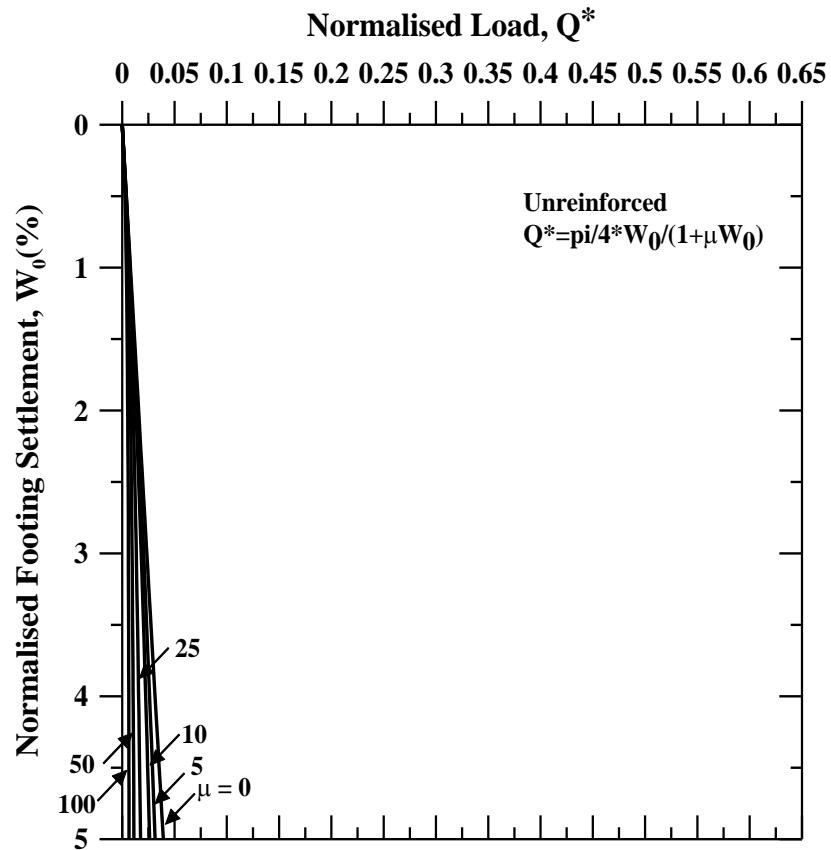


Figure 5.11a: Normalised load settlement curve.

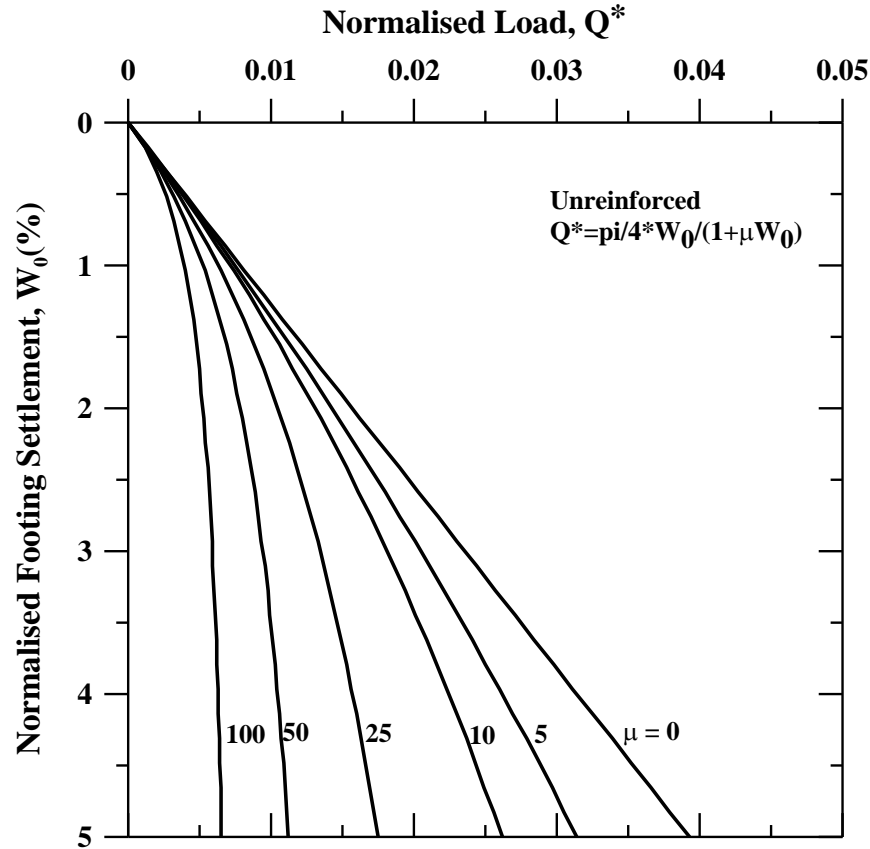


Figure 5.11b: Normalised load settlement curve. (Magnified view)

Figure 5.11: Normalised load settlement curve for the unreinforced ground (different μ)

The influence of the model parameters α and μ on the load settlement behaviour of a rigid circular footing resting on geocell reinforced ground has been plotted in Figures 5.12 and 5.13. As expected, geocells of high shear stiffness ($\alpha = 0.5$) bears very high load and shows significant improvement with increase in shear layer width ratio (R_g) whereas geocells of low shear stiffness ($\alpha = 2$) has very low bearing capacity and negligible improvement with increase in R_g .

The normalised load settlement curves were also plotted with varying subsoil conditions (μ) and constant shear stiffness of the soil (α) as shown in Figure 5.13. Theoretically, infinitely stiff subsoil ($\mu = 0$) bears a high load but comparable difference in the load bearing capacity cannot be found with variation in ultimate bearing capacity of the subsoil. The increase in geocell layer width doesn't bring in any further improvement in soils that are infinitely stiff, however, for lower stiff soils there is considerable improvement in load carrying capacity.

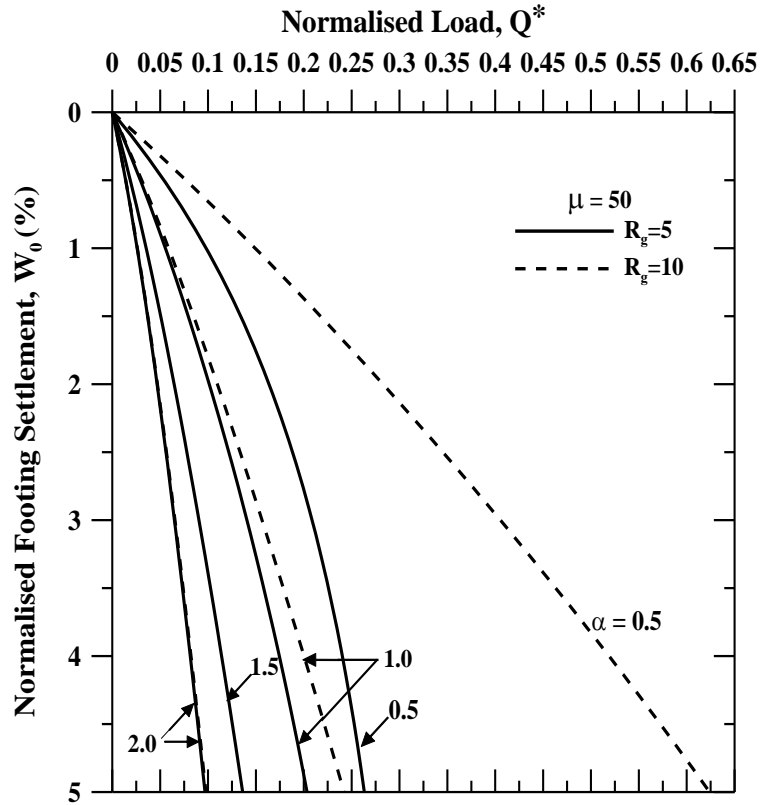


Figure 5.12: Normalised load settlement curve (different α and constant μ)

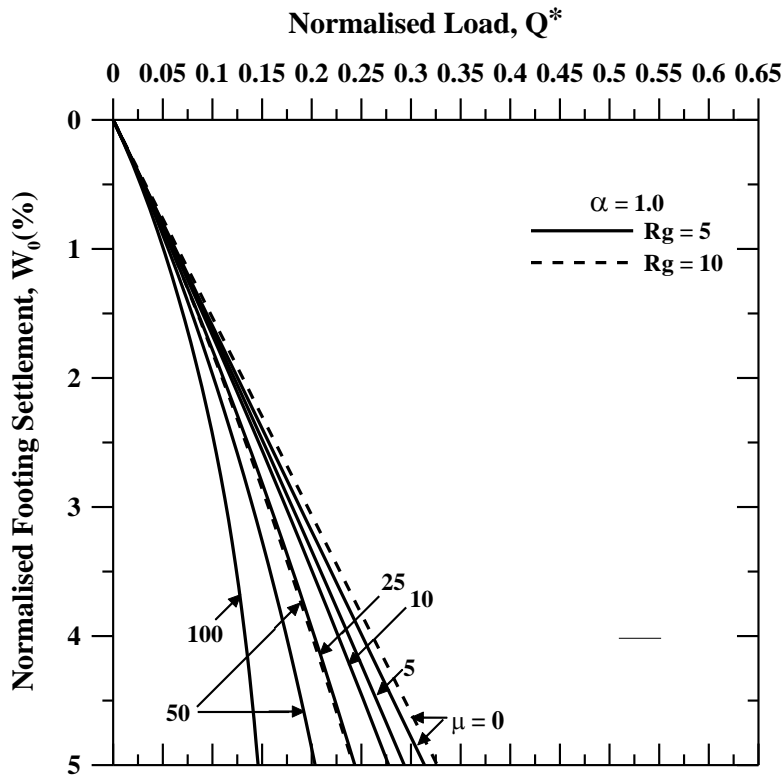


Figure 5.13: Normalised load settlement curve (different μ and constant α)

Figure 5.14a shows the variation of improvement factor, I_f with change in inverse of geocell layer stiffness (α) keeping shear layer width ratio (R_g) and normalised settlement constant. It was observed that there is a clear trend of decrease in improvement factor with increase in geocell layer stiffness. The Improvement factors also increased with increase in normalised settlement which indicates that footing undergoes higher settlement due to the higher load that is applied on the geocell reinforced soil.

Figure 5.14b shows the variation of I_f with α for constant geocell layer width ratio, R_g and normalised settlement. An interesting observation that was made from the analysis is that for subsoil with theoretically infinite stiffness, the I_f obtained is low. This is due to the high stiffness that it possesses and further improvement with the aid of geocell is not significant.

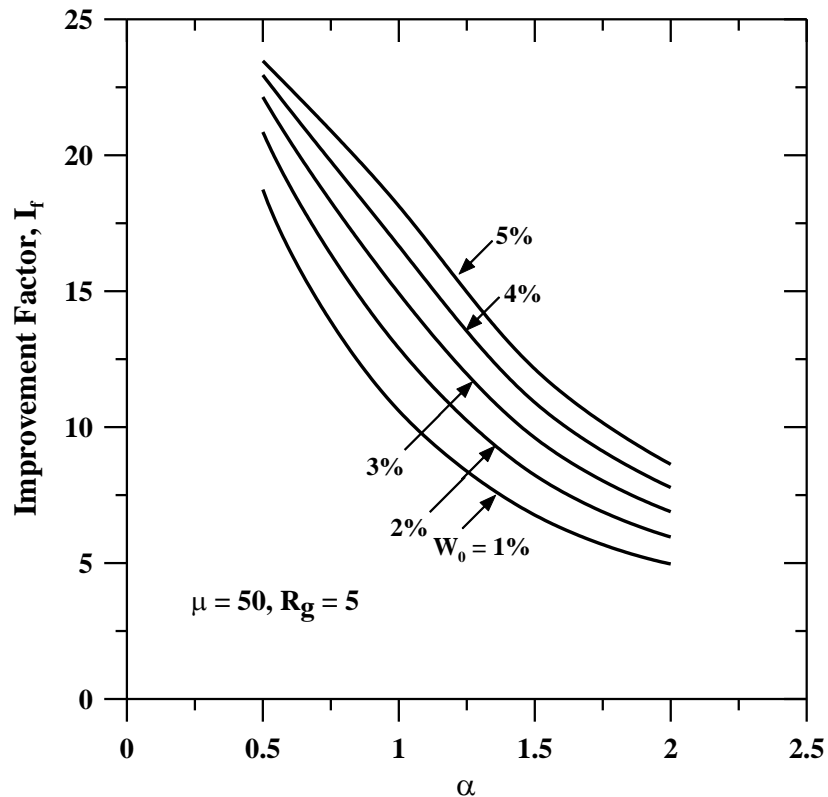


Figure 5.14a: Variation of I_f with α (Constant R_g and μ and varying W_0)

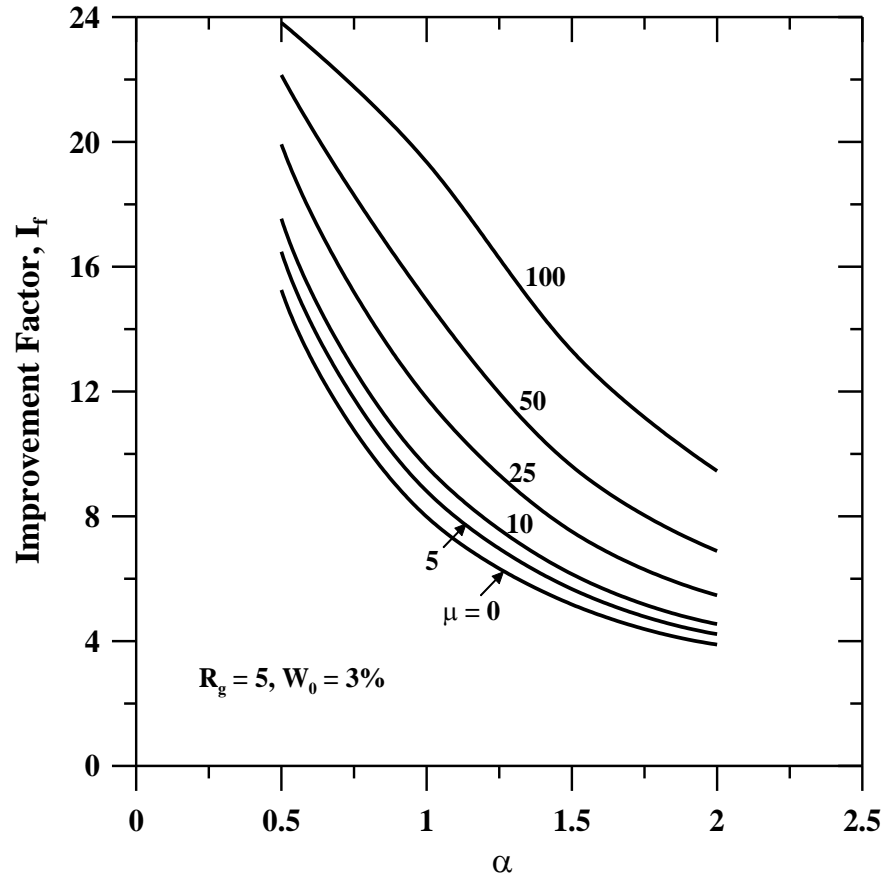


Figure 5.14b: Variation of I_f with α (Constant R_g and W_0 with varying μ)

Figure 5.14: Variation of I_f with α

Figure 5.15a shows the variation of Improvement factor (I_f) with Shear layer width ratio, R_g keeping geocell layer stiffness and settlement constant. The subsoil conditions were varied and the I_f remains low for highly stiff soils as reported earlier. Increase in geocell layer width ratio, R_g beyond 5 has negligible influence on highly stiff soils but for soils of marginal stiffness there is a negligible improvement beyond $R_g=5$.

The variation of improvement factor (I_f) with shear layer width ratio, R_g is shown in Figure 5.15b with constant subsoil conditions and normalised settlement. As reported earlier the improvement is negligible beyond 5. But for very high stiff geocell layer ($\alpha=0.5$) there is considerable improvement even beyond $R_g=5$.

Curves were also plotted for variation in improvement factor (I_f) with shear layer width ratio, R_g for a constant geocell layer stiffness and subsoil condition, but varying the footing

settlement. There is a clear trend of increase in improvement with increase in normalised settlement.

It could be clearly understood from the analysis that providing geocell layer width beyond 5 is not an economical option and has to be avoided unless and until in cases differential settlements are anticipated.

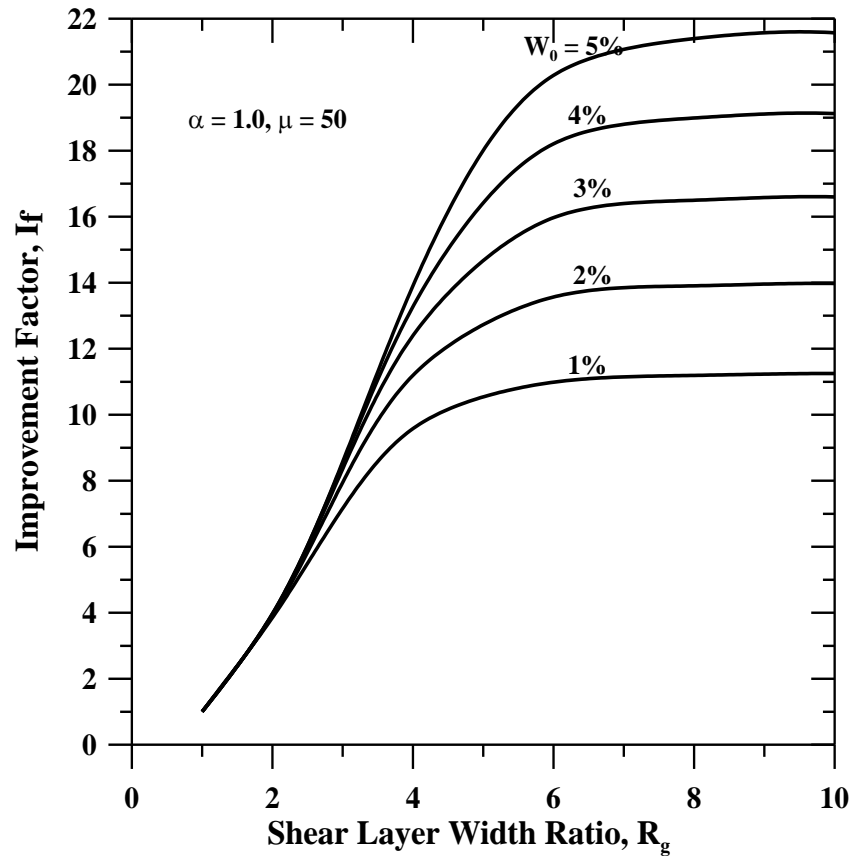


Figure 5.15a: Variation of I_f with R_g (Constant α and μ and varying W_0)

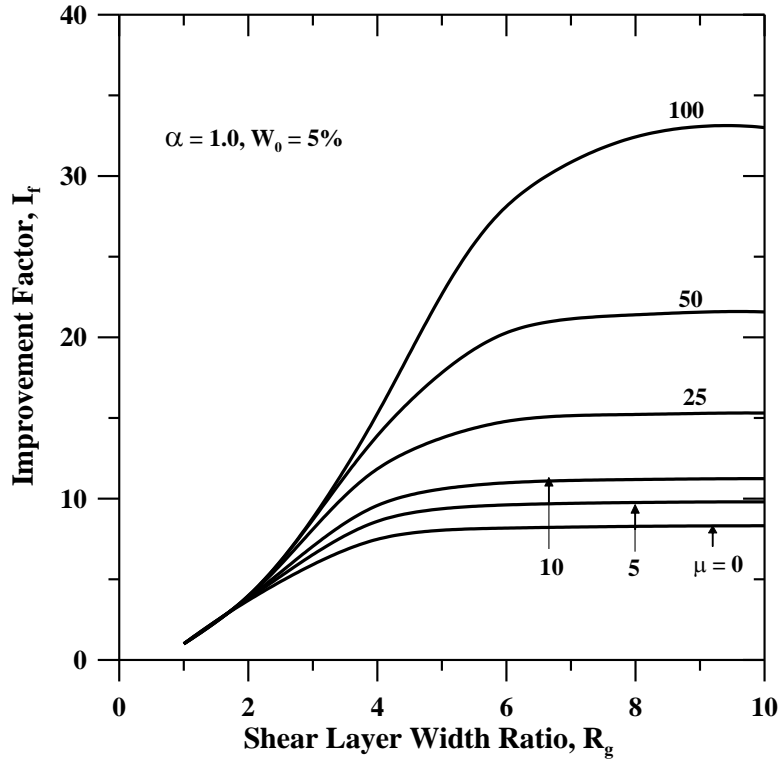


Figure 5.15b: Variation of I_f with R_g (Constant α and W_0 and varying μ)

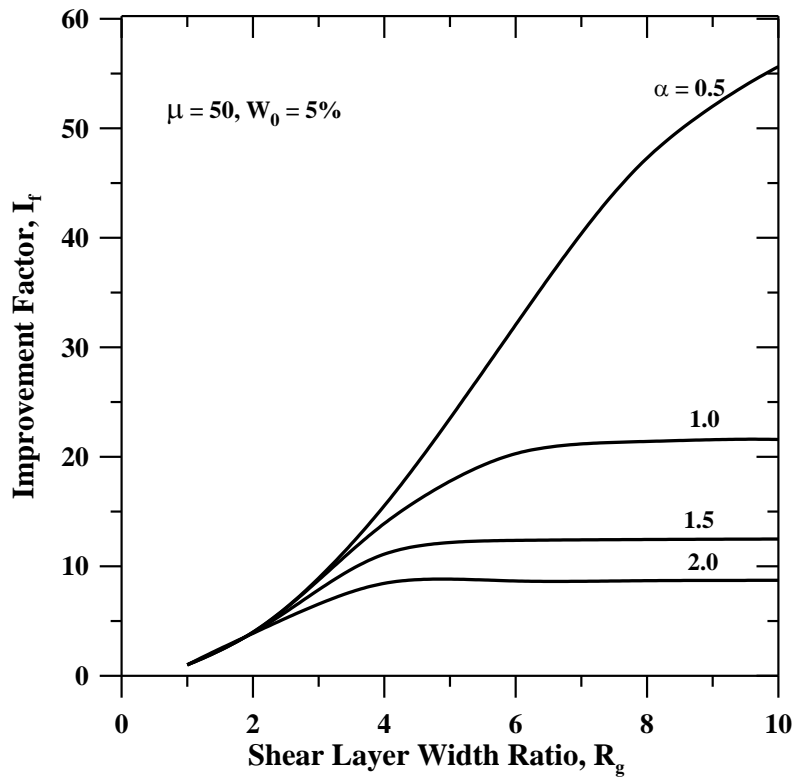


Figure 5.15c: Variation of I_f with R_g (Constant μ and W_0 and varying α)

Figure 5.15: Variation of I_f with R_g

5.5 Summary

Elasto-plastic behaviour of rigid circular footing on geocell reinforced sand beds overlying soft soils has been analysed. Pasternak elastic model was used to idealise the circular footing resting on geocell reinforced soft soils. Following important conclusions are drawn from the study.

- Linear analysis to obtain the load settlement pattern is used when the footing undergoes very low settlements of the order of 1% where the actual load settlement pattern is linear.
- For higher settlements nonlinear response of the footing was used in the analysis.
- To check the validity of the results, the nonlinear model was validated both numerically and theoretically.
- The non-dimensional model parameters, α (inverse of the normalised shear stiffness of the geocell reinforced soil) and μ (inverse of the normalised ultimate bearing capacity) played an instrumental role in modelling the behaviour of circular footing resting on geocell reinforced soils.
- There is significant improvement in ground with the introduction of geocell reinforcement.
- Geocell reinforcement with high stiffness (low α) is able to bear very high load with uniform distribution of the same which enables commendable improvement of very soft soils.
- Low value of μ ($\mu = 0$) represents soils of infinite stiffness which doesn't require further reinforcement and it reflects in the improvement factors that were reported.
- It's is always economical to limit the shear layer width ratio (geocell layer width) to 5, beyond which it provides negligible improvement.

In summary, the model proposed was successful in helping understand the behaviour of rigid circular footing resting on geocell reinforced soils. Geocell reinforcement of soft soils shows a clear trend of improvement.

Chapter 6

Stress Dependent Behaviour of Rigid Strip Footing on Geocell Reinforced Soils

6.1 Problem Statement

The present approach improves the previous model discussed in Chapter 2 by incorporating the confinement effect of the geocell reinforced ground. The major shortcoming in the model discussed earlier is that it doesn't account for the variation in shear modulus in the geocell layer from the centre to the edge of the geocell layer. The present chapter explains the behaviour of geocell reinforced granular layer (associates stress dependency) over soft soil under rigid strip footing as shown in Figure 6.1.

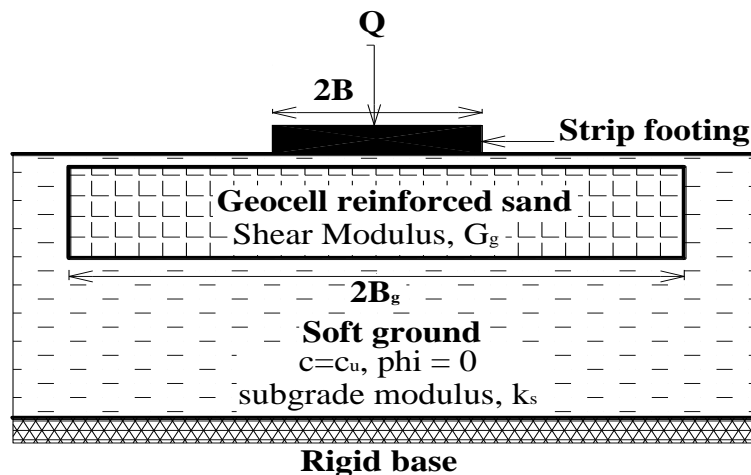


Figure 6.1: Definition sketch of strip footing on geocell reinforced foundation bed

Two parameter elastic model was used to idealize the model (Figure 6.2a). The corresponding deflection profile as per Pasternak model is shown in Figure 6.2b. Since rigid footing is considered the settlement under the loaded strip footing is uniform and the pattern varies from the edge of the footing to the edge of the geocell as described by Pasternak's Equation. The linear and nonlinear response models were analysed for low and high settlements respectively. Soil- Geocell properties were varied to arrive at the optimum parameters of the soil-geocell to obtain economic improvement of the soft ground.

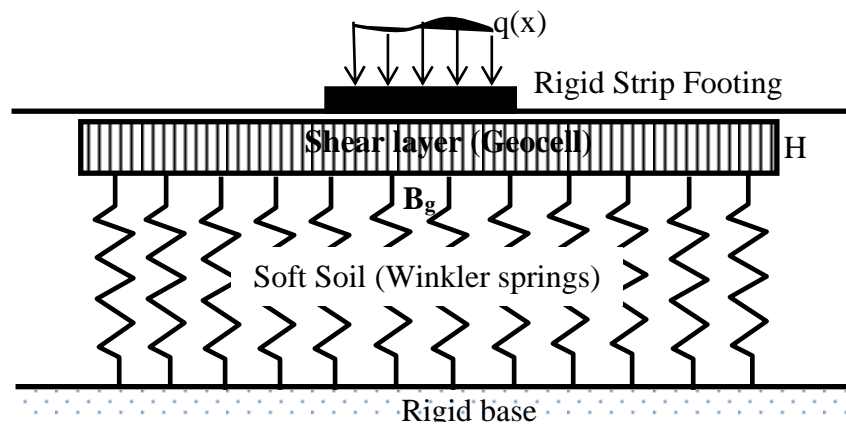


Fig. 6.2a Idealized Pasternak shear layer over Winkler springs

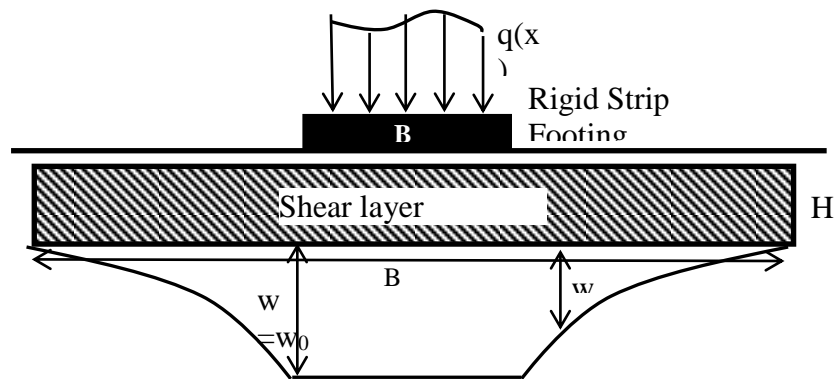


Fig. 6.2b Deflection profile of Pasternak shear layer over Winkler springs

Figure 6.2: Problem definition and deflected profile of the foundation system

6.2 Mathematical Formulation

6.2.1 Linear formulation

The governing equation for the load-deflection pattern of the problem, with the aid of Pasternak model incorporating the stress dependent behaviour is presented below:

$$q(x) = k_s \cdot w_o ; \quad 0 \leq |x| \leq \frac{B}{2} \quad (6.1)$$

$$k_s \cdot w - G_g \cdot H \cdot \frac{d^2 w}{dx^2} = 0 ; \quad \frac{B}{2} \leq |x| \leq \frac{B_g}{2} \quad (6.2)$$

Representing the terms in non-dimensional form, let $X = \frac{x}{B}$, $W = \frac{w}{B}$

Simplifying Equation 6.2 the governing equation reduces to

$$\frac{d^2 W}{dX^2} - \alpha^2 W = 0 \text{ Where } \alpha^2 = \left(\frac{k_s \cdot B^2}{G_g \cdot H} \right) \quad (6.3)$$

Equation (6.3) represents the deflection profile from the edge of the footing to the edge of the geocell. It is well established that the modulus of deformation or the shear modulus of the soil is directly proportional to the confining stress. As per Janbu's relation the shear modulus is a function of confining stress as follows:

$$G = G_0 \left(\frac{\sigma'}{\sigma_0'} \right)^n \quad (6.4)$$

The forces acting on the elemental area in the shear layer is shown in Figure 6.3.

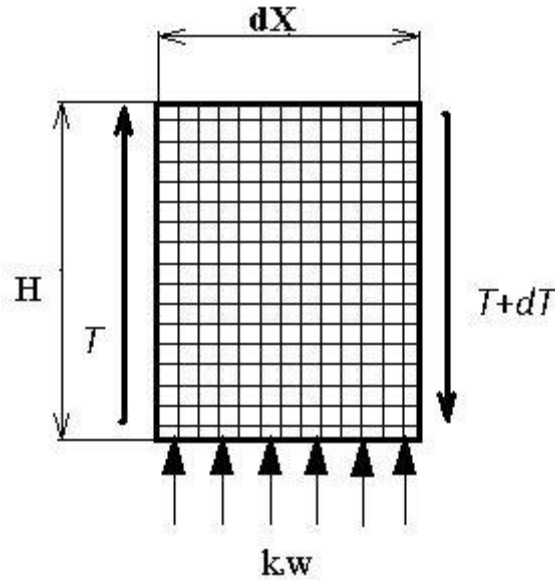


Figure 6.3: Forces acting on an elemental area

Equating forces in vertical direction (Figure 6.3)

Assume the downward forces acting on the element to be zero

$$(k_s w) dx + \tau H - (\tau + \Delta \tau) H = 0 \quad (6.5)$$

Dividing throughout by dx

$$k_s w - \frac{\Delta \tau}{\Delta x} H = 0 \quad (6.6)$$

The shear stress is expressed in terms of shear strain as

$$T = G \frac{dw}{dx} \quad (6.7)$$

Differentiating

$$\frac{\Delta T}{dX} = G \frac{d^2 w}{dx^2} + \frac{dw}{dx} \frac{dG}{dx} \quad (6.8)$$

$$\frac{dG}{dx} = \frac{G_0}{(\sigma_0')^n} n (\sigma_0' + \Delta \sigma')^{n-1} \frac{d\Delta \sigma'}{dx} \quad (6.9)$$

Let us assume the incremental stress, $\Delta \sigma = (k_s w)/2$ (i.e. the average of upward and downward stresses).

Let us represent the initial stress as

$$\sigma_0' = C k_s B \quad (6.10)$$

Substituting,

$$k_s w - G_0 \left(\frac{\sigma_0'}{\sigma_0'} \right)^n H \frac{d^2 w}{dx^2} - \frac{dw}{dx} \frac{G_0}{(\sigma_0')^n} n (\sigma_0' + \Delta \sigma')^{n-1} \frac{d\Delta \sigma'}{dx} H = 0 \quad (6.11)$$

Expressing the eqn. in non-dimensional form

Let $W = w/B$, $X = x/B$,

$$\left(\frac{C + \frac{W}{2}}{C} \right)^n \frac{d^2 W}{dX^2} + \frac{1}{2} \left(\frac{dW}{dX} \right)^2 \frac{1}{C^n} n \left(C + \frac{W}{2} \right)^{n-1} - \alpha^2 W = 0 \quad \text{where } \alpha^2 = \frac{k_s B^2}{G_0 H} \quad (6.12)$$

Equation (6.12) represents the deflection profile from the edge of the footing to the edge of the geocell layer taking into account the geocell properties (α) and confining stresses (C). The parameter, n is assumed as 0.5 in the present analysis.

The load deflection of the formulation is as follows:

$$q(x) \cdot B = Q = k_s B w_0 + 2 \int_{B/2}^{B_s/2} k_s w dx \quad (6.13)$$

Dividing Equation 6.13 with $(k_s B^2)$ yields

$$Q^* = W_0 + 2 \int_{0.5}^{R_g/2} W dX \quad (6.14)$$

6.2.1.1 Validation

Equation (6.12) is a modification of Equation (6.3) incorporating the confinement effect to obtain the deflection profile of rigid strip footing on geocell reinforced soil. Equation (6.12) reduces to Equation (6.3) when $n = 0$. The stress dependent model was validated against the theoretical solution and the results are in good agreement as shown in Figure 6.4. The deviations between the numerical and theoretical results may be due to the truncation and round off errors in finite difference method.

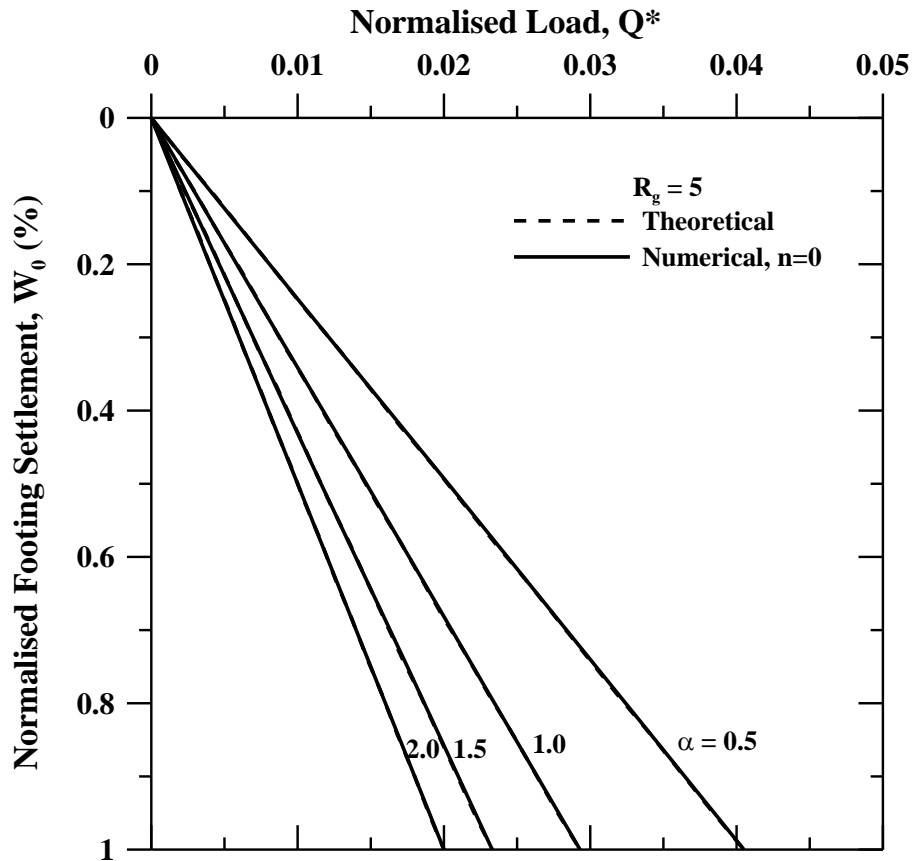


Figure 6.4: Comparison of numerical (after linearization) and theoretical results.

6.2.1.2 Results

The deflection profiles from the edge of the footing to the edge of the geocell are shown in Figure 6.5. The solid lines represent the model that predicts the settlement pattern near to the actual behaviour incorporating the confining stresses in the geocell layer. In normal analysis the shear modulus of the geocell is taken as constant throughout the shear layer whereas the improved model considers the variation in shear modulus of the geocell layer. The improved model shows uniform distribution of load with high bearing capacity.

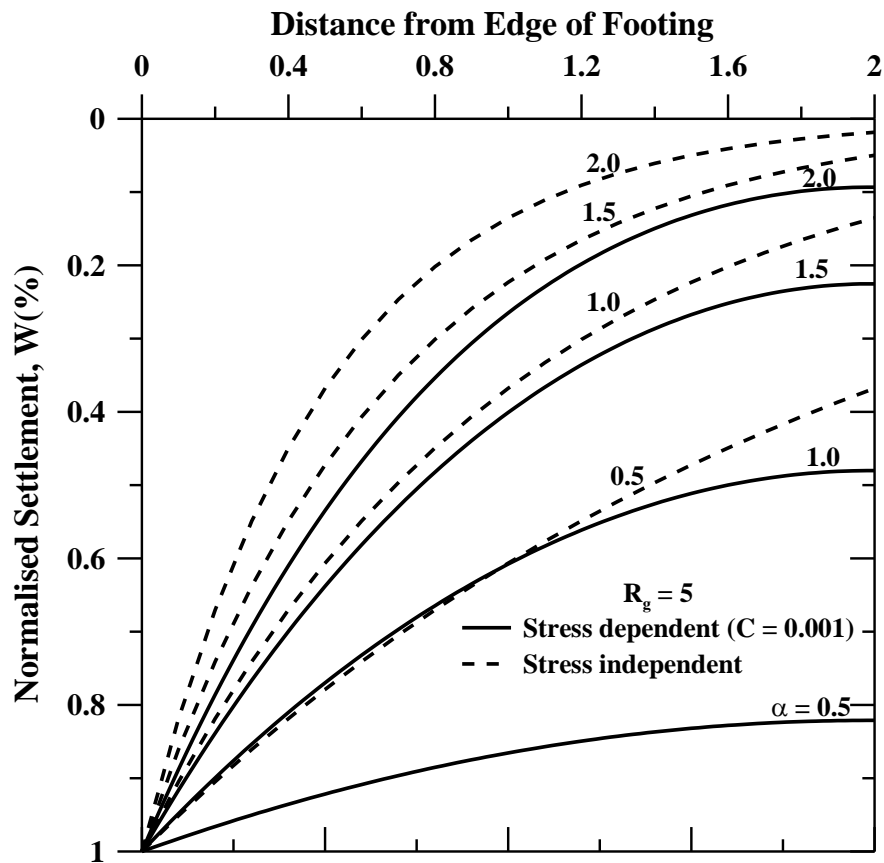


Figure 6.5: Settlement Profile from the edge of the footing to the edge of the geocell layer

The corresponding load settlement with variation in geocell layer stiffness is plotted in Figure 6.6. As expected the model incorporating the confining effect/stress dependency is able to withstand higher loads. The previous model under predicts the actual behaviour. The linear load settlement curve is applicable for very low normalized settlements of the order of 1%.

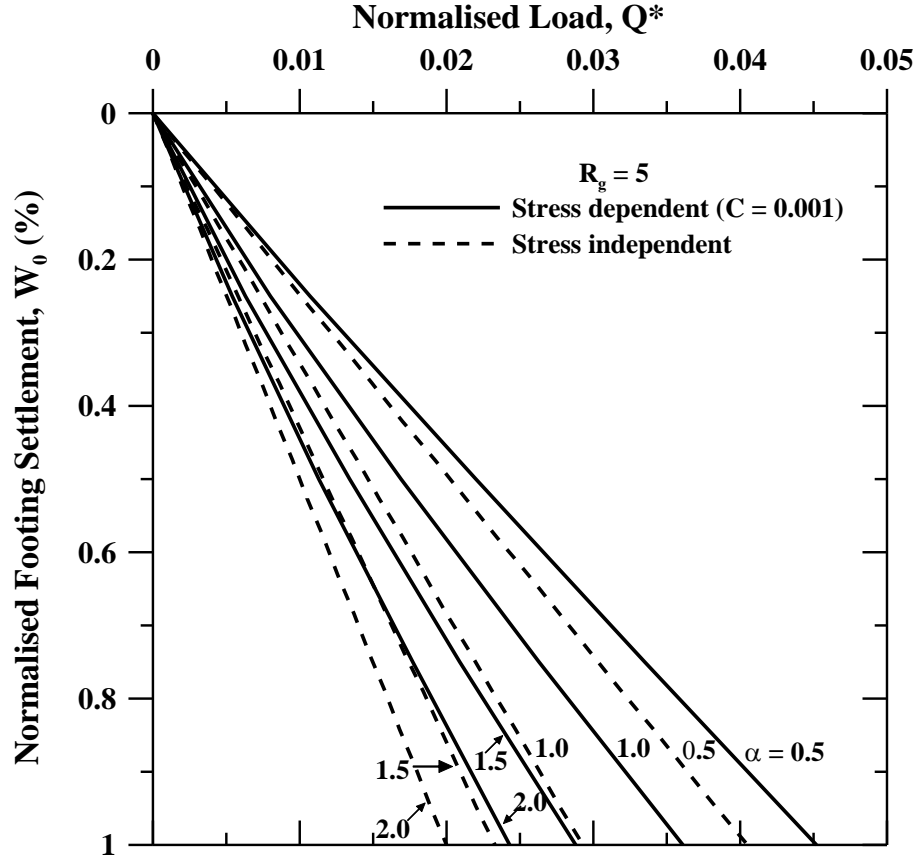


Figure 6.6: Linear load settlement curve (Variation in α)

6.2.2 Nonlinear formulation

The nonlinear stress displacement response of the soil can be represented by hyperbolic relation presented by Kondner (1963)

$$q(x) = \frac{k_s \cdot w_0}{1 + \frac{k_s \cdot w_0}{q_u}} \quad \text{For} \quad 0 \leq x \leq \frac{B}{2} \quad (6.15)$$

$$\frac{k_s \cdot w}{1 + \frac{k_s \cdot w}{q_u}} - G_s H \frac{d^2 w}{dx^2} = 0 \quad \text{For} \quad \frac{B}{2} \leq x \leq \frac{B_g}{2} \quad (6.16)$$

To represent the terms in non-dimensional form, let $X = \frac{x}{B}$, $W = \frac{w}{B}$

Simplifying Equation 6.16 the governing equation reduces to

$$\frac{d^2 W}{dX^2} - \alpha^2 \frac{W}{1 + \mu W} = 0 \quad \text{Where} \quad \alpha^2 = \left(\frac{k_s \cdot B^2}{G_s H} \right) \quad \text{and} \quad \mu = \frac{k_s \cdot B}{q_u} \quad (6.17)$$

Equating forces in vertical direction

Assume $p=0$

$$\left(\frac{k_s w}{1 + \frac{k_s w}{q_u}} \right) dx + \tau H - (\tau + \Delta \tau) H = 0 \quad (6.18)$$

Dividing throughout by dx

$$\left(\frac{k_s w}{1 + \frac{k_s w}{q_u}} \right) - \frac{\Delta \tau}{\Delta x} H = 0 \quad (6.19)$$

$$\left(\frac{k_s w}{1 + \frac{k_s w}{q_u}} \right) - G_0 \left(\frac{\sigma'}{\sigma_0'} \right)^n H \frac{d^2 w}{dx^2} - \frac{dw}{dx} \frac{G_0}{(\sigma_0')^n} n (\sigma_0' + \Delta \sigma')^{n-1} \frac{d\Delta \sigma'}{dx} H = 0 \quad (6.20)$$

In non-dimensional form,

$$\left[\frac{C + \frac{1}{2} \left(\frac{W}{1 + \mu W} \right)}{C} \right]^n \frac{d^2 W}{dX^2} + \frac{1}{2} \frac{1}{C^n} n \left[C + \frac{1}{2} \frac{W}{1 + \mu W} \right]^{n-1} \frac{dW}{dX} \frac{d \left(\frac{W}{1 + \mu W} \right)}{dX} - \alpha^2 \frac{W}{1 + \mu W} = 0 \quad (6.21)$$

Equation (6.21) represents the settlement profile as a function of compaction coefficient, C; inverse of normalized shear stiffness geocell reinforced soil (α), inverse of normalized ultimate bearing capacity of subsoil (μ).

Now the load deflection equation of the formulation is

$$q_f(x) \cdot B = Q_f = \frac{k_s B w_0}{1 + \frac{k_s w_0}{q_u}} + 2 \int_{B/2}^{B_s/2} \frac{k_s w}{1 + \frac{k_s w}{q_u}} dx \quad (6.22)$$

$$Q_f = \frac{k_s B^2 W_0}{1 + \mu W_0} + 2 \int_{B/2}^{B_s/2} \frac{k_s B W}{1 + \mu W} dx \quad (6.23)$$

$$Q_f = \frac{k_s B^2 W_0}{1 + \mu W_0} + 2 \int_{0.5}^{R_s/2} \frac{k_s B^2 W}{1 + \mu W} dX \quad (6.24)$$

$$\frac{Q_f}{k_s B^2} = Q^* = \frac{W_0}{1 + \mu W_0} + 2 \int_{0.5}^{R_s/2} \frac{W}{1 + \mu W} dX \quad (6.25)$$

6.2.3 Finite Difference Formulation

In this study, linear and nonlinear formulations had to be solved using numerical methods. Finite difference method was employed for obtaining the solution. Central difference scheme (Crank-Nicolson method, 1947) was used for discretizing the terms of first order and forward difference scheme (Explicit method) was used for first order terms. The linear governing differential equation was discretized as follows:

$$\left(\frac{C + \frac{W_i}{2}}{C} \right)^n \frac{W_{i+1} - 2W_i + W_{i-1}}{(\Delta X)^2} + \frac{1}{2} \left(\frac{W_{i+1} - W_i}{\Delta X} \right)^2 \frac{1}{C^n} n \left(C + \frac{W_i}{2} \right)^{n-1} - \alpha^2 W_i = 0 \quad (6.26)$$

The equation has to be linearized, to solve using the iterative Gauss Siedel method.

$$\text{Let } h(i) = \left[\frac{C + W_i / 2}{C} \right]^n \text{ where } n=0.5 \quad (6.27)$$

$$h(i) \frac{W_{i+1} - 2W_i + W_{i-1}}{(\Delta X)^2} + \frac{1}{2} \left(\frac{W_{i+1} - W_i}{\Delta X} \right)^2 \frac{1}{C^n h(i)} n - \alpha^2 W_i = 0 \quad (6.28)$$

The governing differential equation is solved to obtain the deflection pattern and the corresponding load deflection equation is solved.

The nonlinear stress dependent model involved high complexity and had to be linearized twice to arrive at the solution. The stress dependent model in finite difference form (Central and forward difference scheme) is represented as follows:

$$\left[\frac{C + \frac{1}{2} \left(\frac{W_i}{1 + \mu W_i} \right)}{C} \right]^n \frac{W_{i+1} - 2W_i + W_{i-1}}{(\Delta X)^2} + \frac{1}{2} \frac{1}{C^n} n \left[C + \frac{1}{2} \frac{W_i}{1 + \mu W_i} \right]^{n-1} \frac{W_{i+1} - W_i}{\Delta X} \frac{\frac{W_{i+1}}{1 + \mu W_{i+1}} - \frac{W_i}{1 + \mu W_i}}{\Delta X} - \alpha^2 \frac{W_i}{1 + \mu W_i} = 0 \quad (6.29)$$

The complexity involved in Equation (6.26) can be reduced by linearizing the equation as follows:

$$\text{Let } g(i) = \frac{W_i}{1 + \mu W_i} \quad (6.30)$$

$$h(i) = \left[\frac{C + g(i)/2}{C} \right]^n \quad \text{Where } n=0.5 \quad (6.31)$$

The equation can be rewritten in the linearized form as

$$h(i) \frac{W_{i+1} - 2W_i + W_{i-1}}{(\Delta X)^2} + \frac{1}{2} \frac{1}{Ch(i)} n \frac{W_{i+1} - W_i}{\Delta X} \frac{\frac{W_{i+1}}{1 + \mu W_{i+1}} - \frac{W_i}{1 + \mu W_i}}{\Delta X} - g(i) \alpha^2 = 0 \quad (6.32)$$

The linearized equation is solved to obtain the deflection pattern and the nonlinear load deflection curves.

6.2.4 Boundary Conditions

The settlement of the rigid strip footing is considered as uniform under the loaded footing area. Hence the normalised settlement (W) at the edge of the footing is equal to the normalised footing settlement (W_0). The slope of the settlement profile (gradient of the settlement profile, dW/dX) is zero at the edge of the geocell layer, ie $R=R_g/2$. These two boundary conditions has been instrumental in solving both linear and non-linear ordinary differential equations.

In mathematical form it can be written as:

$$@R = 0.5, W = W_0$$

$$@R = R_g/2, dW/dX = 0$$

6.3 Validation

6.3.1 Numerical Validation

At very high settlement, the load-settlement curve, Equation (6.25) converges to a constant Q^* , obtained from Equation (6.33).

$$Q^* = \frac{1}{\mu} + 2 \int_{0.5}^{\frac{R_g}{2}} \frac{1}{\mu} dx = \frac{1}{\mu} + \frac{2}{\mu} \left(\frac{R_g}{2} - 0.5 \right) \quad (6.33)$$

To check the accuracy of the stress dependent model, a trial was carried out at 75% settlements to determine whether it matches with the result obtained from Equation (6.33). For $R_g = 5$ and $\mu = 50$, Equation (6.33) yields the solution 0.1. The result obtained from numerical (MATLAB) analysis is 0.0974. The percentage error is -2.73%. This error is due to truncation and round off errors in finite difference method.

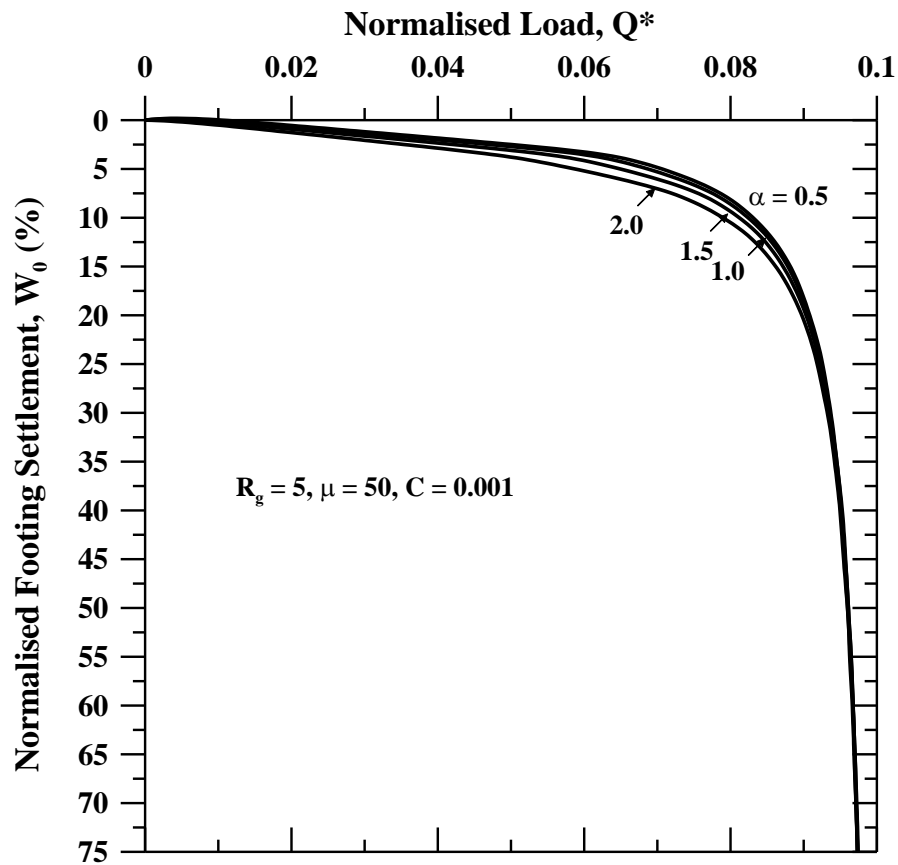


Figure 6.7: Normalized load settlement curve at very high settlement.

6.3.2 Theoretical Validation

The model incorporating stress dependency (Equation 6.21) reduces to the nonlinear model (Equation 6.17) when Janbu's parameter, $n=0$. Similar analysis was carried out on the stress dependent model by substituting $n=0$ and results of nonlinear and stress dependent model were found to be in good agreement.

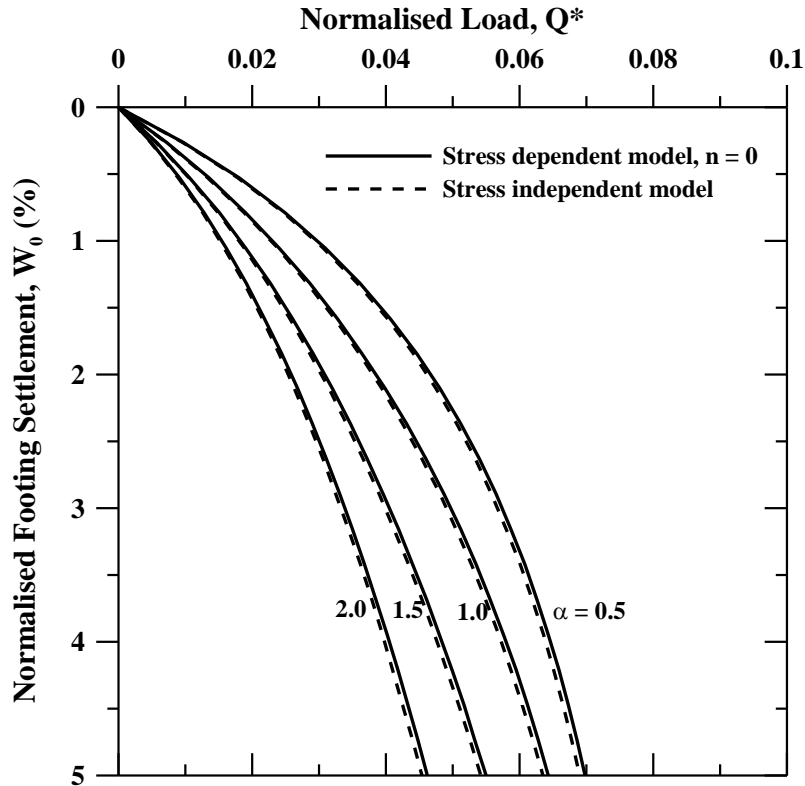


Figure 6.8: Normalized load settlement curve – Comparison of stress dependent and nonlinear model

6.3.3 Experimental Validation

Efficiency of the current model was reviewed with the help of experimental investigations on strip footing on geocell reinforced sand bed that were conducted by Moghaddas et al. From the experimental data the modulus of subgrade reaction, ultimate bearing capacity, static shear modulus of geocell reinforced layer (obtained from elastic modulus) were determined and the values of inverse of shear modulus of the geocell reinforced soil (α) and the inverse of the ultimate bearing capacity of the subsoil (μ) were calculated.

Figure 6.9 shows the load settlement curve of the nonlinear model, stress dependent model and experimental data for various thickness of the geocell reinforced layer. The prediction of the nonlinear model were valid for low normalized settlements of the order of 5% and for higher normalized settlements stress dependent model predicts better. Three cases of the experimental test were analyzed and over the complete range of 0-20% the results are in good agreement both qualitatively and quantitatively.

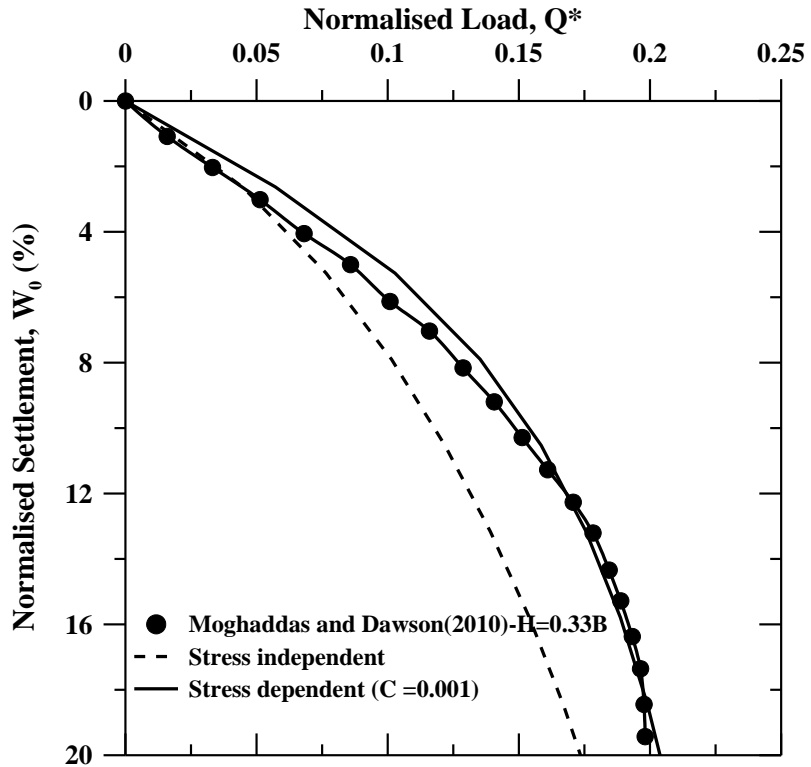


Figure 6.9a: Normalized load settlement curve ($H=0.33B$)

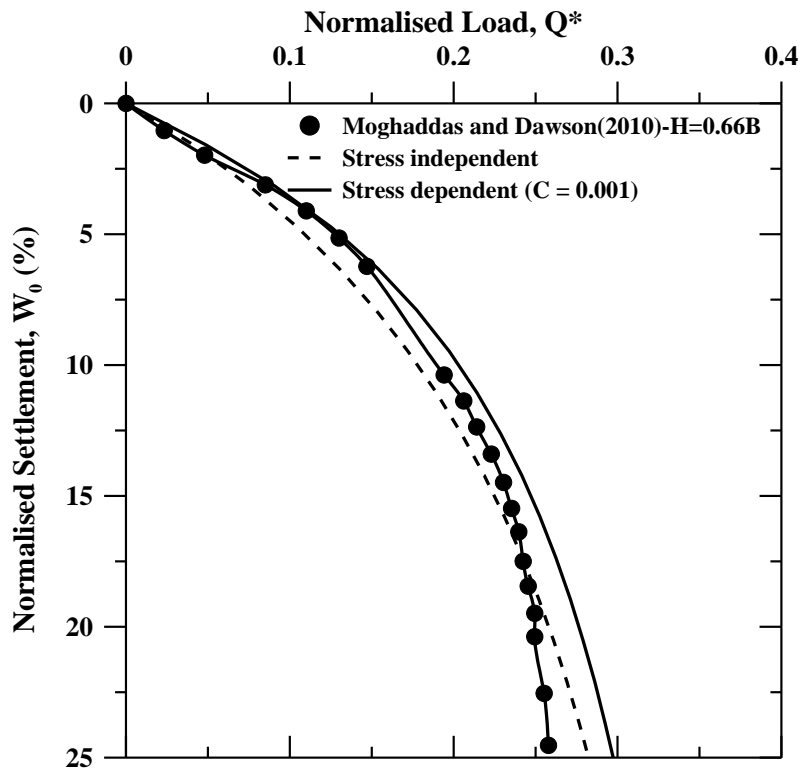


Figure 6.9b: Normalised load settlement curve ($H=0.66B$)

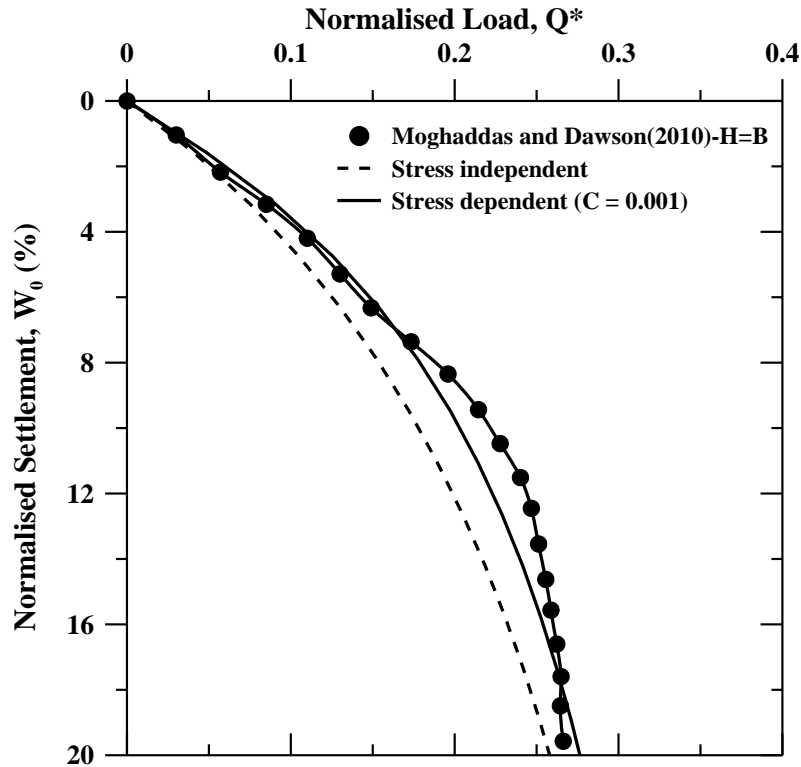


Figure 6.9c: Normalized load settlement curve (H=B)

Figure 6.9: Normalized load settlement curve – Comparison of the stress dependent and nonlinear model with experimental data

6.4 Results and Discussion

The deflection profile from the edge of the footing to the edge of the geocell layer as described by Pasternak model incorporating the nonlinear response and stress dependent behaviour are shown in Figure 6.10. Equation (6.17) representing the deflection pattern as a function of α and μ is plotted as dashed line in Figure 6.10. From the figure it's clear that the nonlinear model without stress dependency doesn't distribute the load uniformly and for geocells with high shear stiffness the behaviour varies significantly. The corresponding load settlement pattern is shown in Figure 6.11. The load settlement pattern shows minimal variation with increase in geocell layer stiffness when the confinement effect of the geocell is also taken into account. But similar trend of variation as the nonlinear model is observed here. The load taken by geocells of high shear stiffness is high but the variation is comparable with that of geocells of low shear stiffness.

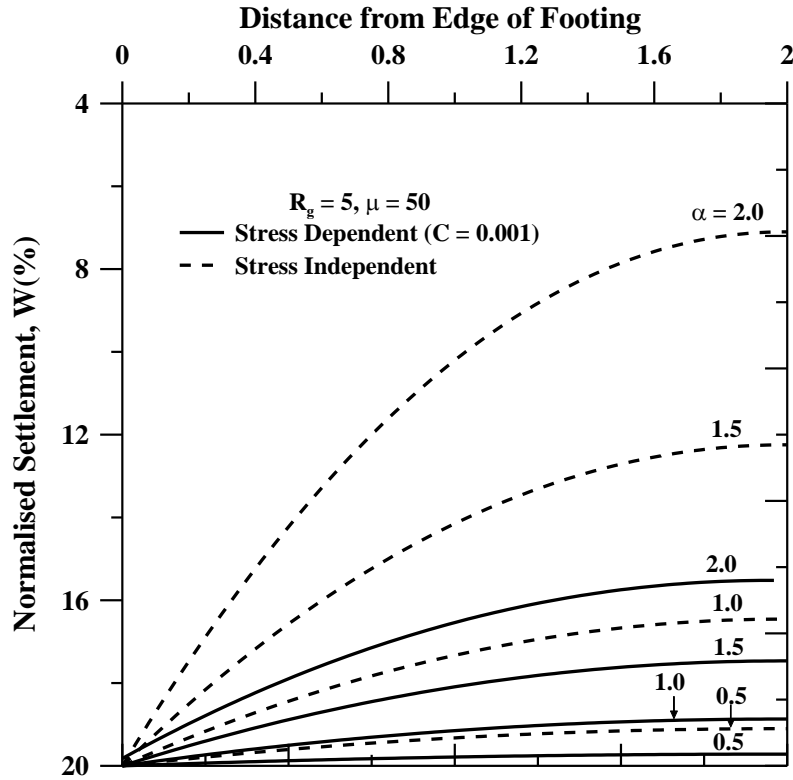


Figure 6.10: Deflection profile from the edge of the footing to the edge of the geocell

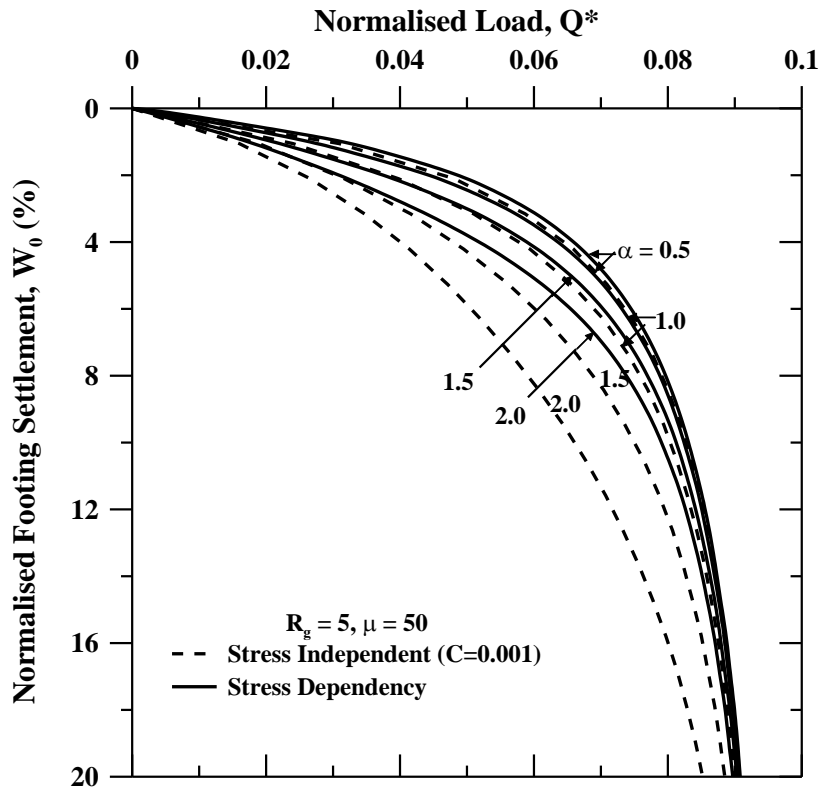


Figure 6.11: Normalized load settlement curve (Variation in α)

The deflection profile from the edge of the footing to the edge of the geocell with variation in subsoil conditions is shown in Figure 6.12. There is minimal effect on the settlement pattern with variation in subsoil condition for the model with incorporation of confinement effect whereas the previous nonlinear model shows significant variation in settlement pattern with variation in subsoil conditions. It was also observed from the figure that there is a uniform distribution of load for soils with low ultimate bearing capacity than stiffer soils.

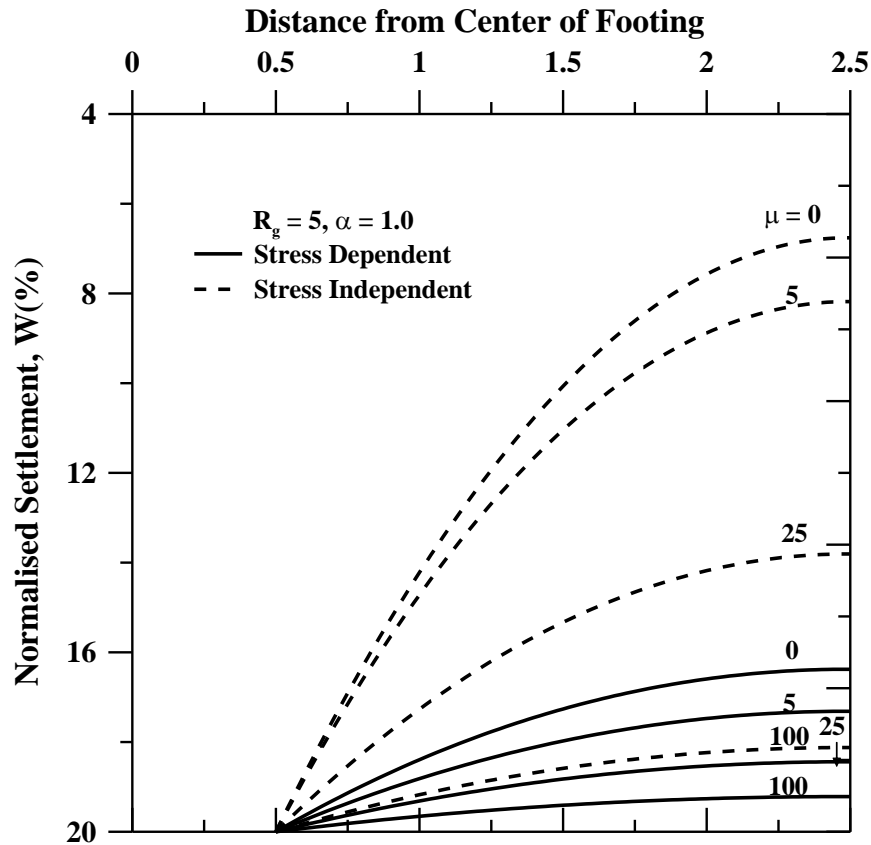


Figure 6.12: Deflection profile from the edge of the footing to the edge of the geocell

The corresponding normalized load settlement curve is plotted in Figure 6.13. The variation in load taken by the geocell reinforced soil is high especially when the subsoil is of high strength. Due to the all-round confinement the geocell offers the soil is able to withstand higher stresses.

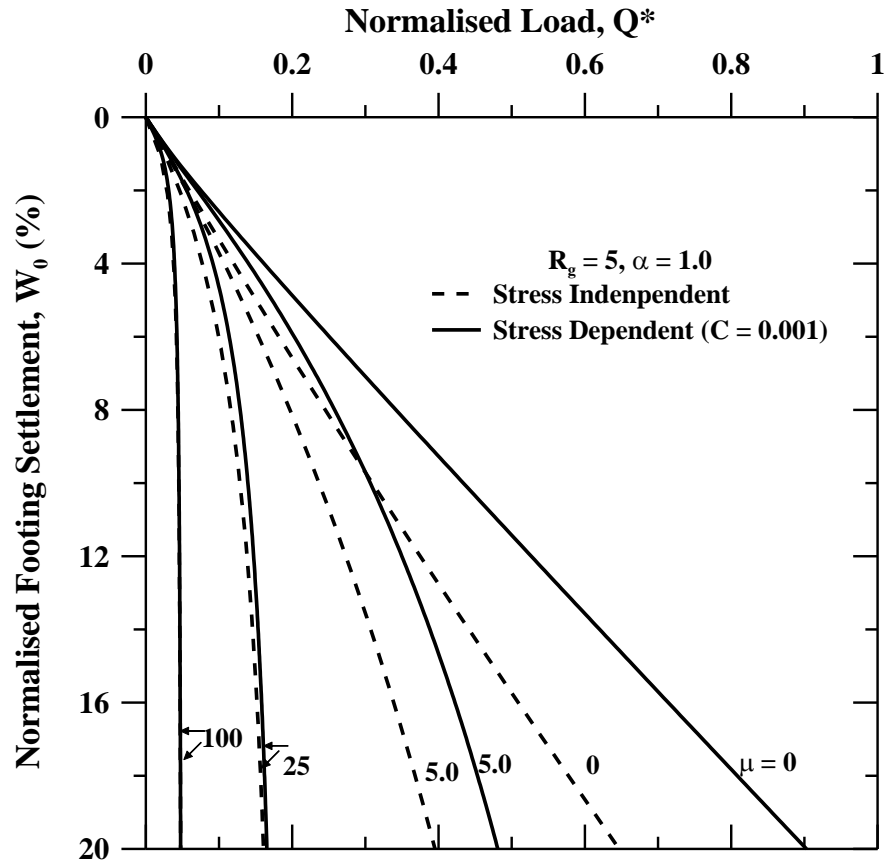


Figure 6.13: Normalized load settlement curve (Variation in μ)

Figure 6.14 shows the normalized load settlement curve for various compaction coefficients over the range of 0-20%. The variation in pattern of load settlement curve with stress dependency is significant over the range of 0-20% and further converges to constant value. The variation in load settlement curve was found to be maximum for lower range of μ values.

The variation in improvement factor (I_f) with inverse of normalized shear stiffness (α) is plotted in Figure 6.15. Figure 6.15a shows the variation of I_f with subsoil stiffness and an interesting observation that was inferred from the plot is that for soils of high stiffness ($\mu=0$) the improvement factors that are reported is low because the load bearing capacity of the soil with high stiffness is very high and further improvement with the inclusion of geocell is marginal. Figure 6.15b shows improvement with variation in normalized settlement and as expected higher improvement is shown at higher settlements. It could be also seen that there is a clear trend of decrease in improvement with low geocell layer stiffness ($\alpha = 2$) especially for soils with high ultimate bearing capacity and lower range of settlements (3-10%). For high range of settlements and soils with low stiffness the improvement remains almost the same with increase in α .

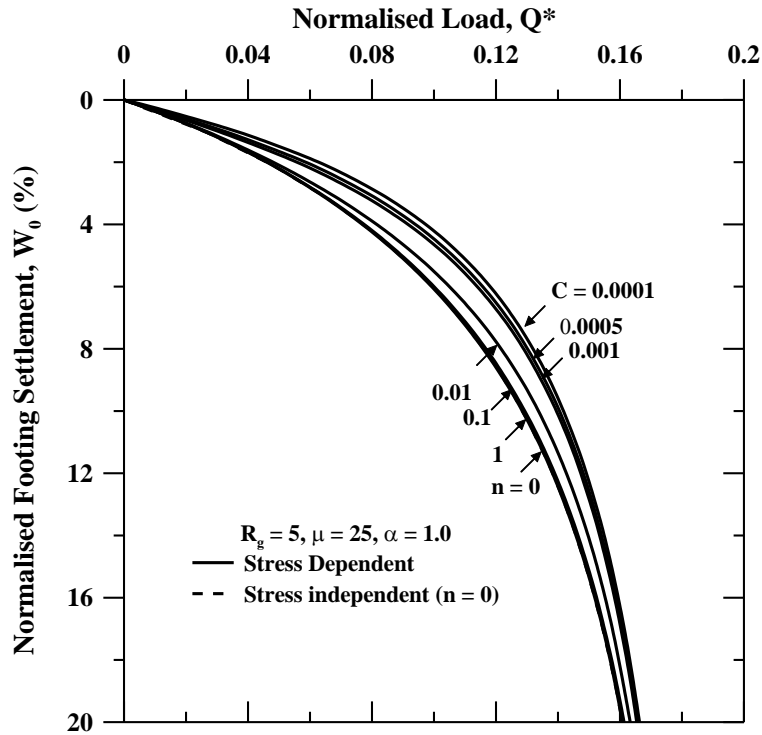


Figure 6.14a: Normalized load settlement curve for varying C ($\mu = 25$, $\alpha = 1$)

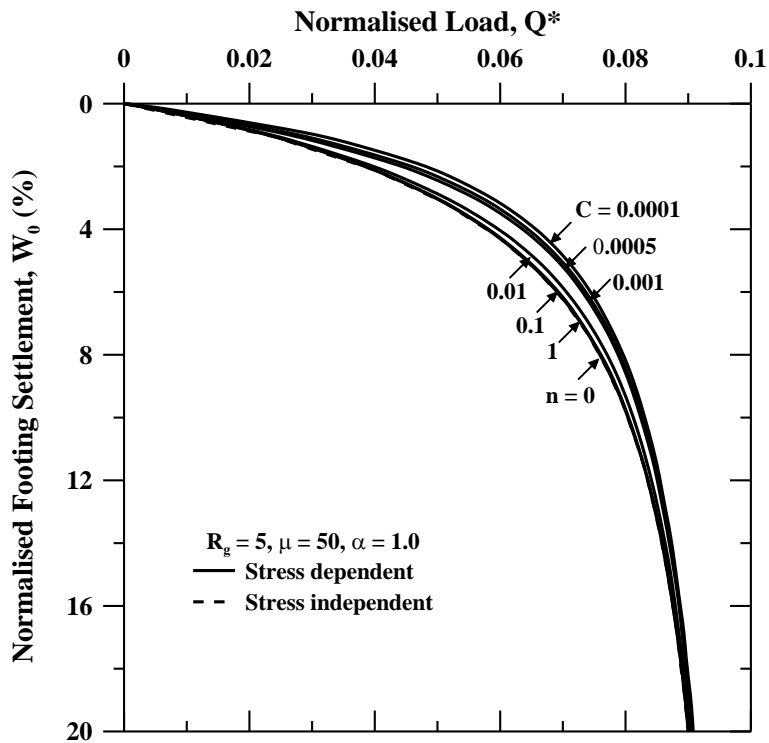


Figure 6.14b: Normalized load settlement curve for varying C ($\mu = 50$, $\alpha = 1$)

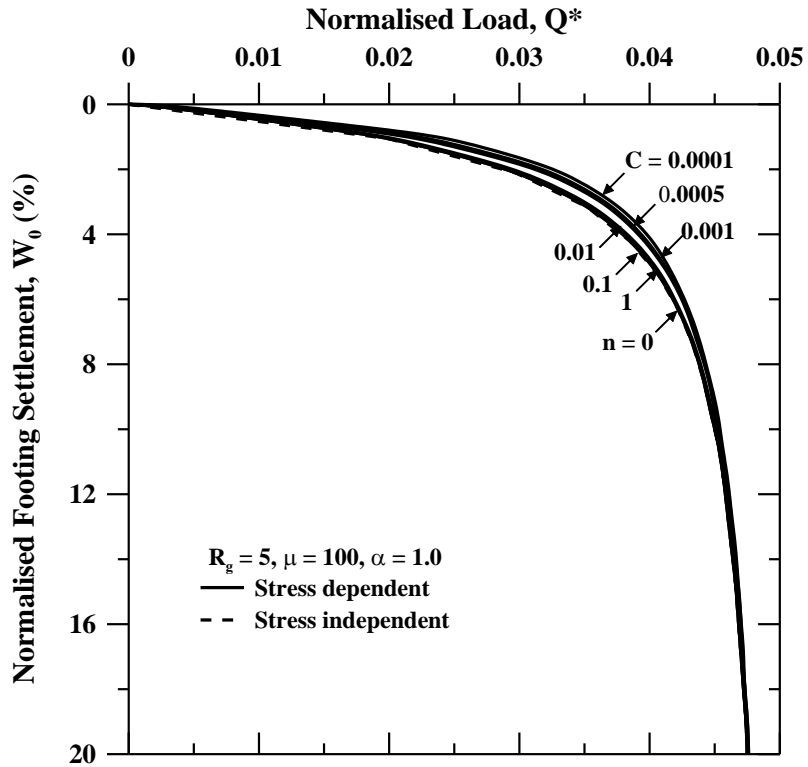


Figure 6.14c: Normalized load settlement curve for varying C ($\mu = 100, \alpha = 1$)

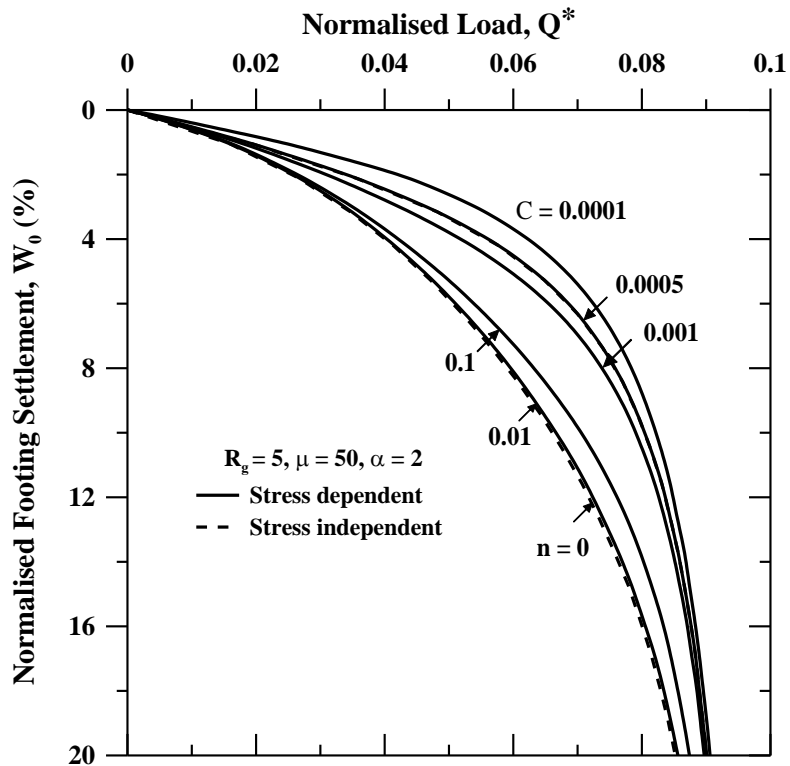


Figure 6.14d: Normalized load settlement curve for varying C ($\mu = 50, \alpha = 2$)

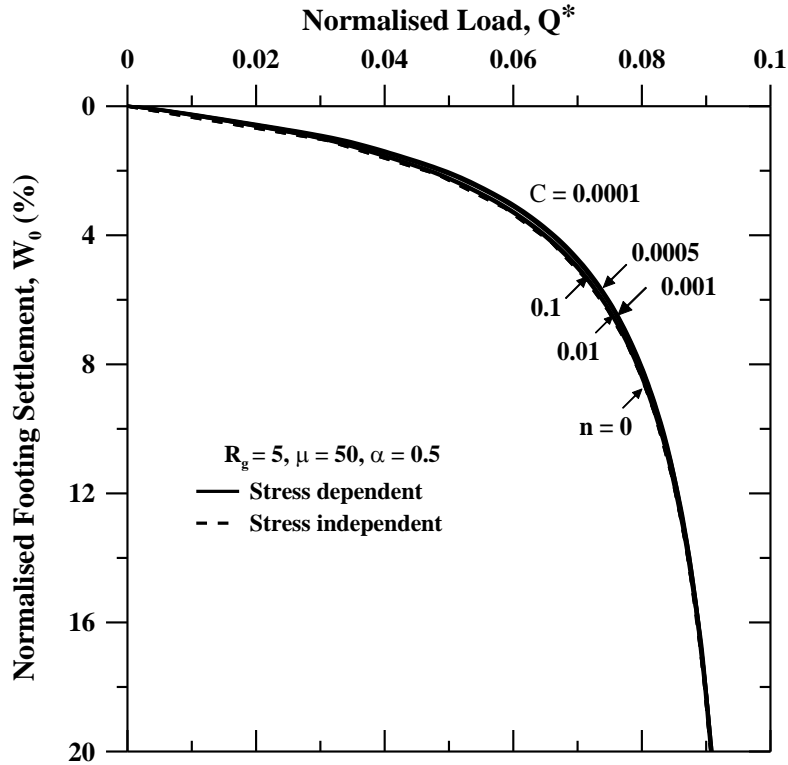


Figure 6.14e: Normalized load settlement curve for varying C ($\mu = 50, \alpha = 0.5$)

Figure 6.14: Normalized load settlement curve (Variation in C)

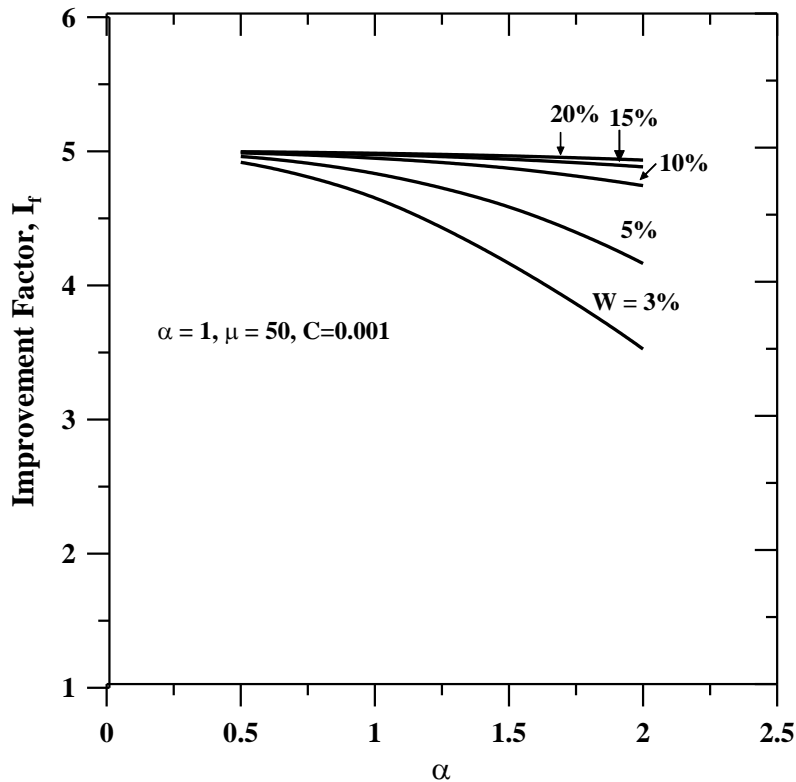


Figure 6.15a: Variation of I_f with α (Varying W_0)

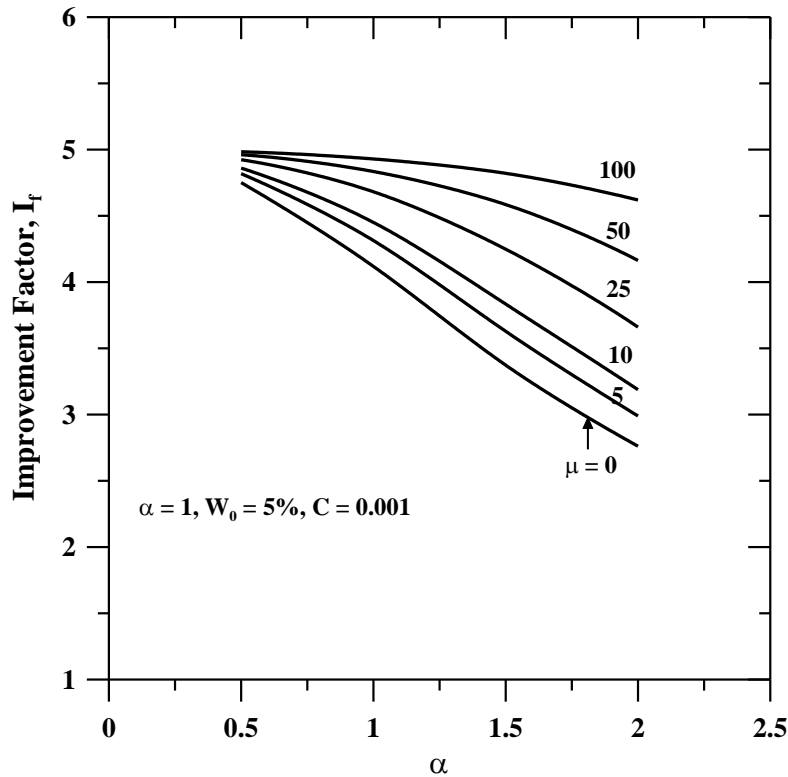
Figure 6.15a: Variation of I_f with α (Varying W_0)**Figure 6.15: Variation of improvement factor (I_f) with inverse of normalized shear stiffness (α)**

Figure 6.16 shows the variation of improvement factor (I_f) with shear layer width ratio (R_g) by varying various parameters (μ , C , α , W_0). There is a clear trend of improvement with increase in geocell layer width but the improvement remains stagnant beyond R_g 5 in usual cases. For subsoil of low stiffness, providing R_g beyond 5 also gives significant improvement (Figure 6.16a). Similarly, there is a convincing improvement after R_g 5 for geocell layer of high stiffness, however improvement is negligible for geocell layers of low stiffness ($\alpha=2$, Figure 6.16b). The compaction factor, C that determines the confining stress in geocells were varied for constant soil-geocell properties and normalized settlement and there was a clear trend of improvement with increase in geocell layer width ratio even up to 10. The improvement factor that is reported is very high by incorporating the impact of confining stresses (Figure 6.16c). The improvement of the soil increase at a constant rate at settlements of the order of 15% but for lower settlements of the order of 5% there isn't a further improvement for shear layer width ratio beyond 5.

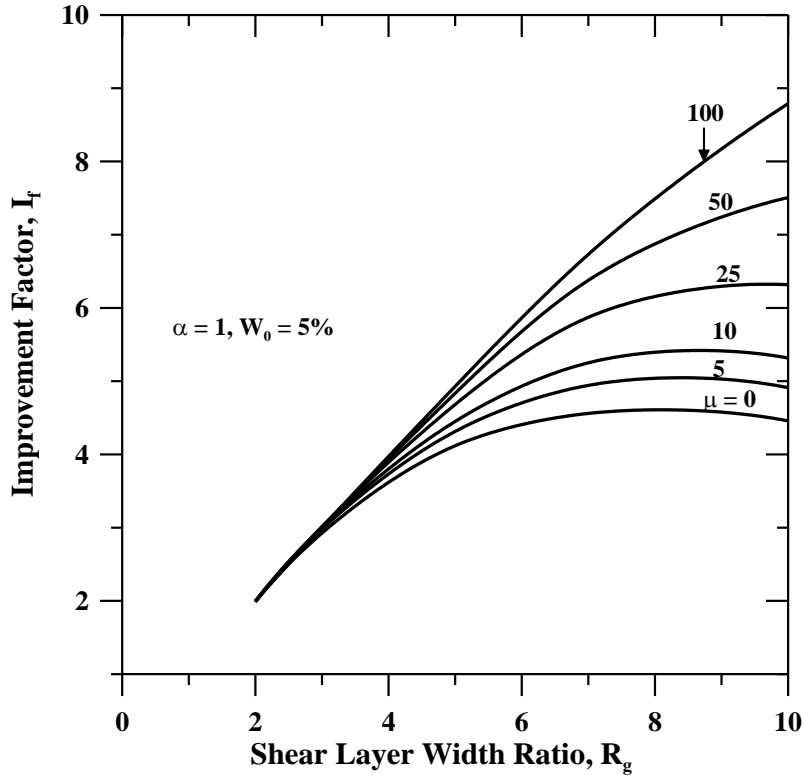


Figure 6.16a: Variation of I_f with R_g (Varying μ)

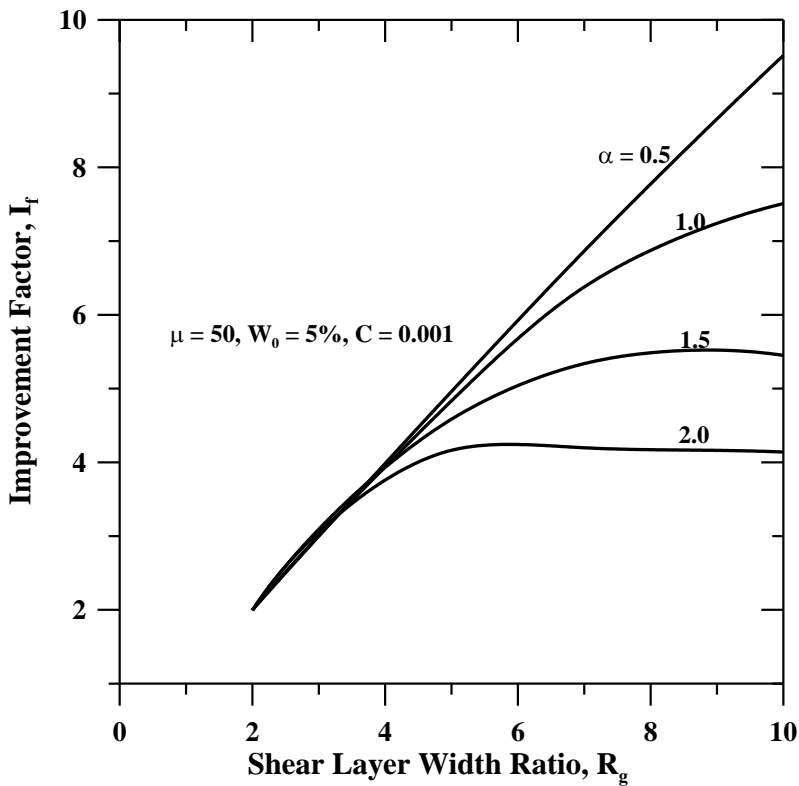


Figure 6.16b: Variation of I_f with R_g (Varying α)

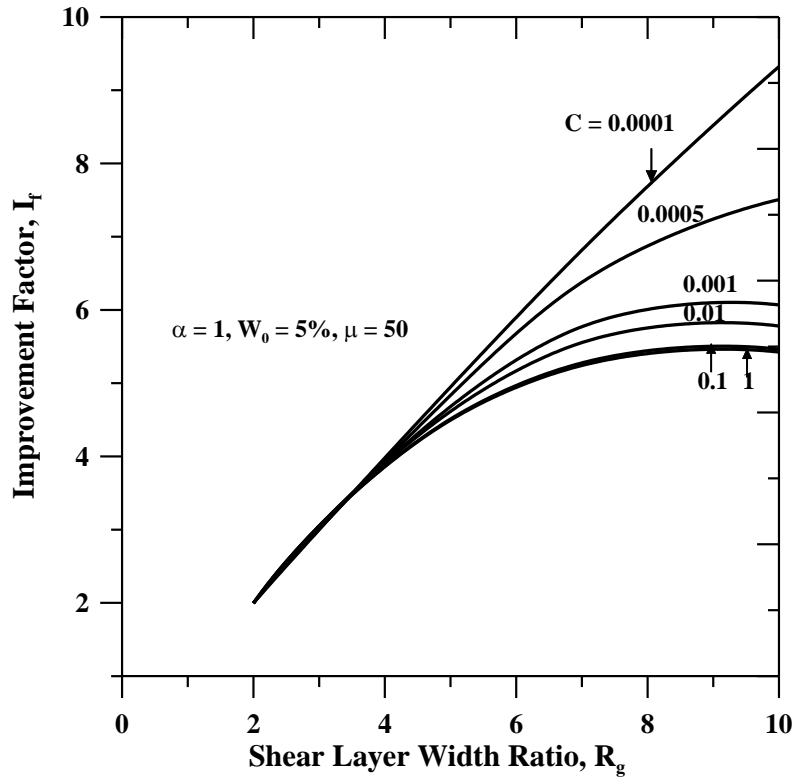


Figure 6.16c: Variation of I_f with R_g (Varying C)

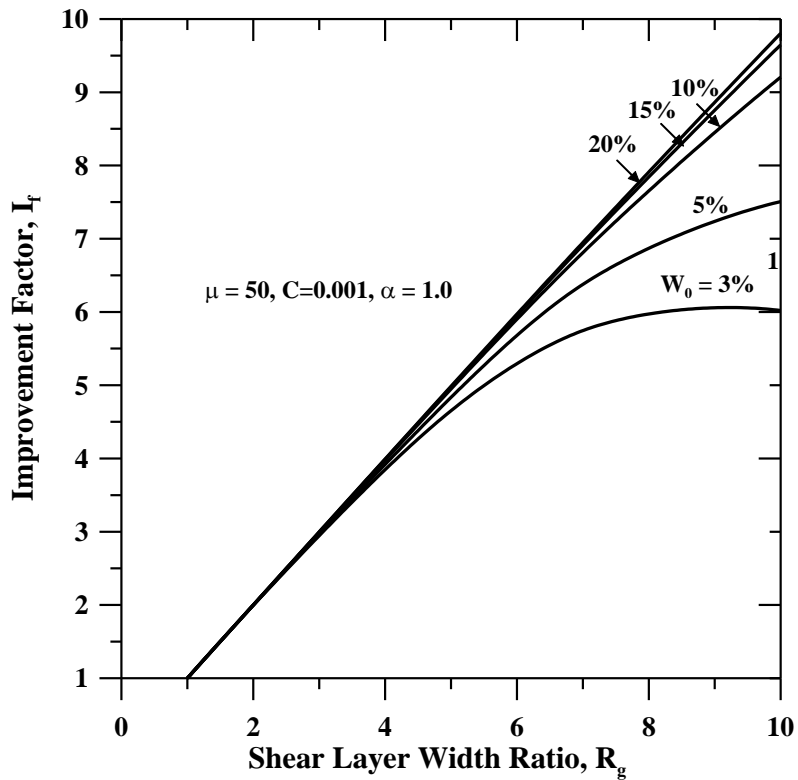


Figure 6.16b: Variation of I_f with R_g (Varying W_0)

Figure 6.16: Variation of improvement factor (I_f) with shear layer width ratio (R_g)

6.5 Summary

An endeavor has been made to numerically simulate the elasto-plastic behaviour of rigid strip footing on geocell reinforced beds incorporating the stress dependency of the geocell layer. Linear and nonlinear responses were studied at low and high settlements respectively. With the aid of foundation models viz. Pasternak model the deflection profiles were obtained numerically (finite difference scheme) and the loads were calculated. Some of the important observations that were drawn from the study are listed below:

- Linear response model which is the simplest approach has to be used for low settlements ($W_0 \approx 1\%$) and nonlinear response has to be taken into account for higher settlements.
- The nonlinear stress independent model performs well for lower settlements but for higher settlements the model that incorporates stress dependency has to be used.
- The parameters that were analyzed in the current study are inverse of the normalized shear stiffness (α), inverse of the normalized ultimate bearing capacity (μ), Compaction coefficient (C) and normalized settlement (W_0).
- To check the consistency and accuracy of the code, it was validated by comparing the model with the nonlinear stress independent model by reducing it into stress independent model. The model was also compared with experimental results. It was also checked numerically whether it converges to a constant value at higher settlements. The current model was found to perform well for the above mentioned cases.
- The current model is an improvement of the previous nonlinear stress independent model as it incorporates the actual behaviour of geocell which derives its strength from the all-round confinement effect. The previous model under predicts the load bearing capacity of geocell reinforced ground.
- There is a clear trend of improvement with increase in the shear stiffness of the geocell reinforced ground at low settlements and high stiffness of the subsoil whereas there isn't any considerable improvement at higher settlements and low stiffness of the subsoil.
- It was also reported that there is an increase in load bearing capacity with higher values of geocell layer width but to be on the economical side it is always good to restrict the geocell layer width to 5.
- The design charts that are proposed could be used for designing geocell reinforced foundations of strip footing.

- Lower value of C induces the confinement effect or stress dependent behaviour and as it increases or tends to infinity it behaves similar to nonlinear stress independent model. Appropriate value of C has to be chosen based on initial stresses.
- The improvement that is brought to soft subsoil is significant with the introduction of geocell reinforcement and the soft soil is able to withstand higher loads.

In summary, the present approach of calculating the improvement factors or loads is a better approach as it accounts for the confining stresses in the geocell from which the geocell reinforced subsoil derives its strength.

Chapter 7

Stress Dependent Behaviour of Rigid Circular Footing on Geocell Reinforced Soils

7.1 Problem Statement

The present chapter deals with an improvement of the previous approach (nonlinear stress independent response) discussed in Chapter 5 by incorporating the confining stresses of the geocell reinforced soil. The present study gives a brief exposition of the behaviour of a rigid circular footing resting on geocell reinforced soft soil taking into account the variation of shear modulus of geocell reinforced soil (stress dependency). The definition sketch of the rigid circular footing resting on geocell reinforced soil is shown in Figure 7.1.

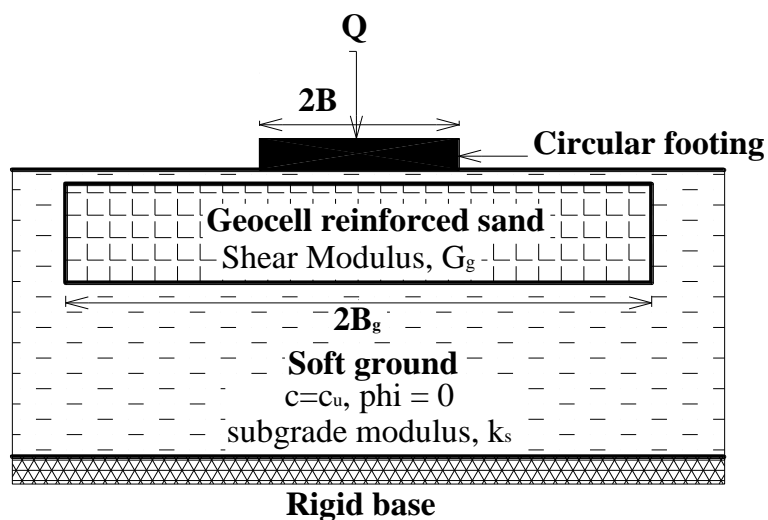


Figure 7.1: Definition sketch of circular footing on geocell reinforced soils

The system is idealised by considering two parameter elastic Pasternak model as shown in Figure 7.2. The corresponding deflection profile is shown in Figure 7.3. Since circular footing is involved, axisymmetric modelling is done. Uniform displacement is considered beneath the

footing and second order differential equation was used to represent the deflection profile from the edge of the footing to the edge of the geocell. The present chapter discusses the mathematical formulation that incorporates the stress dependency; linear and nonlinear response models for low and high settlements respectively and the improvement brought about in the soft ground are reported.

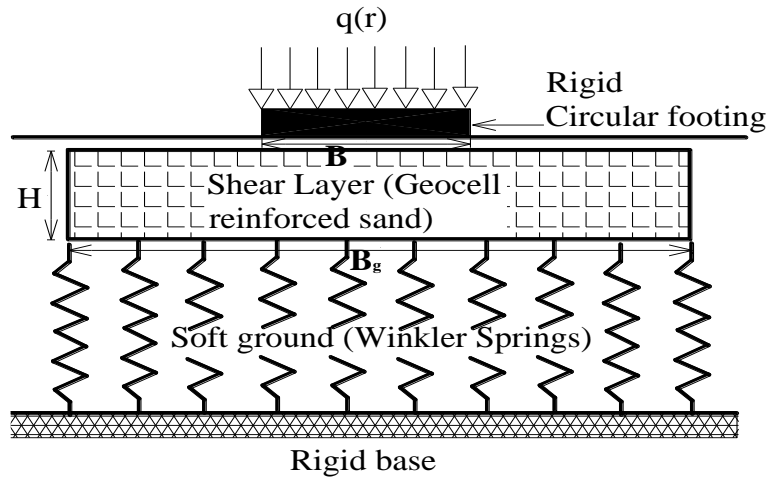


Figure 7.2: Idealisation of Geocell reinforced soils – Pasternak model

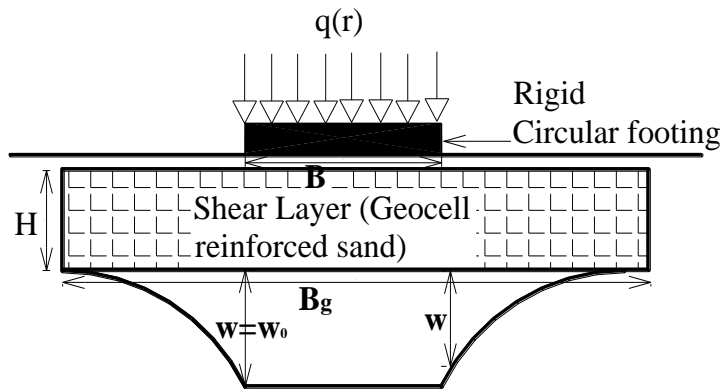


Figure 7.3: Cross – sectional view of the deflection profile of rigid circular footing.

7.2 Mathematical Formulation

The governing equation as described by Pasternak is improved by incorporating the stress dependent behaviour from which geocell derives its major strength. Linear and nonlinear

formulations are discussed below which are applicable for low and high settlements respectively. The current section gives a brief review regarding the same.

7.2.1 Linear Formulation

The governing equation for the load-deflection pattern of the problem considering the shear layer representing the geocell mattress, as described in Pasternak model, is as follows:

$$q(r) = k_s \cdot w_o \quad \text{for } |r| \leq \frac{B}{2} \quad (7.1)$$

$$k_s w - G_g H \left(\frac{d^2 w}{dr^2} + \frac{1}{r} \frac{dw}{dr} \right) \quad \text{for } |r| \geq \frac{B}{2} \quad (7.2)$$

Let r be the radial distance from the central axis, w be the settlement.

Expressing the terms in non-dimensional form,

Let $R=r/B$ and $W=w/B$ where B is the diameter of the footing.

Simplifying Equation (7.2) the governing differential equation reduces to

$$\frac{d^2 W}{dR^2} + \frac{1}{R} \frac{dW}{dR} - \alpha^2 W = 0 \quad \text{Where } \alpha^2 = \frac{k_s B^2}{G_g H} \quad (7.3)$$

Equation (7.3) represents the deflection profile from the edge of circular footing to the edge of the geocell layer. To attend to the confining stresses that acts on the geocell reinforced layer, Janbu's (equation 7.2) relation that accounts for the variation of shear modulus is used.

The quarter symmetric plan view of a circular footing resting on geocell mattress with all the dimensions is shown in Figure 7.4. The vertical forces acting on an elemental block taken from the strip is shown in Figure 7.5.

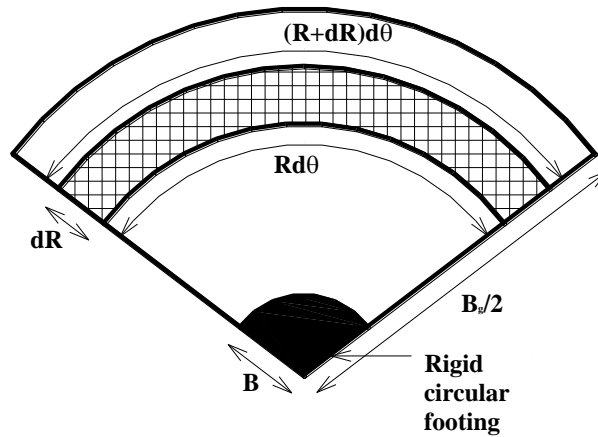


Figure 7.4: Plan view of a circular strip of a circular footing.

Equating forces in vertical direction (Figure 7.5)

$$k_s w (r \Delta \theta \Delta r) + \tau (r \Delta \theta) H - (\tau + \Delta \tau) (r + \Delta r) \Delta \theta H = p (r \Delta \theta \Delta r) \quad (7.4)$$

$$k_s w (r \Delta \theta \Delta r) + \tau (r \Delta \theta) H - H (\tau r \Delta \theta + \tau \Delta r \Delta \theta + \Delta \tau r \Delta \theta + \Delta \tau \Delta r \Delta \theta) = p (r \Delta \theta \Delta r) \quad (7.5)$$

Neglecting the higher order terms and simplifying the equation,

$$k_s w (r \Delta \theta \Delta r) - H (\tau \Delta r \Delta \theta + \Delta \tau r \Delta \theta) = p (r \Delta \theta \Delta r) \quad (7.6)$$

Dividing Equation (7.6) by $r \Delta \theta \Delta r$

$$k_s w - H \left[\frac{\tau}{r} + \frac{\Delta \tau}{\Delta r} \right] = p \quad (7.7)$$

$$\text{Shear stress, } \tau = G \frac{dw}{dr} \quad (7.8)$$

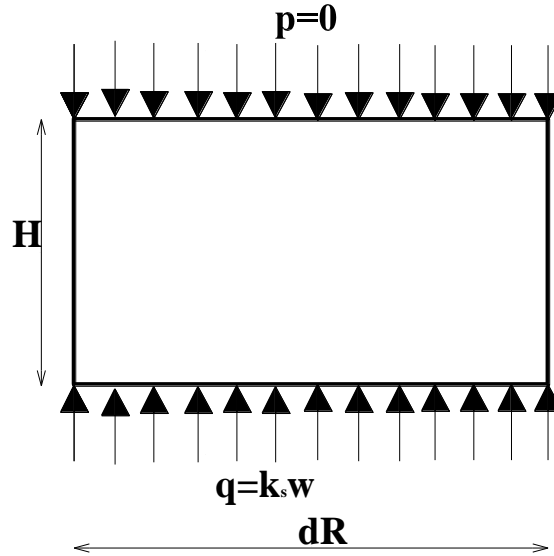


Figure 7.5: Vertical reaction components on an elemental block.

$$k_s w - H \left(\frac{G}{r} \frac{dw}{dr} + \frac{\Delta}{\Delta r} \left(G \frac{dw}{dr} \right) \right) = p \quad (7.9)$$

$$k_s w - \left[GH \frac{\Delta w}{r \Delta r} + H \left(G \frac{d^2 w}{dr^2} + \frac{dw}{dr} \frac{dG}{dr} \right) \right] = p \quad (7.10)$$

The effective stress is represented by

$$\sigma' = \sigma_0' + \Delta \sigma \quad (7.11)$$

The shear modulus of the soil is proportional to the confining stress

$$G = G_0 \left(\frac{\sigma'}{\sigma_0'} \right)^n \quad \text{Lambe and Whitman (1969)} \quad (7.12)$$

(When $n=0$, the shear modulus becomes independent of confining pressure)

Substituting Equation (7.11) in Equation (7.12)

$$G = G_0 \left(\frac{\sigma_0' + \Delta\sigma}{\sigma_0'} \right)^n \quad (7.13)$$

The derivative of the shear modulus is represented by

$$\frac{dG}{dr} = \frac{G_0}{(\sigma_0')^n} \frac{d(\sigma_0' + \Delta\sigma)^n}{dr} \quad (7.14)$$

$$\frac{dG}{dr} = \frac{G_0}{(\sigma_0')^n} n(\sigma_0' + \Delta\sigma)^{n-1} \frac{d\Delta\sigma}{dr} \quad (7.15)$$

Substituting Equation (7.12) and Equation (7.15) in Equation (7.12) gives

$$k_s w - \left[G_0 \left(\frac{\sigma'}{\sigma_0'} \right)^n H \frac{\Delta w}{r \Delta r} + H \left(G_0 \left(\frac{\sigma'}{\sigma_0'} \right)^n \frac{d^2 w}{dr^2} + \frac{dw}{dr} \frac{G_0}{(\sigma_0')^n} n(\sigma_0' + \Delta\sigma)^{n-1} \frac{d\Delta\sigma}{dr} \right) \right] = p \quad (7.16)$$

Let's us assume $p=0$.

$$\text{The initial stress is assumed as, } \sigma_0' = C * k_s D_f \quad (7.17)$$

Where C is the compaction coefficient.

The incremental stress is assumed as (average of upward and downward acting pressure)

$$\Delta\sigma = \frac{q}{2} = \frac{k_s w}{2} \quad (7.18)$$

Substituting Equation. (7.17), (7.18) in eqn. (7.16)

$$k_s w - G_0 \left(\frac{Ck_s B + \frac{k_s w}{2}}{Ck_s B} \right)^n H \frac{\Delta w}{r \Delta r} + H G_0 \left(\frac{Ck_s B + \frac{k_s w}{2}}{Ck_s B} \right)^n \frac{d^2 w}{dr^2} + H \frac{dw}{dr} \frac{G_0}{(Ck_s B)^n} n \left(Ck_s B + \frac{k_s w}{2} \right)^{n-1} \frac{k_s d(w)}{dr} = p \quad (7.19)$$

Representing the equation in non-dimensional form

$$k_s WB - G_0 \left(\frac{Ck_s B + \frac{k_s WB}{2}}{Ck_s B} \right)^n H \frac{\Delta W}{RB \Delta R} + HG_0 \left(\frac{Ck_s B + \frac{k_s WB}{2}}{Ck_s B} \right)^n \frac{1}{B} \frac{d^2 W}{dR^2} + \quad (7.20)$$

$$H \frac{dW}{dR} \frac{G_0}{(Ck_s B)^n} n \left(Ck_s B + \frac{k_s WB}{2} \right)^{n-1} \frac{k_s}{2} \frac{d(W)}{dR} = 0$$

$$\left(\frac{C + \frac{W}{2}}{C} \right)^n \frac{1}{R} \frac{\Delta W}{\Delta R} + \left(\frac{C + \frac{W}{2}}{C} \right)^n \frac{d^2 W}{dR^2} + \frac{dW}{dR} \frac{1}{(C)^n} n \left(C + \frac{W}{2} \right)^{n-1} \frac{1}{2} \frac{dW}{dR} - \alpha^2 W = 0 \quad (7.21)$$

Now the load deflection equation of the formulation is

$$Q = \int_0^{2\pi} \int_0^{B/2} k_s w_o r dr d\theta + \int_0^{2\pi} \int_{B/2}^{B_g/2} k_s w r dr d\theta \quad (7.22)$$

$$Q = \int_0^{2\pi} \int_0^{1/2} k_s B^3 W_o R dR d\theta + \int_0^{2\pi} \int_{1/2}^{R_g/2} k_s B^3 W R dR d\theta \quad (7.23)$$

$$Q^* = \int_0^{2\pi} \int_0^{1/2} W_o R dR d\theta + \int_0^{2\pi} \int_{1/2}^{R_g/2} W R dR d\theta \quad \text{where } Q^* = \frac{Q}{k_s B^3} \quad (7.24)$$

$$Q^* = \frac{\pi}{4} W_0 + 2\pi \int_{0.5}^{R_g/2} W R dR \quad (7.25)$$

7.2.1.1 Validation

Equation (7.21), the stress dependent pattern of deflection profile from the edge of the footing to the edge of the geocell reduces to equation (7.2) when $n=0$ (stress independency). The stress dependent model (substituting $n=0$) was validated against the numerical solution obtained for stress independency. Figure 7.6 depicts the normalized load settlement curves for both stress dependent and stress independent analysis. The results were found to be in good agreement since in both the cases finite difference method was employed for the analysis.

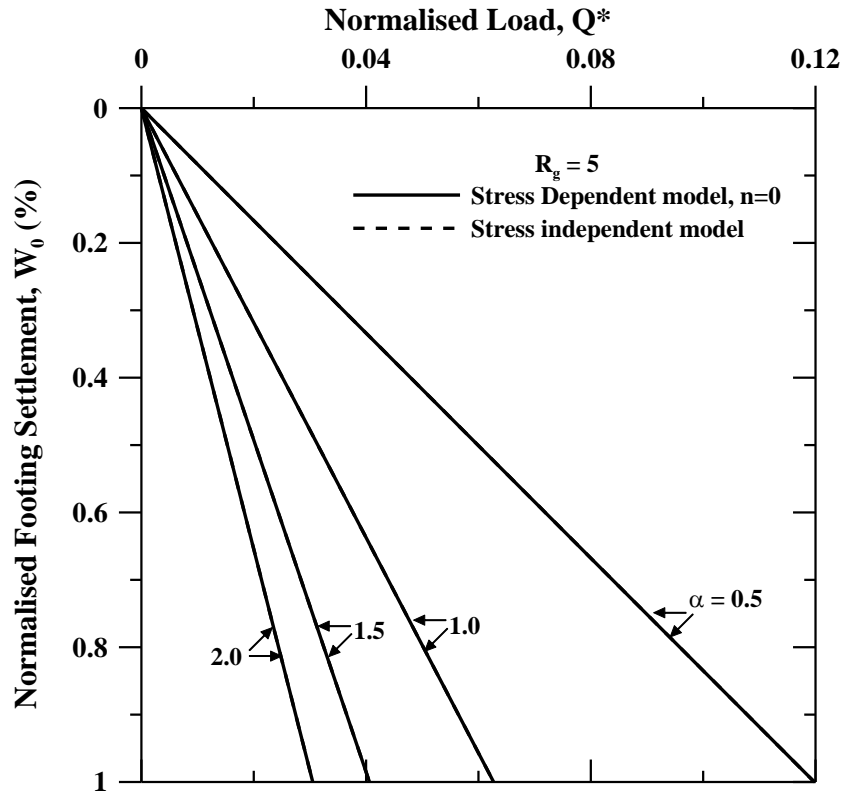


Figure 7.6: Comparison of stress dependent and independent results

7.2.1.2 Results

The deflection profile from the edge of the footing to the edge of the geocell by varying the parameter, α is shown in Figure 7.7. The solid line represents the deflection pattern that incorporates stress dependency and the dashed lines represent stress independency. It is clear from the plot that the stress independent model underestimates the exact behaviour since incorporation of stress dependency leads to uniform distribution of loads in the geocell layer.

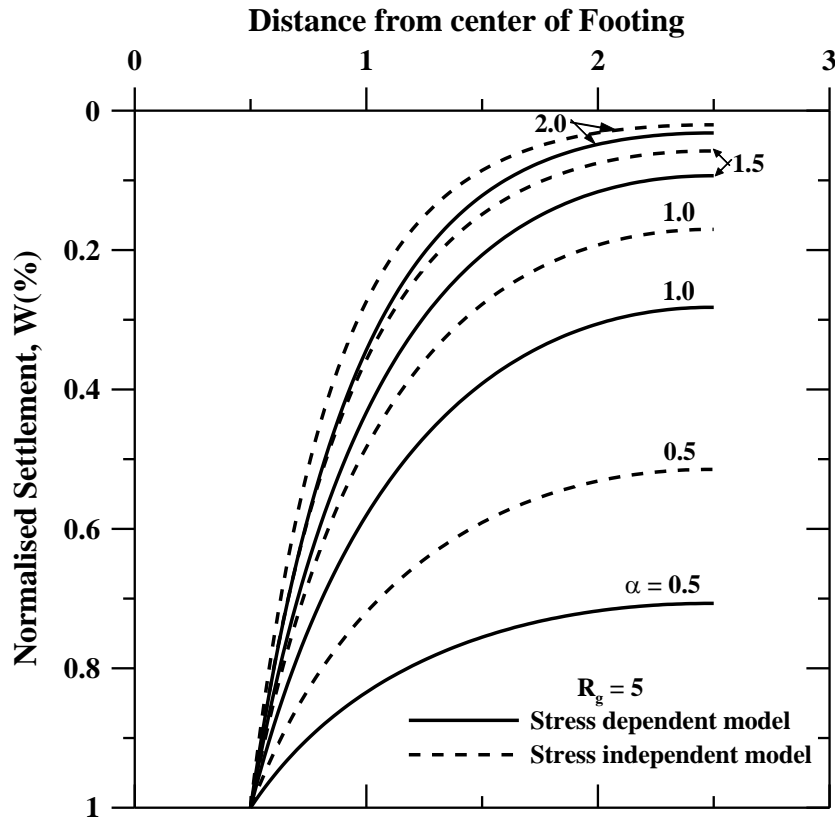


Figure 7.7: Settlement profile from the edge of the footing to the edge of the geocell layer (varying α)

The corresponding load settlement pattern is shown in Figure 7.8 for a footing settlement of the order of 1%. The variation between stress dependent and independent model shows considerable difference for geocells of high stiffness.

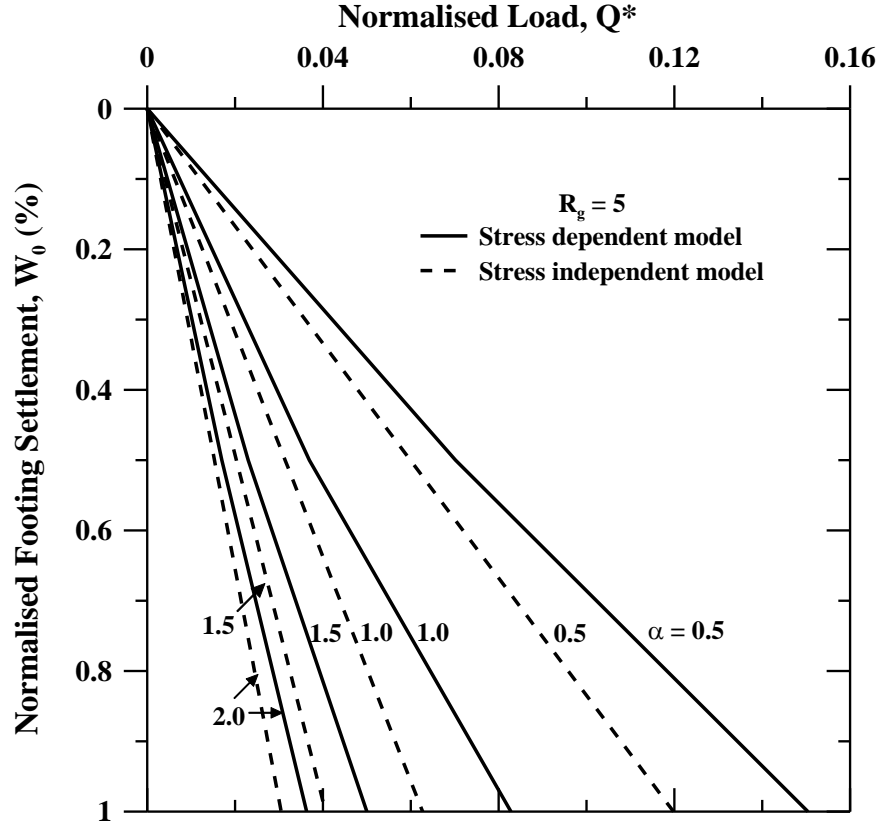


Figure 7.8: Normalized load settlement curve (Varying α)

7.2.2 Nonlinear formulation

The nonlinear stress displacement response of the soil can be represented by the hyperbolic relation presented by Kondner (1963) as follows:

$$q(r) = \frac{k_s w_0}{1 + \frac{k_s w_0}{q_u}} \quad \text{for } |r| \leq \frac{B}{2} \quad (7.26)$$

$$\frac{k_s w_0}{1 + \frac{k_s w_0}{q_u}} - G_g H \left(\frac{d^2 w}{dr^2} + \frac{1}{r} \frac{dw}{dr} \right) = 0 \quad \text{for } |r| \geq \frac{B}{2} \quad (7.27)$$

Simplifying Equation (7.27) the governing differential equation that describes the deflection from the edge of the footing to the edge of the geocell reduces to

$$\frac{d^2 W}{dR^2} + \frac{1}{R} \frac{dW}{dR} - \frac{\alpha^2 W}{1 + \mu W} = 0 \quad (7.28)$$

Where $\alpha^2 = \frac{k_s B^2}{G_g H}$ and $\mu = \frac{k_s B}{q_u}$

Equation (7.28) that defines the deflection pattern is a function of inverse of normalized shear stiffness, inverse of normalized ultimate bearing capacity. However, geocell derives its major strength from the all-round confinement the system offers. The vertical forces that act on an elemental block is shown in Figure 7.9.

Equating forces in vertical direction (Figure 7.9)

$$\frac{k_s w}{1 + \frac{k_s w}{q_u}} (r \Delta \theta \Delta r) + \tau (r \Delta \theta) H - (\tau + \Delta \tau) (r + \Delta r) \Delta \theta H = p (r \Delta \theta \Delta r) \quad (7.29)$$

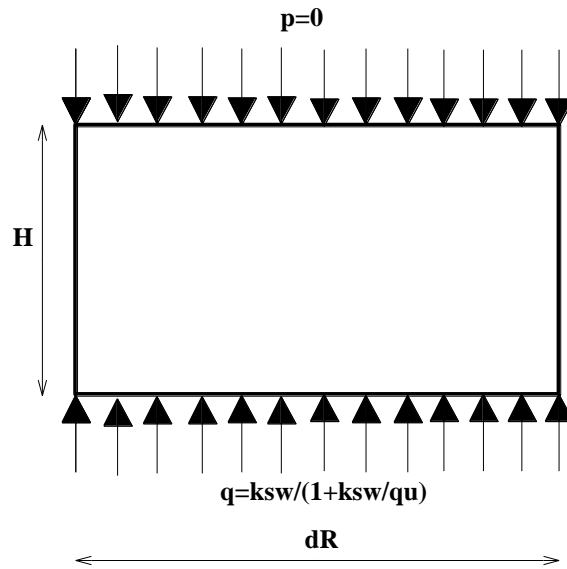


Figure 7.9: Vertical reaction components on an elemental block.

$$\frac{k_s w}{1 + \frac{k_s w}{q_u}} (r \Delta \theta \Delta r) + \tau (r \Delta \theta) H - H (\tau r \Delta \theta + \tau \Delta r \Delta \theta + \Delta \tau r \Delta \theta + \Delta \tau \Delta r \Delta \theta) = p (r \Delta \theta \Delta r) \quad (7.30)$$

Neglecting the higher order terms and simplifying the equation,

$$\frac{k_s w}{1 + \frac{k_s w}{q_u}} (r \Delta \theta \Delta r) - H (\tau \Delta r \Delta \theta + \Delta \tau r \Delta \theta) = p (r \Delta \theta \Delta r) \quad (7.31)$$

Dividing Equation (7.31) by $r \Delta r \Delta \theta$

$$\frac{k_s w}{1 + \frac{k_s w}{q_u}} - H \left[\frac{\tau}{r} + \frac{\Delta \tau}{\Delta r} \right] = p \quad (7.32)$$

$$\text{Shear stress, } \tau = G \frac{dw}{dr} \quad (7.33)$$

$$\frac{k_s w}{1 + \frac{k_s w}{q_u}} - H \left(\frac{G}{r} \frac{dw}{dr} + \frac{\Delta}{\Delta r} \left(G \frac{dw}{dr} \right) \right) = p \quad (7.34)$$

$$\frac{k_s w}{1 + \frac{k_s w}{q_u}} - \left[GH \frac{\Delta w}{r \Delta r} + H \left(G \frac{d^2 w}{dr^2} + \frac{dw}{dr} \frac{dG}{dr} \right) \right] = p \quad (7.35)$$

The effective stress is represented by

$$\sigma' = \sigma_0' + \Delta \sigma \quad (7.36)$$

The shear modulus of the soil is proportional to the confining stress

$$G = G_0 \left(\frac{\sigma'}{\sigma_0'} \right)^n \quad \text{Lambe and Whitman(1969)} \quad (7.37)$$

(When n=0, the shear modulus becomes independent of confining pressure)

Substituting Eq.7.26 in Eq. 7.37

$$G = G_0 \left(\frac{\sigma_0' + \Delta \sigma}{\sigma_0'} \right)^n \quad (7.38)$$

The derivative of the shear modulus is represented by

$$\frac{dG}{dr} = \frac{G_0}{(\sigma_0')^n} \frac{d(\sigma_0' + \Delta \sigma)^n}{dr} \quad (7.39)$$

$$\frac{dG}{dr} = \frac{G_0}{(\sigma_0')^n} n (\sigma_0' + \Delta \sigma)^{n-1} \frac{d\Delta \sigma}{dr} \quad (7.40)$$

Substituting Eq. 9 and Eq.12 in Eq. 7 we get

$$\frac{k_s w}{1 + \frac{k_s w}{q_u}} - \left[G_0 \left(\frac{\sigma'}{\sigma_0'} \right)^n H \frac{\Delta w}{r \Delta r} + H \left(G_0 \left(\frac{\sigma'}{\sigma_0'} \right)^n \frac{d^2 w}{dr^2} + \frac{dw}{dr} \frac{G_0}{(\sigma_0')^n} n (\sigma_0' + \Delta \sigma)^{n-1} \frac{d\Delta \sigma}{dr} \right) \right] = p \quad (7.41)$$

In our analysis we take p=0 (since no load is acting beyond the footing)

$$\text{The initial stress is assumed as, } \sigma_0' = C * k_s D_f \quad (7.42)$$

Where C is a constant.

The incremental stress is assumed as (average of upward and downward acting pressure)

$$\Delta\sigma = \frac{q}{2} = \frac{\left(\frac{k_s w}{1 + \frac{k_s w}{q_u}} \right)}{2} \quad (7.43)$$

Substituting equations. (7.37), (7.42), (7.43) in (7.41)

$$\frac{k_s w}{1 + \frac{k_s w}{q_u}} - G_0 \left(\frac{\frac{k_s w}{1 + \frac{k_s w}{q_u}}}{Ck_s B + \frac{q_u}{2}} \right)^n H \frac{\Delta w}{r \Delta r} + HG_0 \left(\frac{\frac{k_s w}{1 + \frac{k_s w}{q_u}}}{Ck_s B + \frac{q_u}{2}} \right)^n \frac{d^2 w}{dr^2} + \quad (7.44)$$

$$H \frac{dw}{dr} \frac{G_0}{(Ck_s B)^n} n \left(\frac{\frac{k_s w}{1 + \frac{k_s w}{q_u}}}{Ck_s B + \frac{q_u}{2}} \right)^{n-1} k_s d \left(\frac{w}{1 + \frac{k_s w}{q_u}} \right) \frac{1}{dr} = p$$

Representing the equation in non-dimensional form

$$\frac{k_s WB}{1 + \frac{k_s WB}{q_u}} - G_0 \left(\frac{\frac{k_s WB}{1 + \frac{k_s WB}{q_u}}}{Ck_s B + \frac{q_u}{2}} \right)^n H \frac{\Delta W}{RB \Delta R} + HG_0 \left(\frac{\frac{k_s WB}{1 + \frac{k_s WB}{q_u}}}{Ck_s B + \frac{q_u}{2}} \right)^n \frac{1}{B} \frac{d^2 W}{dR^2} + \quad (7.45)$$

$$H \frac{dW}{dR} \frac{G_0}{(Ck_s B)^n} n \left(\frac{\frac{k_s WB}{1 + \frac{k_s WB}{q_u}}}{Ck_s B + \frac{q_u}{2}} \right)^{n-1} \frac{k_s}{2} \frac{d}{dR} \left(\frac{WB}{1 + \frac{k_s WB}{q_u}} \right) = 0$$

Multiply equation (7.45) by B/ (G₀H)

$$\text{Let } \mu = \frac{k_s B}{q_u} \quad \text{and} \quad \alpha^2 = \frac{k_s B^2}{G_s H}$$

$$\left(\frac{C + \frac{W}{1 + \mu W}}{C} \right)^n \frac{1}{R} \frac{\Delta W}{\Delta R} + \left(\frac{C + \frac{W}{1 + \mu W}}{C} \right)^n \frac{d^2 W}{dR^2} + \frac{\Delta W}{\Delta R} \frac{1}{(C)^n} n \left(\frac{C + \frac{W}{1 + \mu W}}{C} \right)^{n-1} \frac{1}{2} \frac{d}{dR} \frac{W}{1 + \mu W} - \frac{\alpha^2 W}{1 + \mu W} = 0 \quad (7.46)$$

Equation (7.46) represents the deflection profile as a function of compaction coefficient (C), inverse of normalized shear stiffness (α), inverse of normalized ultimate bearing capacity (μ). To obtain the deflection pattern, numerical methods viz. finite difference method has to be employed.

Now the load deflection equation of the formulation is

$$Q = \int_0^{2\pi} \int_0^{B/2} \frac{k_s W_0}{1 + \frac{k_s}{q_u} W_0} r dr d\theta + \int_0^{2\pi} \int_{B/2}^{R_g/2} \frac{k_s W}{1 + \frac{k_s}{q_u} W} r dr d\theta \quad (7.47)$$

Changing the limits of integration and expressing in non-dimensional form

$$Q = \int_0^{2\pi} \int_0^{B/2} k_s B^3 \frac{W_0}{1 + \mu W_0} R dR d\theta + \int_0^{2\pi} \int_{1/2}^{R_g/2} k_s B^3 \frac{W}{1 + \mu W} R dR d\theta \quad (7.48)$$

$$Q^* = \int_0^{2\pi} \int_0^{1/2} \frac{W_0}{1 + \mu W_0} R dR d\theta + \int_0^{2\pi} \int_{1/2}^{R_g/2} \frac{W}{1 + \mu W} R dR d\theta \quad \text{where } Q^* = \frac{Q}{k_s B^3} \quad (7.49)$$

$$Q^* = \frac{\pi}{4} \left(\frac{W_0}{1 + \mu W_0} \right) + 2\pi \int_{1/2}^{R_g/2} \frac{W}{1 + \mu W} R dR \quad (7.50)$$

7.2.3 Finite difference formulation

Both the equations involved in obtaining linear and nonlinear load settlement curves were difficult to solve analytically. Finite difference method, numerical method for approximating the solution of differential equations was employed. Central difference scheme (Crank – Nicolson method, 1947) was employed to discretise second order terms and forward difference scheme (Explicit method) was used to discretise first order terms. The normalised length, L has been divided into '(n-1)' number of elements with 'n' number of node points.

The mesh size (dX) can be written as $dX=L/n$ (refer figure 5.6). Writing the equation for any interior node 'i', for the linear ordinary differential equation leads to the following:

$$\begin{aligned} & \left(\frac{C + \frac{W_i}{2}}{C} \right)^n \frac{1}{R} \frac{W_{i+1} - W_i}{\Delta R} + \left(\frac{C + \frac{W_i}{2}}{C} \right)^n \frac{W_{i+1} - 2W_i + W_{i-1}}{(\Delta R)^2} \\ & + \frac{W_{i+1} - W_i}{\Delta R} \frac{1}{(C)^n} n \left(C + \frac{W_i}{2} \right)^{n-1} \frac{1}{2} \frac{W_{i+1} - W_i}{\Delta R} - \alpha^2 W_i = 0 \end{aligned} \quad (7.51)$$

To simplify equation (7.51), the equation is written in the following form:

$$h(i) \frac{1}{R} \frac{W_{i+1} - W_i}{\Delta R} + h(i) \frac{W_{i+1} - 2W_i + W_{i-1}}{(\Delta R)^2} + \frac{W_{i+1} - W_i}{\Delta R} \frac{1}{(C)^n} n \frac{1}{2h(i)} \frac{W_{i+1} - W_i}{\Delta R} - \alpha^2 W_i = 0 \quad (7.52)$$

$$\text{Where } h(i) = \left(\frac{C + \frac{W_i}{2}}{C} \right)^n$$

Gauss-Seidel iterative procedure is used to obtain the solution. The nonlinear stress dependent model involved high complexity and had to be linearized twice to arrive at the solution. The stress dependent model in finite difference form (Central and forward difference scheme) is represented as follows:

$$\begin{aligned} & \left(\frac{C + \frac{W_i}{1 + \mu W_i}}{C} \right)^n \frac{1}{R_i} \frac{W_{i+1} - W_i}{\Delta R} + \left(\frac{C + \frac{W_i}{1 + \mu W_i}}{C} \right)^n \frac{W_{i+1} - 2W_i + W_{i-1}}{(\Delta R)^2} \\ & + \frac{W_{i+1} - W_i}{\Delta R} \frac{1}{2C} \left(\frac{C + \frac{W_i}{1 + \mu W_i}}{C} \right)^{n-1} \frac{\frac{W_{i+1}}{1 + \mu W_{i+1}} - \frac{W_i}{1 + \mu W_i}}{\Delta R} - \alpha^2 \frac{W_i}{1 + \mu W_i} = 0 \end{aligned} \quad (7.53)$$

Since the discretised equation is in nonlinear form direct approaches viz. Gauss elimination, Gauss-Seidel, Tridiagonal matrix method etc. cannot be employed. The nonlinear algebraic equation (5.16) has to be linearized.

$$\text{Let } g(i) = \frac{W_i}{1 + \mu W_i} \text{ and } h(i) = \left(\frac{C + \frac{g(i)}{2}}{C} \right)^n$$

Equation (7.53) can be rewritten as

$$h(i) \frac{1}{R_i} \frac{W_{i+1} - W_i}{\Delta R} + h(i) \frac{W_{i+1} - 2W_i + W_{i-1}}{(\Delta R)^2} + \frac{W_{i+1} - W_i}{\Delta R} \frac{1}{2Ch(i)} \frac{g(i+1) - g(i)}{\Delta R} - \alpha^2 g(i) = 0 \quad (7.54)$$

An initial guess for g_i was adopted and the iterative Gauss-Siedel procedure for obtaining solution

7.2.4 Boundary Conditions

The settlement of the rigid strip footing is considered as uniform under the loaded footing area. Hence the normalised settlement (W) at the edge of the footing is equal to the normalised footing settlement (W_0). The slope of the settlement profile (gradient of the settlement profile, dW/dX) is zero at the edge of the geocell layer, ie $R=R_g/2$. These two boundary conditions has been instrumental in solving both linear and non-linear ordinary differential equations.

In mathematical form it can be written as:

$$@R = 0.5, W = W_0$$

$$@R = R_g/2, dW/dX = 0$$

7.3 Validation

To check the accuracy and consistency of the results, the current model has been validated in various ways. The nonlinear model was initially checked against the linear solution, Limit theorem was applied to check the solution at very high settlements and the present model was also compared against an experimental data.

7.3.1 Theoretical Validation

The complete solution of the nonlinear stress dependent equation (7.46) reduces to the nonlinear equation (7.28) when $n=0$ which represents the deflection profile for stress independency and accounts for the nonlinear stress strain relationship as per Kondner (1963).

Analysis was done for same geocell layer width ratio, R_g and the results were found to overlap for various values of α (Figure 7.10) since finite difference method was employed to obtain the solution in both the cases.

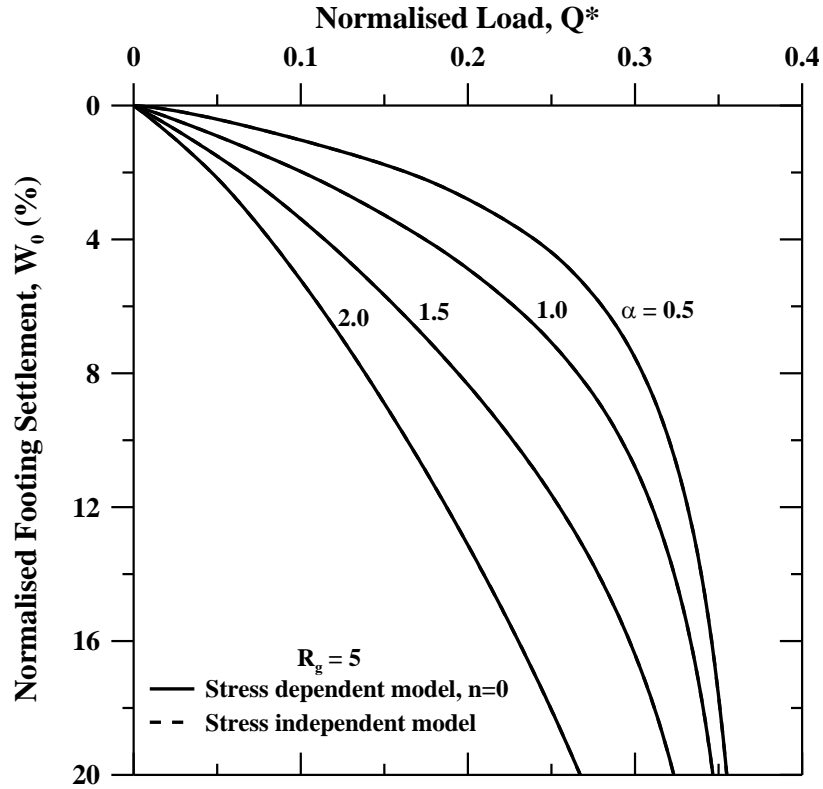


Figure 7.10: Normalized load settlement curve (Validation of stress dependent model against stress independent model)

7.3.2 Numerical Validation

At very high settlements the normalized load settlement equation (7.54) converges to constant limiting value as follows:

$$Q^* = \frac{\pi}{4\mu} R_g^2 \quad (7.55)$$

The constant limiting value, Q^* for the parameters $R_g=5$ and $\mu = 50$ is 0.3926. From MATLAB analysis the value of Q^* at 75% settlement is 0.3824 (Figure 7.11). The percentage error is -2.6% which is due to truncation and round off errors that occurs in finite difference method and may also be due to the 75% settlement criterion that was considered.

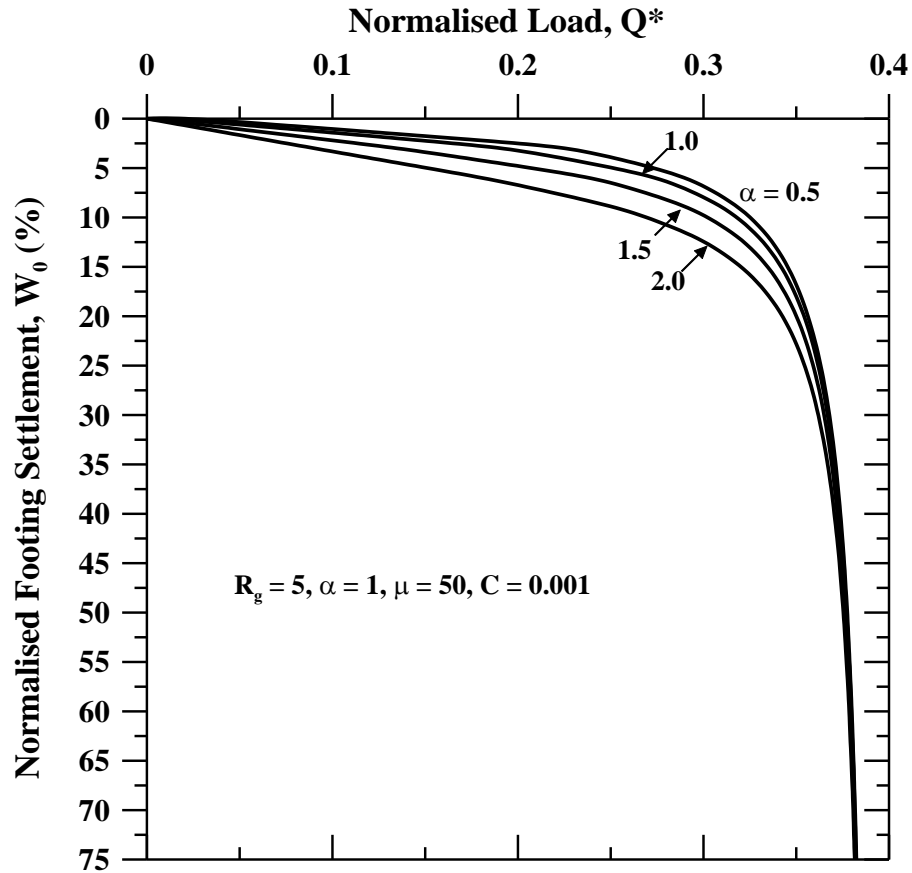


Figure 7.11: Normalized load settlement curve at high settlements

7.3.3 Experimental Validation

To check the validity of the present model to exercise the same for practical application, the results from the present study were compared with the results from model studies on circular footing supported on geocell reinforced sand underlain by soft clay conducted by Das et al (2003). The stress dependent and independent models were compared for two cases of geocell heights. It was seen from the analysis that the stress dependent model was found to perform better than stress independent case especially for higher range of settlements (Figure 7.12). The shear modulus of the geocell system (from the relation considering elastic modulus, shear modulus and Poisson ratio of the soil), ultimate bearing capacity of the subsoil were calculated to obtain the model parameters α and μ in the study.

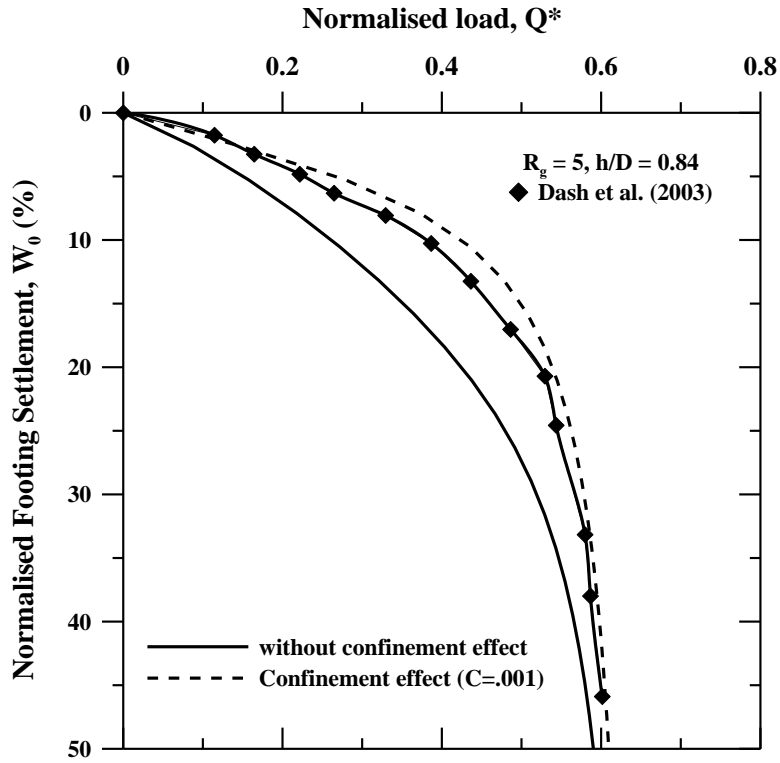


Figure 7.12: load settlement curve for geocell height, $H/D=0.84$

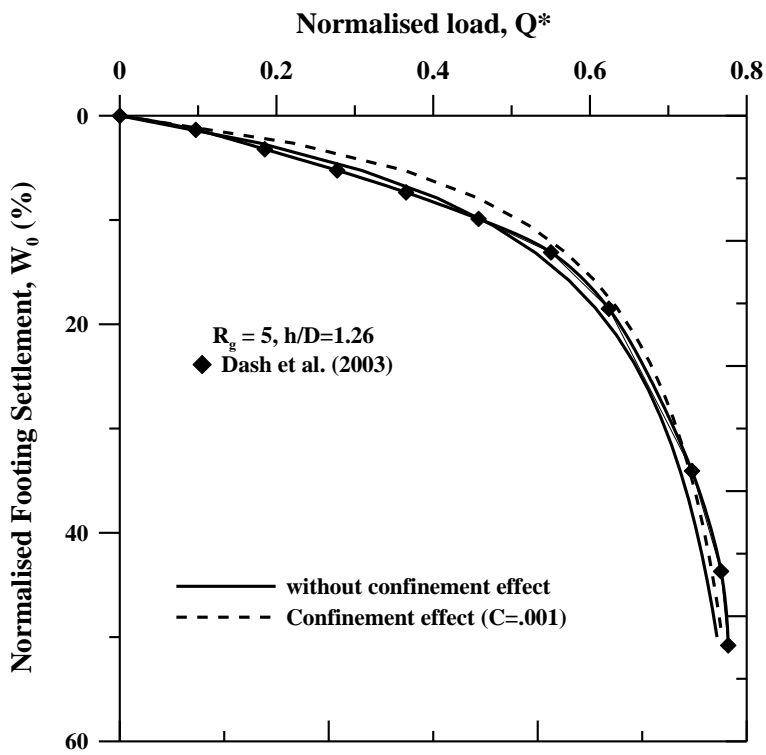


Figure 7.12a: load settlement curve for geocell height, $H/D=1.26$

Figure 7.12: Normalized load settlement curve (Comparison of different models with experimental data)

7.4 Results and Discussion

The present model incorporating stress dependency has extra variables viz. the initial compaction coefficient, C and Janbu's parameter, n that are instrumental in defining the pattern of settlement and the corresponding loads. A lower value of C indicates the initial stresses in the layer are low but the system is able to take higher loads (incremental stresses). Figure 7.13 shows curves of settlement pattern for varying values of C . The explanation that was given above was found to hold good here. Lower values of C shows uniform distribution of loads with a uniform pattern of settlement whereas higher values indicates varying distribution due to lesser stresses that act on the system.

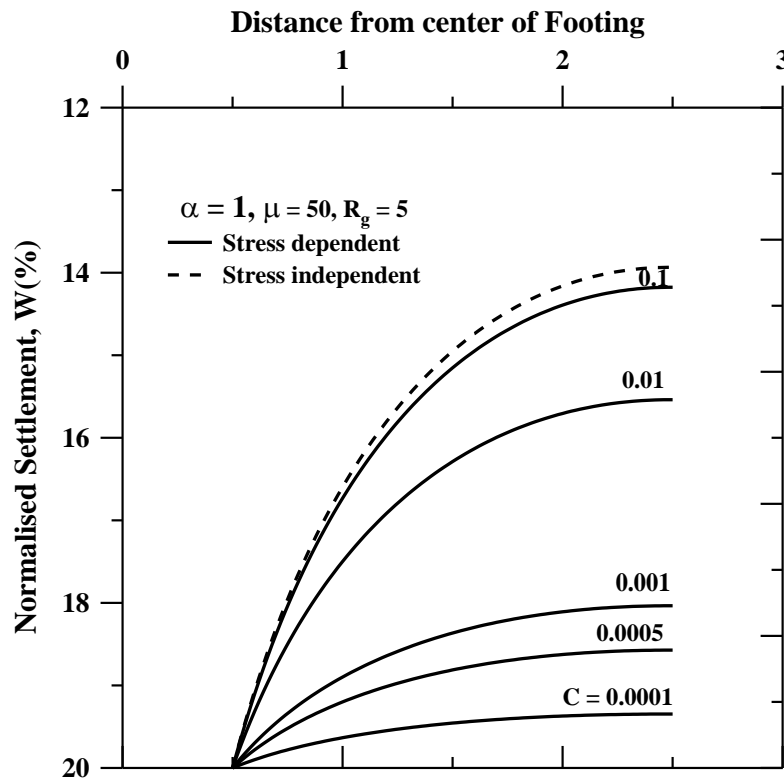


Figure 7.13: Settlement profile for various values of initial compaction coefficients.

The corresponding normalised load settlement curve is shown in Figure 7.14b. The dashed line represents the case of stress independency which is found to lie below the stress dependent case and the apparent variation in behaviour of the models is noticeable over the range of settlement 5-15% of footing settlement. Higher loads are bore by geocell systems with lower values of C (indicating low initial stresses). It is also observed that as C tends to a higher value (tending to infinity) it is similar to the stress dependent model. The analysis was conducted for different μ values and it was inferred from the study that lower values of μ shows considerable variation in load deflection pattern.

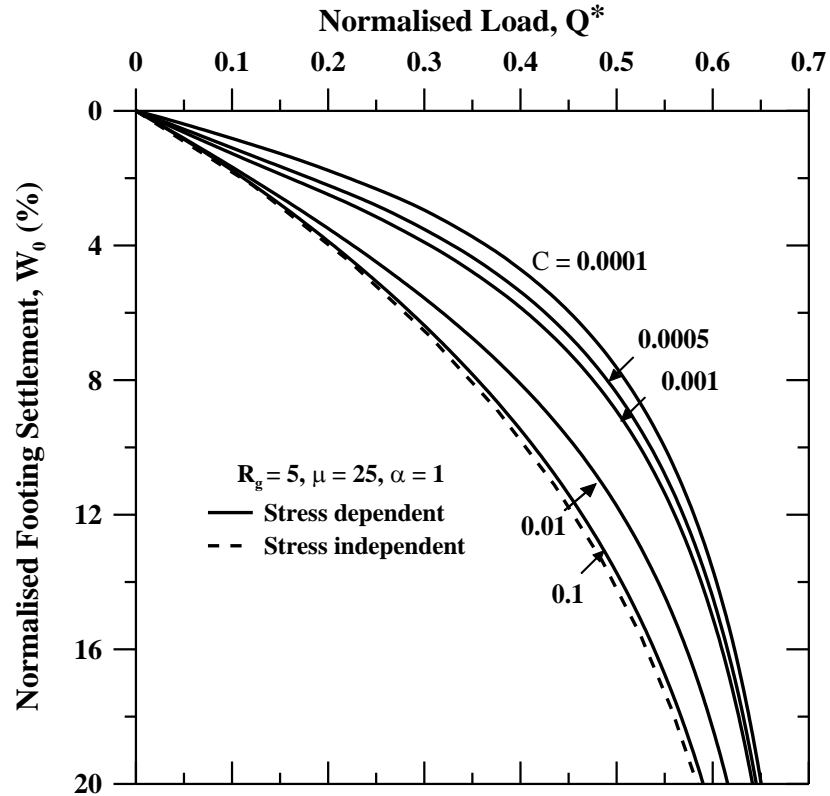


Figure 7.14a: Normalized load settlement curve for varying C ($\mu = 25$)

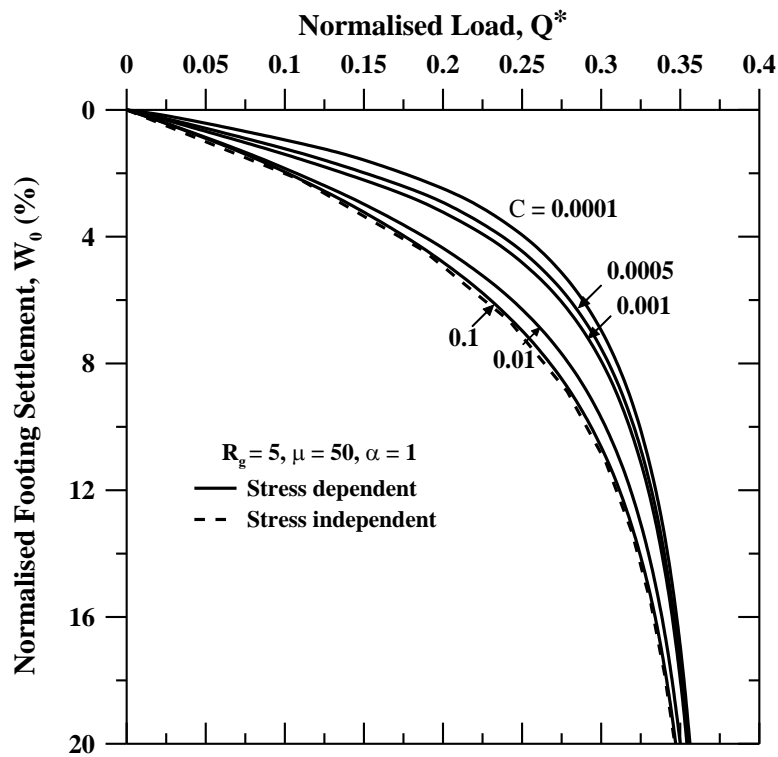


Figure 7.14b: Normalized load settlement curve for varying C ($\mu = 50$)

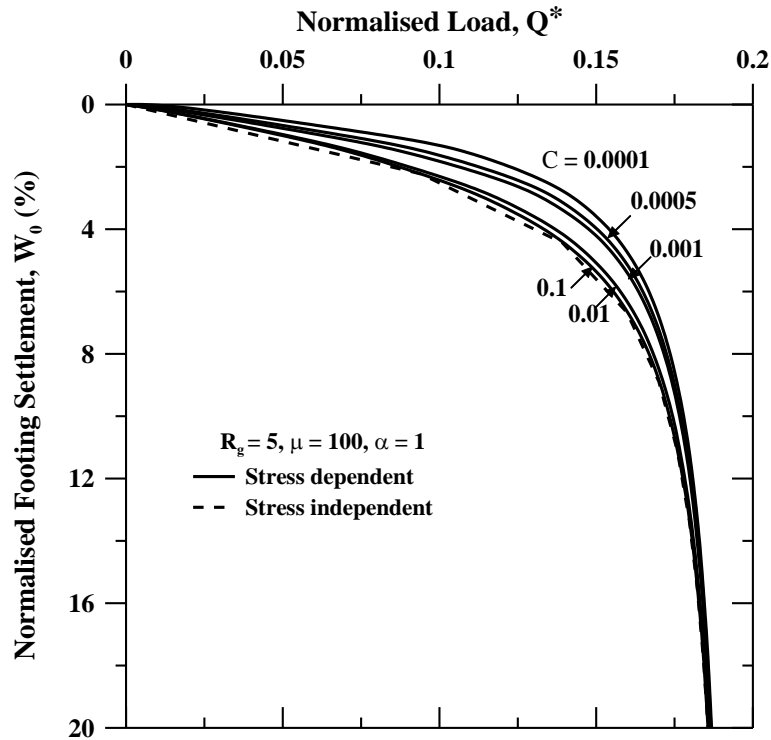


Figure 7.14c: Normalized load settlement curve for varying C ($\mu = 100$)

Figure 7.14: Normalized load settlement curve for varying compaction coefficient, C

The load settlement curve for varying C values were repeated for different μ values. It was found that there is significant variation in load settlement curve with variation in C value for subsoil with high ultimate bearing capacity. The curves in Figure 7.10 infer that the loads that are borne by the system with high subsoil stiffness are very high and the initial compaction stresses play a major role.

Parametric study was also done by varying parameters inverse of normalized shear stiffness of geocell reinforced soil (α), inverse of normalized ultimate bearing capacity (μ), Shear/Geocell layer width ratio (R_g). The settlement pattern for varying shear stiffness for both the cases is presented in Figure 7.9. It was found that higher values of α (low shear stiffness) has significant variation in the settlement curves for stress dependency and independency which indicates a major role for the confining stresses acting on the system whereas for low values of α the variation is not remarkable. The corresponding load settlement curves were plotted in Figure 7.10 and similar observation as reported in settlement pattern was observed. It was found that there is a remarkable variation in load

settlement pattern for higher values of α (low shear stiffness) and the defining trends like geocell with higher shear stiffness bears a higher load is followed here.

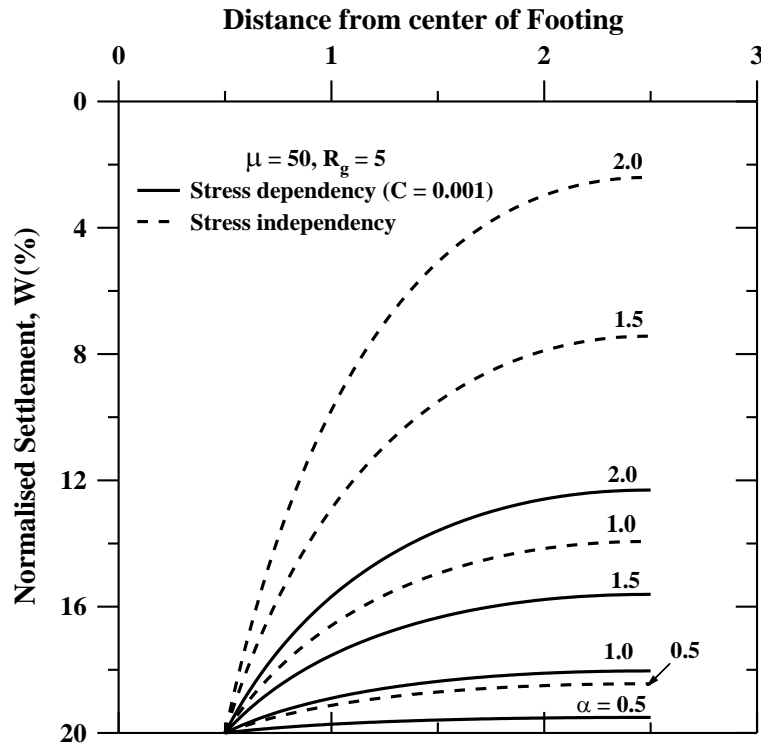


Figure 7.15: Settlement profile for various values α .

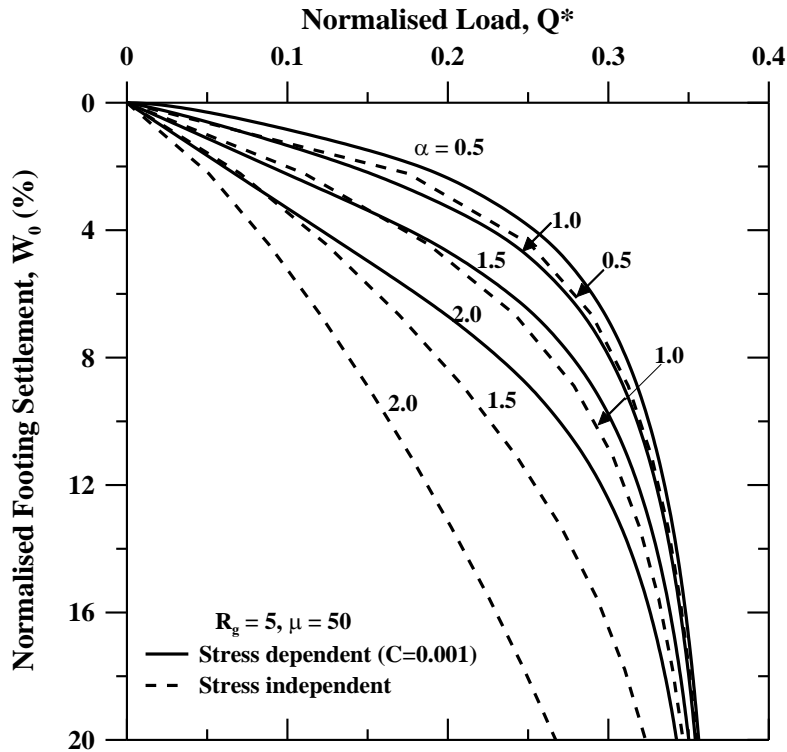


Figure 7.16: Normalized load settlement curve for various α .

The settlement pattern from the edge of the footing to the edge of the geocell layer with varying subsoil conditions is plotted in Figure 7.17. The subsoil with highest stiffness shows the greatest variation while comparing the stress independent and dependent cases. This variation may be due to the unbelievably high loads that is bore by the reinforced ground by incorporating the stress dependent behaviour. High stiffness offered by the ground prevents the uniform movement of the geocell layer which is reflected in the pattern of deflection in high stiff soils. The subsoil with low stiffness gives a uniform deflection to the geocell layer.

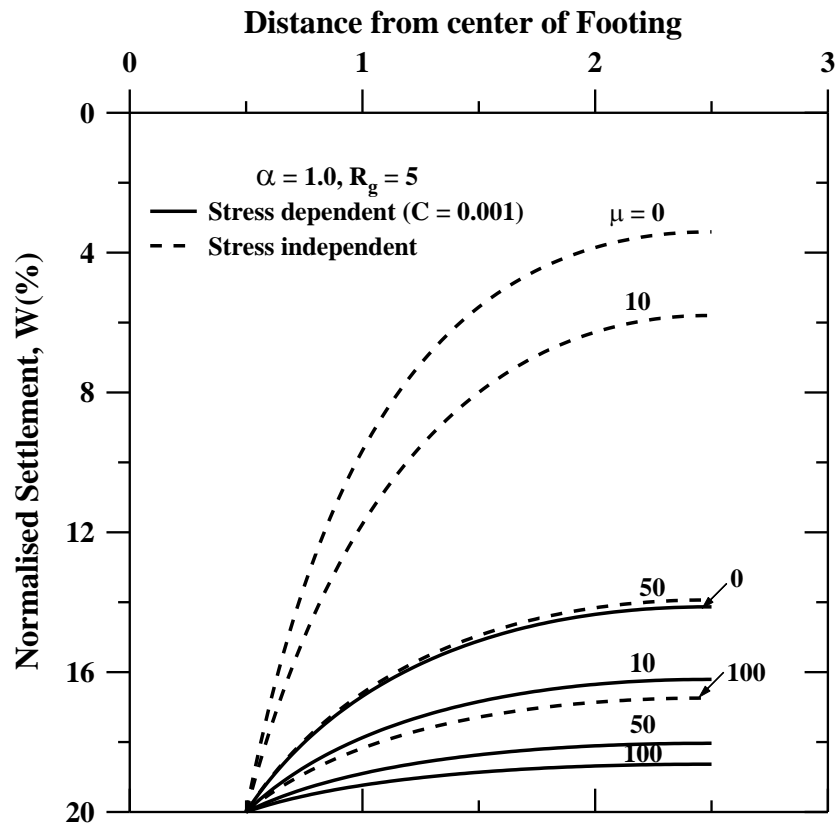


Figure 7.17: Settlement profile for various values μ .

The corresponding load settlement curves are plotted in Figure 7.18. The variation in deflection reported in settlement curve is well explained here. The predicted load carrying capacity is found to be as high as twice the load carrying capacity of the bed when used stress depended and independent models for the case of soil with high stiffness. Negligible variation in load settlement pattern is observed for underlying soils of low stiffness.

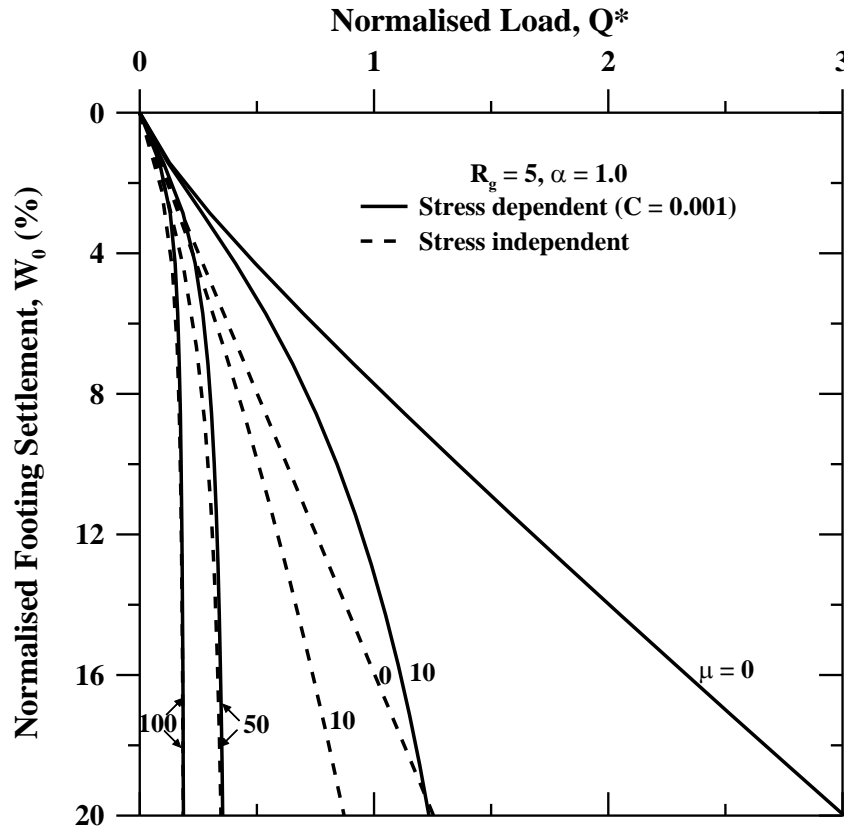


Figure 7.18: Normalized load settlement curve for various μ .

7.4.1. Improvement Factors

Figures 7.19 and 7.20 presents the variation of improvement factor (I_f) with inverse of normalized shear stiffness (α) and shear layer width ratio (R_g) respectively. Figure 7.19a shows the variation of I_f with α for varying subsoil conditions. The geocell layer width, footing settlement and the coefficient, C were kept constant. There is a clear trend of decrease in I_f with increasing value of α with very high values of I_f being reported. The stiffest subsoil ($\mu = 0$) reported the lowest improvement factors since I_f shows the relative performance of the reinforced soil with respect to the unreinforced ground. For the case of stiff subsoil ($\mu=0$) further improvement with the help of geocell reinforcement is not appreciable. Figure 7.19b shows the variation of I_f with α for different W_0 . As expected higher I_f is observed for higher settlement. Figure 7.19c shows the variation of I_f with α by varying the compaction coefficient, C which indicates initial stresses that the geocell reinforced ground is subjected to. This case refers to subsoil with same ultimate bearing capacity for different series of tests. A similar observation as reported from the load settlement curve applies here. The highest improvement in ground is shown by the system with low initial stresses ($C = 0.0001$) which

enables it to withstand higher incremental stresses, hence reporting higher I_f . It can also be seen that the rate of decrease of I_f with α decreases with decrease in the value of C .

Figure 7.20 shows the variation of I_f with R_g . Figure 7.20a shows the variation of I_f with R_g for different values of C keeping the geocell stiffness, subsoil conditions and footing settlement constant. There is a clear progression of improvement with increase in the value of R_g . It was inferred from the study that the improvement brought in to the ground by increasing the geocell width beyond 5 is not significant. But for the case of the system with very low initial stresses ($C = 0.0001$) there is considerable improvement in the efficiency of the system even at $R_g = 10$. But this case occurs in rare circumstances

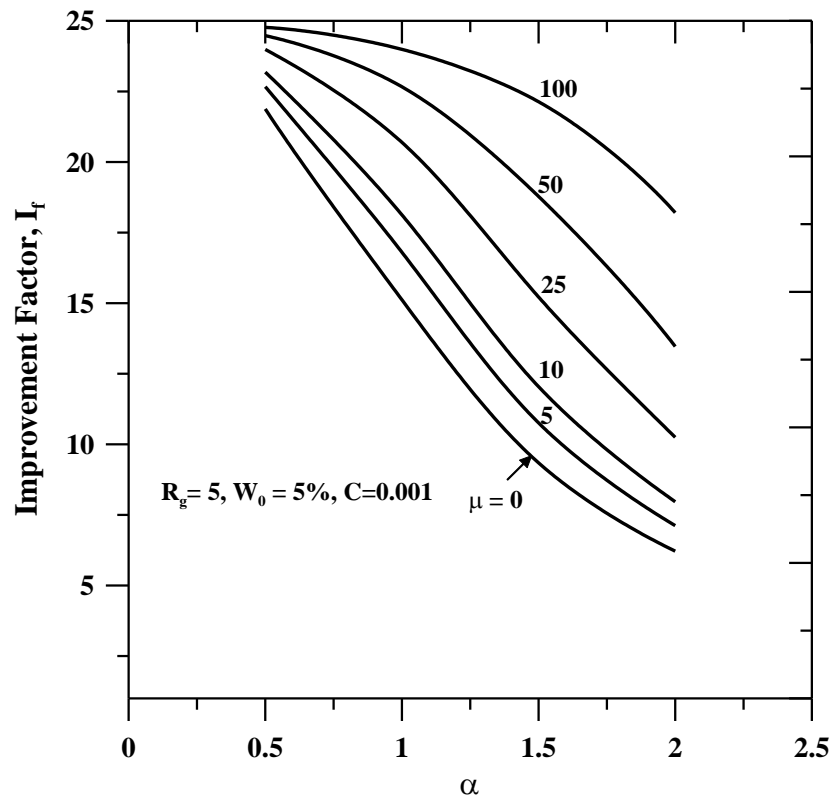


Figure 7.19a: Variation of I_f with α (varying μ)

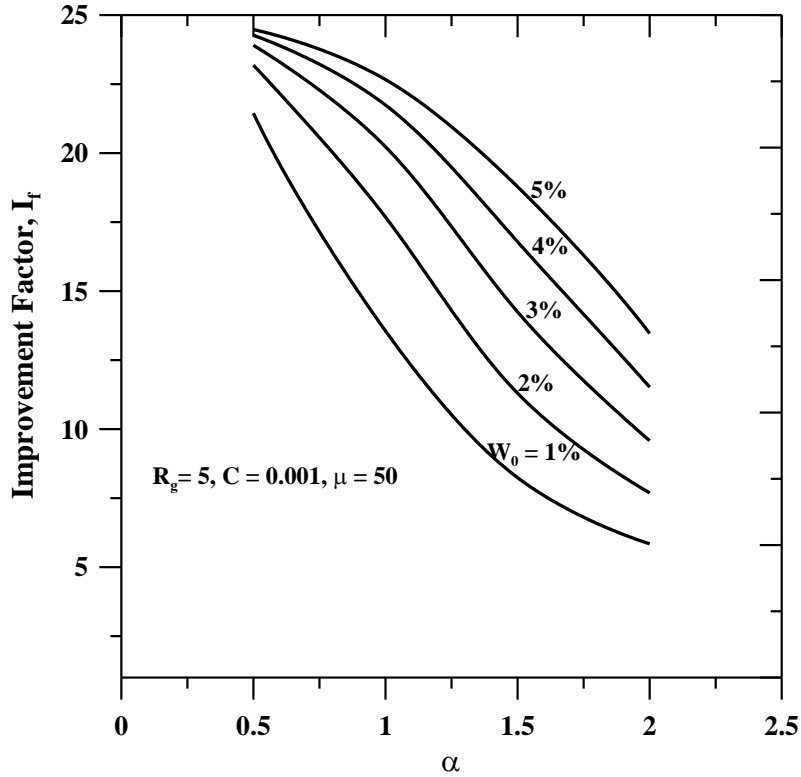


Figure 7.19b: Variation of I_f with α (varying W_0)

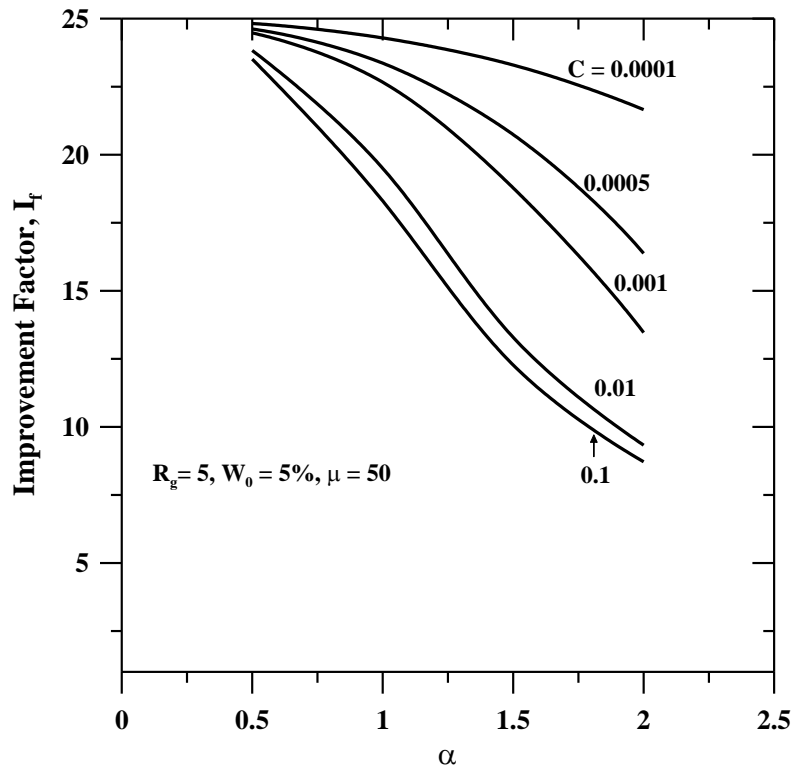


Figure 7.19c: Variation of I_f with α (varying W_0)

Figure 7.19: Variation of Improvement factor (I_f) with inverse of normalized shear stiffness (α)

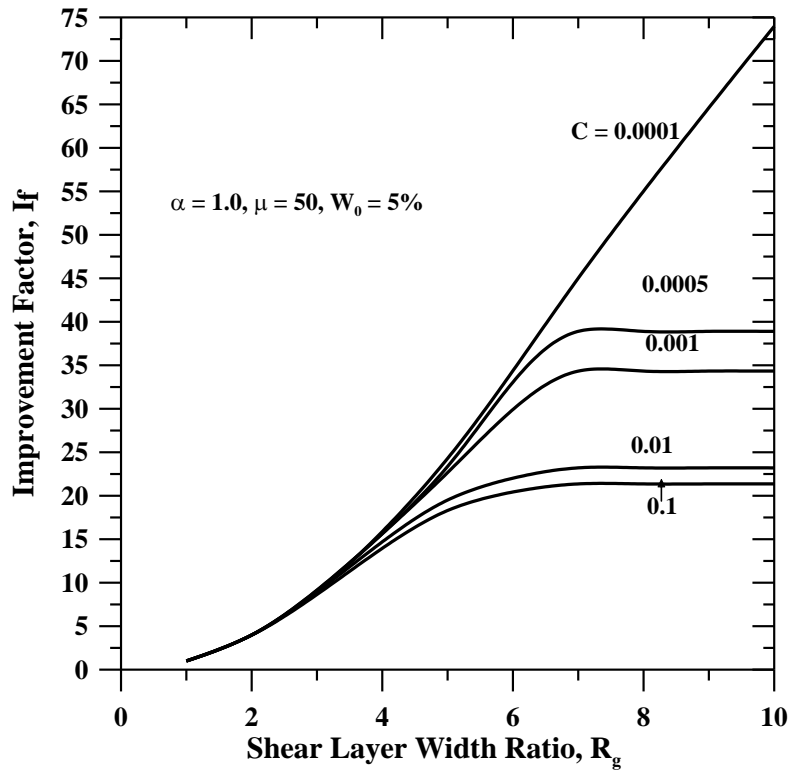


Figure 7.20a: Variation of I_f with R_g (varying C)

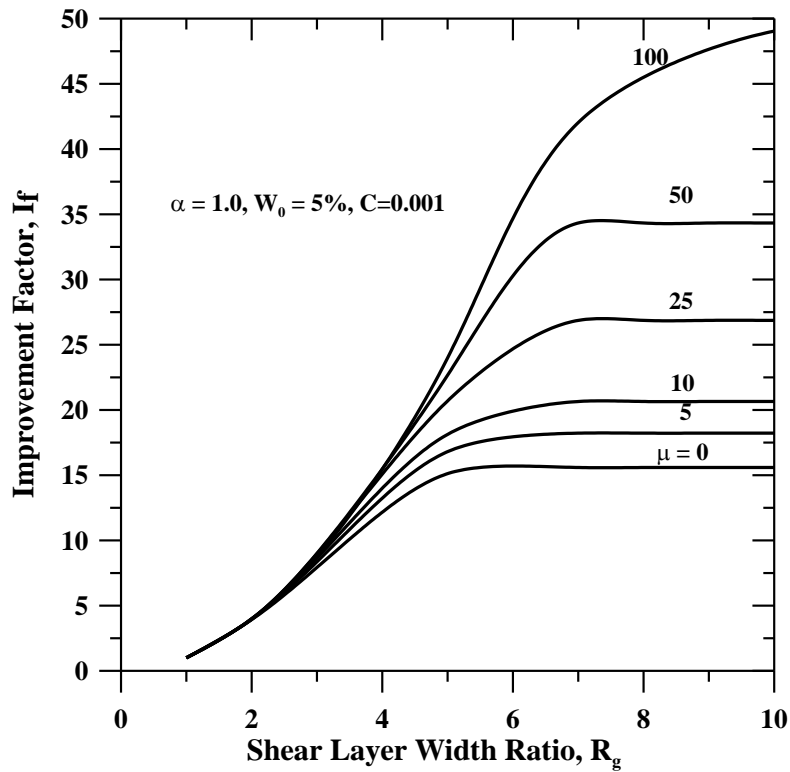


Figure 7.20b: Variation of I_f with R_g (varying μ)

The variation of I_f with R_g for varying subsoil conditions is shown in Figure 7.20b. There is an increase in I_f with R_g up to 5 for all the subsoil conditions beyond which the improvement remains stable for sub soils having intermediate to high stiffness ($\mu = 0$ to 50). There is remarkable improvement in ground for very soft soils ($\mu = 0$) even beyond $R_g = 5$.

The influence of geocell stiffness on the geocell reinforced system is shown in Figure 7.20c. Geocells of intermediate to high stiffness ($\alpha = 0.5$ to 1.5) provides negligible improvement with increase in $R_g \approx 5$ but geocells of low stiffness ($\alpha = 2.0$) shows improvement for geocell widths even up to 10.

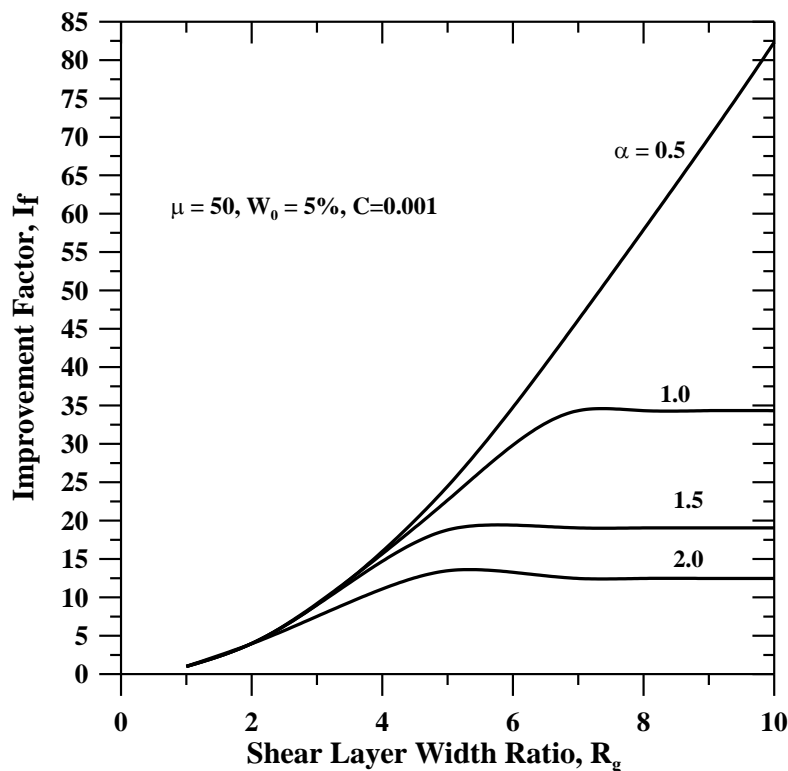


Figure 7.20c: Variation of I_f with R_g (varying α)

From the improvement factors reported from the study, the values of I_f are very high compared to the case of stress independency. The previous model without incorporation of stress dependency underestimates the exact improvement brought in to the geocell system.

7.5 Summary

An attempt was made to improve the Pasternak model by incorporating the stress dependent behaviour of the geocell reinforced soil. Parametric study was done for various parameters viz. compaction coefficient, C and Janbu's parameter, n which play an instrumental role in predicting the stress dependent behaviour. Linear and nonlinear analysis was done to obtain the load settlement curves and corresponding improvement factors for low and high settlements respectively. The following major conclusions drawn from the study are pointed out as below:

- Finite difference method was employed to obtain the numerical solution of linear and nonlinear differential equations and the current analysis involved the incorporation of extra parameters, compaction coefficient, C and Janbu's parameter, n in addition to the model parameters α and μ indicating the inverse of normalized shear stiffness of the geocell reinforced soil and inverse of normalized ultimate bearing capacity respectively.
- The current model was validate in several ways to check the accuracy of the predictions. Initially, the nonlinear data was compared with linear analysis data; the stress dependent model was compared with the stress independent model (reducing the model to stress independent model); the limiting value of Q^* is obtained at high settlements and the result is compared with the data from numerical analysis (MATLAB) which shows good agreement.
- The model was also checked with experimental results to understand the applicability of the current model in practical applications. It was very clear from the comparison that stress dependent model was found to perform better than the stress independent model indicating stress dependent model predicts the behaviour of geocell reinforced system near to the exact behaviour.
- It was observed from the study that the model parameters inverse of normalized shear stiffness, α ; inverse of normalized ultimate bearing capacity, μ ; compaction coefficient, C ; Shear layer width ratio, R_g plays a significant role in predicting the improvement brought about by the geocell reinforced soil.
- Lower value of compaction coefficient, C (Low value of C indicates low initial stresses and higher value of stresses that can be bore by the geocell reinforced system) shows a uniform distribution of loads in the settlement pattern ($C=.0001$) and high loads that can be bore by the reinforced system.

- The stress independent model underestimates the actual predictions and incorporation of stress dependency helps in understanding the actual behaviour of the geocell reinforced system since it takes into account the confining stresses acting on the system.
- The deflection profiles and load deflection patterns obtained for varying values of inverse of normalized shear stiffness of the geocell reinforced soil (α) shows a uniform distribution of loads for geocells of high stiffness ($\alpha = 0.5$) and higher loads bore by the geocell reinforced system and the vice versa occurs for geocells of low stiffness ($\alpha = 2.0$).
- Similarly the settlement profile and the load settlement curve were also plotted for varying subsoil conditions. It was inferred from the study that uniform deflection of the geocell layer was observed when the subsoil is of low stiffness since a subsoil of high stiffness would resist the free movement of the geocell layer. But the loads that can be bore y the system with strong subsoil conditions are very high ($\mu = 0$, indicating infinitely high stiffness for the subsoil).
- To quantify the performance of geocell reinforced system, improvement factors were used. The variation of improvement factors (If) with variation of inverse of normalized shear stiffness (α) and geocell/shear layer width ratio (R_g) was analyzed by varying model parameters, μ , W_0 , C .
- The improvement factors that were reported with incorporation of stress dependent behaviour are very high. As expected the I_f was found to decrease with increase in the value of α indicating higher improvement for the geocell reinforcement with high stiffness. The influence of the model parameters μ , C and W_0 were studied. Subsoil with high stiffness reported lesser improvement factors indicating that further improvement of the system with inclusion of geocell is negligible and is not an economical option.
- As expected, with increase in footing settlement (W_0), the I_f reported is also high. The major factor that governs the stress dependent behaviour, compaction coefficient, C was shown to have a clear increase in improvement with lower values of C . For lower values of C , even system with low geocell stiffness shows a higher improvement of the geocell reinforced system.
- The variation of improvement factor, I_f with geocell layer width, R_g was also analyzed. Various parameters C , μ , α were varied to study the influence of the

same on the improvement. In most of the cases the improvement was found to be constant beyond R_g 5 but in extreme cases where the geocell and subsoil stiffness is very weak and very low initial stresses the improvement was found to be appreciable.

In summary, the present model that incorporates the stress dependent behaviour of the geocell reinforced system helps in predicting the behaviour of the geocell reinforced system near to the actual behaviour. The improvement factors reported from the study could be used for design of geocell reinforced system as it is close to the actual behaviour.

Chapter 8

Conclusions

8.1 General

In the present study, several models were analyzed to check their applicability on footings resting on geocell reinforced soils. Strip and circular footings that has wide range of applicability in geotechnical areas were modelled in the current study. The variation of contact pressure based on geocell width were considered to obtain the approximate bearing capacity improvement. To have a better idea, foundation models viz. Pasternak was used and based on deflection profiles and load settlement curves improvement factors were reported. To understand the exact behaviour of geocell, the confining stresses that act on the geocell system has to be accounted. Pasternak model was improved by considering the effect of confining stresses and the improvement factors that are near to the exact value were reported.

8.2 Conclusions

The methods discussed have proved successful in indicating the potential improvement in bearing capacity the geocell reinforced sand layer brings to the circular and strip footings. The limit bearing capacity of footings (circular and strip) on geocell reinforced beds were reported. This analysis gives an idea of the upper and lower bound values of bearing capacities of the geocell reinforced system. This model doesn't account for the geocell properties or subsoil conditions and hence gives an approximate idea of the order of improvement. The Pasternak model was used further in the study as it is a betterment of the analytical model based on contact pressure variation as it considers the properties of the geocell-subsoil system. The main drawback of assessing the behaviour of the geocell reinforced system with the aid of Pasternak model is that it doesn't consider the effect of all-round confinement which is a major contributing factor that gives strength to the geocell

reinforced system. The major conclusions that were obtained from various study are discussed below:

8.2.1 Limit Bearing Capacities through Contact Pressure Variations

The approach based on contact pressure variation is demonstrative in understanding the pattern of bearing capacity improvement but for exact predictions of the same, numerical investigations using foundation models or experimental studies have to be conducted. The following conclusions are drawn from the study

- The improvement in bearing capacity of circular footing was found to be much higher than the strip footing.
- The assumed variations in contact pressure were found to hold good i.e. uniform pressure distribution (short geocell), linear distribution (intermediate width geocell) and exponential variation (wide geocell). Decay parameter, β has to be chosen appropriately for wide width geocells.
- Increasing geocell layer width ratio, R_g beyond 5 only provides marginal increase in the bearing capacity improvement of the soft ground. Providing very large geocell layer width has wide applications in pavements and improvement of soft grounds where differential settlements are anticipated.
- Appropriate contact pressure has to be chosen for accurate prediction of BCR.

However, for accurate prediction of bearing capacities, present model needs to be improved by using a model that considers the material properties of geocell reinforced footing system as well as incorporating the confining stresses that act on geocell reinforced system.

8.2.2 Nonlinear Pasternak Model for Strip Footings

An improvement of the previous model that accounts for the material properties of the geocell reinforced soil system is discussed here. An attempt has been made to numerically simulate the elasto-plastic behavior of rigid strip footing on geocell reinforced sand beds overlying soft clay beds. The deflection profile of the Pasternak shear layer was analyzed to obtain the load-settlement profiles. Following important conclusions are drawn from this study:

- A non-linear relationship between the normalized load (Q^*) and normalized footing settlement (W_0) in terms of the non-dimensional model parameters α and μ is obtained based on the deflection profile of the Pasternak shear layer. The second order non-linear differential equations were solved using finite difference scheme.

- A good agreement was observed between numerical results and independent experimental data.
- It has been observed that the normalized load-deflection profiles have significant influence on the model parameters viz. the shear layer width ratio, R_g ; inverse of normalized shear stiffness of the reinforced granular layer, α ; inverse of the normalized ultimate bearing capacity of the soft clay bed, μ .
- Lower value of μ represents higher stiffness of the soft foundation clay layer. Besides, lower the value of α represents higher flexural rigidity and stiffness of the Pasternak shear layer with geocell reinforcement.
- It is seen that a stiffer granular-geocell layer ($\alpha=0.5$) sustains a higher load for W_0 of 5% and spreads the load uniformly over the soft foundation soil. Further increase in value of α , the load supported by the geocell-granular layer decreases owing to lower flexural stiffness.
- For a given value of inverse of normalized shear stiffness of reinforced granular layer ($\alpha=1.0$), the settlement profile is uniform for shorter shear layer ($R_g = 5$) than for wider shear layer ($R_g = 10$). This observation concurs with the fact that highly rigid foundations undergo uniform settlements. Besides, there is a reduction in settlement with increase in shear layer width, R_g for a given value of α , even for weaker subsoil conditions (i.e. with increase in μ).
- With decrease in the value of inverse of normalized shear stiffness (α), the load carrying capacity of the composite ground increases. However, the influence of α beyond 1.0 seems insignificant on the load-settlement response, even though there is an increase in the shear layer width ratio.
- The load carrying capacity of the composite ground decreases with increase in the value of μ . This influence of $\mu \leq 10$ is found to be negligible on the load-settlement response as the foundation soils are expected to be very stiff at these values.
- Design charts in terms of improvement factors are presented with respect to various model parameters. For lower values of μ (0-25), it is seen that there is no improvement after increasing the shear layer width ratio (R_g) beyond 5. But significant improvement is brought by soils with low ultimate bearing capacity ($\mu>25$).
- The inclusion of geocell with higher shear stiffness ($\alpha=0.5$) brings in 8 fold increase in the improvement of ground.

In summary, the improvement factors with different model parameters show a clear trend of improvement in bearing capacity of reinforced ground.

8.2.3 Modified Pasternak model – Circular Footing

Elasto-plastic behaviour of rigid circular footing on geocell reinforced sand beds overlying soft soils has been analysed. Pasternak elastic model was used to idealise the circular footing resting on geocell reinforced soft soils. Following important conclusions are drawn from the study.

- Linear analysis to obtain the load settlement pattern is used when the footing undergoes very low settlements of the order of 1% where the actual load settlement pattern is linear.
- For higher settlements nonlinear response of the footing was used in the analysis.
- To check the validity of the results, the nonlinear model was validated both numerically and theoretically.
- The non-dimensional model parameters, α (inverse of the normalised shear stiffness of the geocell reinforced soil) and μ (inverse of the normalised ultimate bearing capacity) played an instrumental role in modelling the behaviour of circular footing resting on geocell reinforced soils.
- There is significant improvement in ground with the introduction of geocell reinforcement.
- Geocell reinforcement with high stiffness (low α) is able to bear very high load with uniform distribution of the same which enables commendable improvement of very soft soils.
- Low value of μ ($\mu = 0$) represents soils of infinite stiffness which doesn't require further reinforcement and it reflects in the improvement factors that were reported.
- It's is always economical to limit the shear layer width ratio (geocell layer width) to 5, beyond which it provides negligible improvement.

In summary, the model proposed was successful in helping understand the behaviour of rigid circular footing resting on geocell reinforced soils. Geocell reinforcement of soft soils shows a clear trend of improvement.

8.2.4 Stress Dependent Model for Strip Footing

The previous Pasternak model doesn't account for the confining stresses that act on the geocell reinforced system with which it derives its maximum strength. An attempt has been made to numerically simulate the elasto-plastic behaviour of rigid strip footing on geocell reinforced beds incorporating the stress dependency of the geocell layer. With the aid of foundation models viz. Pasternak model the deflection profiles were obtained numerically (finite difference scheme) and the loads were calculated. Some of the important observations that were drawn from the study are listed below:

- The nonlinear stress independent model performs well for lower settlements but for higher settlements the model that incorporates stress dependency has to be used.
- The parameters that were analyzed in the current study are inverse of the normalized shear stiffness (α), inverse of the normalized ultimate bearing capacity (μ), Compaction coefficient (C) and normalized settlement (W_0).
- To check the consistency and accuracy of the code, it was validated by comparing the model with the nonlinear stress independent model by reducing it into stress independent model. The model was also compared with independent experimental results. In all the cases, the new model results were well compared with the other models.
- There is a clear trend of improvement with increase in the shear stiffness of the geocell reinforced ground at low settlements and high stiffness of the subsoil whereas there isn't any considerable improvement at higher settlements and low stiffness of the subsoil.
- It was also reported that there is an increase in load bearing capacity with higher values of geocell layer width but to be on the economical side it is always good to restrict the geocell layer width to 5.
- The design charts that are proposed could be used for designing geocell reinforced foundations of strip footing.
- Lower value of C induces the confinement effect or stress dependent behaviour and as it increases or tends to infinity it behaves similar to nonlinear stress independent model. Appropriate value of C has to be chosen based on initial stresses.
- The improvement that is brought to soft subsoil is significant (about 20 folds) with the introduction of geocell reinforcement and the soft soil is able to withstand higher loads.

In summary, the present approach of calculating the improvement factors or loads is a better approach as it accounts for the confining stresses in the geocell from which the geocell reinforced subsoil derives its strength.

8.2.5 Stress Dependent Model for Circular Footing

The above stress dependent model has been extended to understand the behavior of circular footing. The following major conclusions drawn from the study are pointed out as below:

- Validation of the present model has been done with experimental results to understand the applicability of the current model in practical applications. It was very clear from the comparison that stress dependent model was found to perform better than the stress independent model.
- It was observed from the study that the model parameters, including inverse of normalized shear stiffness, α ; inverse of normalized ultimate bearing capacity, μ ; compaction coefficient, C ; Shear layer width ratio, R_g have a significant role in predicting the improvement brought about by the geocell reinforced soil.
- Lower value of compaction coefficient, C (Low value of C indicates low initial stresses and higher value of stresses that can be bore by the geocell reinforced system) shows a uniform distribution of loads in the settlement pattern ($C=0.0001$) and high loads that can be bore by the reinforced system.
- The stress independent model underestimates the actual predictions and incorporation of stress dependency helps in understanding the actual behaviour of the geocell reinforced system since it takes into account the confining stresses acting on the system.
- The deflection profiles and load deflection patterns obtained for varying values of inverse of normalized shear stiffness of the geocell reinforced soil (α) shows a uniform distribution of loads for geocells of high stiffness ($\alpha = 0.5$) and higher loads bore by the geocell reinforced system and the vice versa occurs for geocells of low stiffness ($\alpha = 2.0$).
- Similarly the settlement profile and the load settlement curve were also plotted for varying subsoil conditions. It was inferred from the study that uniform deflection of the geocell layer was observed when the subsoil is of low stiffness since a subsoil of high stiffness would resist the free movement of the geocell layer. But the loads that

can be bore y the system with strong subsoil conditions are very high ($\mu = 0$, indicating infinitely high stiffness for the subsoil).

- To quantify the performance of geocell reinforced system, improvement factors were used. The variation of improvement factors (I_f) with variation of inverse of normalized shear stiffness (α) and geocell/shear layer width ratio (R_g) was analyzed by varying model parameters, μ , W_0 , C .
- The improvement factors that were reported with incorporation of stress dependent behaviour are very high. As expected the I_f was found to decrease with increase in the value of α indicating higher improvement for the geocell reinforcement with high stiffness. The influence of the model parameters μ , C and W_0 were studied. Subsoil with high stiffness reported lesser improvement factors indicating that further improvement of the system with inclusion of geocell is negligible and is not an economical option.
- As expected, with increase in footing settlement (W_0), the I_f reported is also high. The major factor that governs the stress dependent behaviour, compaction coefficient, C was shown to have a clear increase in performance improvement with lower values of C . For lower values of C , even system with low geocell stiffness shows a higher improvement of the geocell reinforced system.
- The variation of improvement factor, I_f with geocell layer width, R_g was also analyzed. Various parameters C , μ , α were varied to study the influence of the same on the improvement. In most of the cases the improvement was found to be constant beyond R_g 5 but in extreme cases where the geocell and subsoil stiffness is very weak and very low initial stresses the improvement was found to be appreciable.

In summary, the model that incorporates the stress dependent behaviour of the geocell reinforced system helps in predicting the behaviour of the geocell reinforced system near to the actual behaviour. The improvement factors reported from the study could be used for design of geocell reinforced system as it is close to the actual behaviour.

8.3 Scope of Further work

The present study has attempted to study the behaviour of rigid footings resting on geocell reinforced soils. The study can be further extended to study the behaviour of flexible foundations on geocell reinforced soils. Different types of loading conditions viz. embankment loading on geocell reinforced soils could also be analyzed. The models can also

be employed to obtain the performance improvement of geocell reinforced pavements and railway ballast.

References

- [1] Akinmusuru, J.O., and Akinbolade, J.A., 1981, 'Stability of loaded footings on reinforced soil'. *Journal of the Geotechnical Engineering Division*, ASCE,107, 819 - 827.
- [2] Alawaji, H.A., 2001, 'Settlement and bearing capacity of geogrid-reinforced sand over collapsible soil'. *Geotextiles and Geomembranes*, 19, 75-88.
- [3] Bathurst R. J. and Jetter, P. M (1989). Large-Scale tests of geo-composite mattresses over peat sub grades. *Transportation Research Record 1188*, Transportation Research Board, Washington, DC, pp. 28 – 36.
- [4] Binquet, J., and Lee, L.K., 1975a, 'Bearing capacity tests on reinforced earth slabs'. *Journal of Geotechnical Engineering Division*, ASCE, 101(12), 1241 -1255.
- [5] Binquet, J., and Lee, L.K., 1975b, 'Bearing capacity analysis of reinforced earth slabs'. *Journal of the Geotechnical Engineering Division*, ASCE, 101(12), 1257-1276.
- [6] Boushehrian, J.H., and Hataf, N., 2003, 'Experimental and numerical investigation of the bearing capacity of model circular and ring footings on reinforced sands'. *Geotextiles and Geomembranes*, 21(5), 241-256.
- [7] Bush, D. I., Jenner, C. G. and Bassett, R. H (1990). The design and construction of geocell foundation mattress supporting embankments over soft ground. *Geotextiles and Geomembranes*, 9, pp. 83-98.
- [8] Cowland, J.W. and Wong, S. C. K (1993). Performance of a road embankment on soft clay supported on a geocell mattress foundation. *Geotextiles and Geomembranes*, 12, pp. 687-705.
- [9] Crank, J. and Nicolson, P (1947). A practical method for numerical evaluation of solutions of partial differential equations of the heat conduction type. *Proc. Camb. Phil. Soc.*, 43 (1), pp. 50–67.
- [10] Das, B.M., Puri, V.K., Omar, M.T., and Evgin, E., 1996a, 'Bearing capacity of strip foundation on geogrid-reinforced sand -scale effects in model tests'.*Proc. of 6th International Conference on Offshore and Polar Engineering*, Los Angeles, May, 527-530.

- [11] Dash, S.K., Krishnaswamy, N. R. and Rajagopal, K (2001a). Bearing capacity of strip footings supported on geocell-reinforced sand. *Geotextiles and Geomembranes*, 19, pp. 235-256.
- [12] Dash, S.K., Sireesh, S., and Sitharam, T.G (2003). Model studies on circular footing supported on geocell reinforced sand underlain by soft clay. *Geotextiles and Geomembranes*, 21, pp. 197-219.
- [13] De Merchant, M. R., Valsangkar, A.J., and Schriver, A. B., 2002, 'Plate load tests on geogrid-reinforced expanded shale light weight aggregate'. *Geotextiles and Geomembranes*, 20, 173-190.
- [14] Deb, K., Basudhar, P. K. and Chandra, S (2007). Generalized Model for Geosynthetic-Reinforced Granular Fill-Soft Soil with Stone Columns. *Int. J. Geomech*, 7, pp. 266-276.
- [15] Filonenko-Borodich, M.M (1940). Some approximate theories of the elastic foundation. *Uch. Zap.Mosk.Gos.Univ.Mech*, 46, pp. 3-18 (in Russian).
- [16] Filonenko-Borodich, M.M (1945). A very simple Model of an elastic foundation capable of spreading the load. *Sb. Tr. Mosk. Elektro. Inst. Inzh. Trans.* No: 53 Transzheldorizdat. (In Russian)
- [17] Fragaszy, J.R., and Lawton, E., 1984, 'Bearing capacity of reinforced sand subgrades'. *Journal of the Geotechnical Engineering Division, ASCE*, 110,1500-1507.
- [18] Gabr, M.A., Dodson, R., and Collin, J.G., 1998, 'A study of stress distribution in geogrid-reinforced sand'. *Geosynthetics in foundation reinforcement and erosion control systems*, ASCE Special publication, 62-76.
- [19] Guido, V. A., Chang, D.K. and Sweeny, M. A., 1986, 'Comparison of geogrid and geotextile reinforced earth slabs'. *Canadian Geotechnical Journal*, 23, 435- 440
- [20] Huang, C.C., and Tatsuoka, F., 1990, 'Bearing capacity of reinforced horizontal sandy ground'. *Geotextiles and Geomembranes*, 9, 51-82.
- [21] Koerner R.M. Designing with geosynthetics, Prentice Hall, Englewood Cliffs, (1990), New Jersey
- [22] Kondner, R. L (1963). Hyperbolic stress-strain response: cohesive soils. *J. Soil Mech. and Found. Div.*, 89(1), pp. 115-14.
- [23] Krishnaswamy, N. R., Rajagopal, K. and Madhavi Latha, G (2000). Model studies on geocell supported embankments constructed over soft clay foundation. *Geotechnical Testing Journal, ASTM*, 23, pp. 45-54.

- [24] Kumar, A., and Saran. S., 2001, 'Isolated strip footings on reinforced sand'. *Journal of the Southeast Asian Geotechnical Society*, 32(3), 117-189.
- [25] Madhav, M. R. and Poorooshab, H. B (1988). A new model for geosynthetic reinforced soil. *Computers and Geotechnics*, 6, pp. 277-290.
- [26] Madhav, M. R. and Poorooshab, H. B (1989). Modified Pasternak model for reinforced soil. *Int. J. Math. Comp. Modelling*, 12, pp. 1505-1509.
- [27] Maheshwari, P., Chandra, S. and Basudhar, P.K (2004). Response of beams on a tensionless extensible geosynthetic-reinforced earth bed subjected to moving loads. *Computers and Geotechnics*, 31, pp. 537-548.
- [28] Mandal, J.N. and Gupta, P (1994) Stability of geocell reinforced soil *Construction and Building Materials*, 8(1), pp. 55-62.
- [29] Mhaiskar, S. Y. and Mandal, J. N (1994). Soft clay subgrade stabilization using geocells. *Geosyntheticworld*, Publication by Wiley Eastern Ltd.
- [30] Michalowski, R.L., 2004, 'Limit loads on reinforced foundation soils'. *Journal of Geotechnical and Geoenvironmental Engineering*, ASCE, 130(4),381-390.
- [31] Mitchael, T. A., and Collin. J.G., 1997, 'Large model spread footing load tests on geosynthetic reinforced soil foundations'. *Journal of Geotechnical and Geoenvironmental Engineering*, ASCE, 123(1), 66-72.
- [32] Moghaddas and Dawson ,2010 'Laboratory model tests for a strip footing supported on geocell reinforced sand beds' *Geotechnical special publications* No: 207.
- [33] Omar, M.T., Das, B.M., Yen, S.C., Puri, V.K., and Cook, E.E., 1993b, 'Ultimate bearing capacity of rectangular footings on geogrid-reinforced sand'. *Geotechnical Testing Journal*, ASTM, 16, 246-252.
- [34] Pasternak, P.L (1954). On a new method of analysis of an elastic foundation by means of two foundation constants (In Russian).
- [35] Patra, C.R., Das, B.M., and Atalar, C., 2005, 'Bearing capacity of embedded strip foundation on geogrid-reinforced sand'. *Geotextiles and Geomembranes*, 454-462.
- [36] Poulos, H. G. and Davis, E (1974). *Elastic solutions for soil and rock mechanics*. Wiley, New York.
- [37] Raymond, G.P., Abdel-Baci, M.S.A., Karpurapu, R., and Bathurst, R.J.,1992, 'Improvement from reinforcement of soil below eccentrically loaded footings'. *Special Publication on Grouting, soil Improvement and Geosynthetic*, *Journal of Geotechnical Engineering*, ASCE, 2, 1104-1115.

- [38] Selvadurai, APS (1979). Elastic analysis of soil-foundation interaction. Elsevier Scientific Publishing Company, Amsterdam, the Netherlands.
- [39] Shimizu, M. and Inui, T (1990). Increase in the bearing capacity of ground with geotextile wall frame. *Proc. of the 4th Int. Conf. on Geotextiles, Geomembranes and Related products*, pp. 254.
- [40] Shin, E.C., Das, B.M., Lee, E.S., and Atalar, C., 2002, 'Bering capacity of strip foundation on geogrid-reinforced sand'. *Geotechnical and Geological Engineering*. 20, 169-180.
- [41] Shukla, SK. Chandra S (1994). A generalized mechanical model for geosynthetic-reinforced foundation soil. *Geotext Geomembr*, 13, pp. 813–825.
- [42] Sitharam, T. G. and Sireesh, S (2005a) Behaviour of embedded footings supported on geogrid-cell reinforced foundation beds. *Geotechnical testing Journal*, ASTM, 28, pp. 452 – 463.
- [43] Verma, B.P., and Char, A.N.R., 1986, 'Bearing capacity tests on reinforced sand subgrades'. *Journal of Geotechnical Engineering*, ASCE, 112, 701- 706.
- [44] Winkler, E. (1867). *Die Lehre von der Elastizitat und Festigkeit*. Dominicus, Prague.
- [45] Yamamoto, K., and Otani, J., 2002, 'Bearing capacity and failure mechanism of reinforced foundations based on rigid plate-finite element formulation'. *Geotextiles and Geomembranes*, 20, 367-393.
- [46] Yetimoglu, T., Wu, J.T.H., and Saglamer, A., 1994, 'Bearing capacity of rectangular footings on geogrid-reinforced sand'. *Journal of Geotechnical Engineering*, ASCE, 120(12), 2083-2099

Publications

- [1] Sireesh S, Madhav M. R., and Faby Mole, P. A. (2012) 'Nonlinear Analysis of Geocell Reinforced Rigid Strip Footings on Soft Soils' In the proceedings of Indian Geotechnical Conference (IGC 2012), New Delhi, 13-15 December, 2012.
- [2] Faby Mole P.A., Sireesh S, Madhav M.R (2013), 'Estimation of bearing capacity of strip footing on geocell reinforced soils', In the proceedings of fourth Indian young geotechnical engineers conference (4IYGEC 2013), IIT Madras, 17-18 May,2013
- [3] Faby Mole, P. A, Sireesh S, Madhav M. R. (2013) 'Prediction of limit bearing capacity of footings on Geocell reinforced soils'(Under review)
- [4] Faby Mole, P. A, Sireesh S, Madhav M. R. (2013) 'Numerical Modelling of Geocell reinforced foundations', Ground improvement journal. (Under review)